

# **A Vector Controlled Drive for Parameter Evaluation of Variable Flux Machines**

**Rajendra Thike**

**A Thesis**

**in**

**The Department**

**of**

**Electrical and Computer Engineering**

**Presented in Partial Fulfillment of the Requirements**

**for the Degree of**

**Master of Applied Science (Electrical and Computer Engineering) at**

**Concordia University**

**Montréal, Québec, Canada**

**November 2016**

**© Rajendra Thike, 2016**

**CONCORDIA UNIVERSITY  
SCHOOL OF GRADUATE STUDIES**

This is to certify that the thesis prepared

By: Rajendra Thike

Entitled: "A Vector Controlled Drive for Parameter Evaluation of Variable Flux Machines"

and submitted in partial fulfillment of the requirements for the degree of

**Master of Applied Science**

Complies with the regulations of this University and meets the accepted standards with respect to originality and quality.

Signed by the final examining committee:

_____	Chair
Dr. R. Raut	
_____	Examiner, External To the Program
Dr. M. Paraschivoiu (MIE)	
_____	Examiner
Dr. A. K. Rathore	
_____	Supervisor
Dr. P. Pillay	

Approved by: \_\_\_\_\_  
Dr. W. E. Lynch, Chair  
Department of Electrical and Computer Engineering

\_\_\_\_\_20\_\_\_\_\_

\_\_\_\_\_

Dr. Amir Asif, Dean  
Faculty of Engineering and Computer  
Science

# Abstract

## A Vector Controlled Drive for Parameter Evaluation of Variable Flux Machines

Rajendra Thike

Variable flux machine is a new class of permanent magnet machines that combine the flux controllability in wound field synchronous machines, and the high efficiency due to permanent magnets. An AlNiCo based variable flux machine whose air-gap flux is varied by applying a direct axis current pulse is considered in this work.

This thesis review the  $dq$  model of permanent magnet machines, which is then modified to account for flux controllability in variable flux machines. The existing inductance measurement methods are analyzed, and a vector control technique that is fast in the measurement of current dependent inductances at various magnetization level, is proposed. The accuracy of the method is assessed by comparing it with the flux linkage calculation method.

The variable flux machines are designed with small air-gap lengths to reduce the magnet thickness, and the magnetization current. Due to this reason, saturation and cross-magnetization effects causes changes in the flux produced by one coil, when current in other coil is changed and vice versa. If the cross-magnetization effects are neglected, accurate control of the magnet flux would require a slower current controller. This would need a longer duration pulse to change the magnetization level. The longer the pulse duration, the more severe is the torque ripple. For high performance drives, consideration of cross-magnetization effects is required. Therefore, this thesis proposes a vector controlled technique to evaluate the cross-magnetization effects in variable flux machines. The proposed technique is able to measure the self and cross-coupled inductances at any magnetization level using an

existing drive. The  $dq$  model of variable flux machine is then modified to account for the cross-magnetization effects.

The cross-coupled inductances are used to evaluate the static torque-angle characteristics of the machine. Two methods using the vector control technique are presented to experimentally measure the static torque-angle characteristics. The benefit of using a vector control drive is that the effects of heating and unequal phase resistances are taken care automatically. The measured torque-angle characteristics are compared with the calculated and finite element method simulation ones. Finally, the same vector control technique is used to evaluate the torque ripple performance of the VFM. This technique is not only useful in evaluating the designed machine, but it is also useful to evaluate design software.

# Acknowledgments

This thesis represents not only the fruits of my hard work, but also the support, guidance and wishes of many amazing people I met here at Concordia. They have been a family far from home. Compared to the first day I came to Concordia, I find myself equipped with sound analytic and laboratory skills in power electronics, electric machines and drives. Moreover, I have gained a better communication skills. Thanks to my colleagues at the power electronics and energy research group who have profoundly contributed to laboratory and equipment handling skills.

I would like to express my sincere gratitude to my advisor, Prof. Pragasen Pillay, NSERC/Hydro-Québec Senior Industrial Research Chair at Concordia University for providing me an opportunity to work with electric machines. He has provided not only the financial support, but the guardianship in a completely new socio-economic and cultural environment which I consider the most important factor for an international student who is half the globe from home. Prof. Pillay is a deeply caring person who has created a family environment in his research group. His timely and valuable guidance is the reason behind the successful completion of this thesis.

I would like to acknowledge the Department of Electrical and Computer Engineering at Concordia University for an excellent academic environment.

I would like to thank my colleague Dr. Lesedi Masisi from South Africa for introducing me to the experimental work in machines and drives. He is a very nice guy who spent several of his valuable days to familiarize me with the skills needed to work with electric machines.

Special thank goes to Mr. Chirag Desai for helping me with appropriate tools to prepare my experimental setup. Brother Akrem Aljehaimi, with whom I had worked together for troubleshooting the problems in the experimental work helped me a lot. And I would like to appreciate Dr. R. Sudharshan Kaarthik for his valuable insights and troubleshooting skills with the analog and digital measurement systems. Without his consultations, a timely experimental result would not have been possible.

I would like to appreciate the continuous inspiration from Dr. John Wanjiku. He is an ideal colleague to work with, highly responsible yet enjoys the life to the fullest. He helped me in reviewing the thesis. I would like to remember my colleague Amirmasoud Takbash for sharing his knowledge and insightful discussion in electric machines. I would like to mention Dr. Maher Al-Badri, Dr. Abhijit Choudhury, Dr. Maged Ibrahim, Jemimah Akiror, Sara Maroufian, Samhita Dey, Nazli Kalantari, Mohammad Hosein, Mohammad Masadeh and Mahmud Bijan for all the works in strengthening the group, and all the fun, celebrations, barbecues and parties. The time spent at PEER lab was enjoyable.

Most importantly, I would like to remember the love, encouragement and patience from my family. My mother, who deeply missed her son and always tried to hide her tears whenever I talked with her. I would like to respect her love. And I would like to thank god for everything I have.

This thesis was financially supported in part by the R&D program of the Natural Sciences and Engineering Research Council Chair entitled “Design and Performance of Special Electrical Machines” at Concordia University.

# Contents

<b>List of Figures</b>	<b>x</b>
<b>List of Tables</b>	<b>xiv</b>
<b>1 Introduction</b>	<b>1</b>
1.1 Electric Machines for EV Applications . . . . .	2
1.2 Permanent Magnet Synchronous Machine . . . . .	6
1.2.1 PMSM Modeling . . . . .	8
1.2.2 PMSM Parameters Measurements . . . . .	10
1.3 Variable Flux Machines . . . . .	12
1.3.1 VFM Classifications . . . . .	14
1.3.2 Advantages of the VFM . . . . .	16
1.4 Cross Magnetization . . . . .	17
1.5 Research Objective . . . . .	19
1.6 Organization of the Thesis . . . . .	20
1.7 Publications . . . . .	21
<b>2 Fundamentals of AlNiCo based VFMs</b>	<b>22</b>
2.1 Characteristics of AlNiCo Magnets . . . . .	24
2.2 Characteristics of a VFM . . . . .	26
2.2.1 Measurement of VFM Characteristics . . . . .	27

2.3	Modeling of a VFM . . . . .	29
2.3.1	Basic model of the VFM . . . . .	29
2.3.2	VFM Drive . . . . .	31
2.3.3	Experimental Tests . . . . .	32
2.4	Review on VFM Parameter Measurement . . . . .	35
2.4.1	Inductance Measurement . . . . .	36
2.5	Inductance Measurement Method for the VFM . . . . .	40
2.5.1	Discussion on General Methods of Inductance Measurement . . . . .	40
2.5.2	The Proposed Method . . . . .	41
2.5.3	q-axis Inductance Measurement . . . . .	41
2.5.4	d-axis Inductance Measurement . . . . .	42
2.5.5	Experimental Setup and Control Structure . . . . .	43
2.5.6	Results . . . . .	46
2.6	Comparison of Techniques . . . . .	48
2.7	Summary . . . . .	49
<b>3</b>	<b>Cross Magnetization Effects in VFMs</b>	<b>51</b>
3.1	Cross-Magnetization in PM Machines . . . . .	52
3.2	Cross-Magnetization in VFMs . . . . .	53
3.3	VFM Model including Cross-Magnetization . . . . .	53
3.3.1	Apparent and Incremental Inductances . . . . .	55
3.3.2	Cross-Coupling Inductance Evaluation . . . . .	55
3.3.3	Experimental Tests . . . . .	57
3.3.4	Results and Discussions . . . . .	58
3.4	Summary . . . . .	65
<b>4</b>	<b>Torque Performance of VFMs</b>	<b>66</b>

4.1	Steady State Torque Calculation . . . . .	67
4.2	Measurement of Static Torque-Angle Characteristics . . . . .	72
4.2.1	Method I: Varying Rotor Position . . . . .	73
4.2.2	Method II: Varying Current Vector . . . . .	75
4.3	Torque Angle Comparison . . . . .	78
4.4	Torque Ripple Performance . . . . .	82
4.4.1	Torque Ripple Measurement . . . . .	82
4.5	Summary . . . . .	85
<b>5</b>	<b>Conclusions And Recommendations</b>	<b>86</b>
5.1	Conclusion . . . . .	86
5.2	Future Works . . . . .	88
	<b>Bibliography</b>	<b>89</b>
	<b>Appendix A Machine Specifications</b>	<b>98</b>

# List of Figures

Figure 1.1	General overview of motor drives. . . . .	3
Figure 1.2	Different topologies for radial field PMSMs. . . . .	7
Figure 1.3	Three phase stationary coils and equivalent $dq$ coils . . . . .	8
Figure 1.4	Dynamic equivalent circuits of PMSM neglecting core losses. . . . .	10
Figure 1.5	Circuit diagram to measure inductances using a DC source. . . . .	12
Figure 1.6	Categorization of VFMs according to the method of flux control. . .	14
Figure 1.7	Measured permeability variation of M19G29 electrical steel. . . . .	18
Figure 2.1	Variable flux machine using AlNiCo magnets. . . . .	23
Figure 2.2	AlNiCo magnets operation under demagnetizing field . . . . .	25
Figure 2.3	Linearized BH loop of AlNiCo magnets . . . . .	25
Figure 2.4	Circuit diagram to measure VFM characteristics. . . . .	26
Figure 2.5	Measured magnetization characteristics of a prototyped VFM . . . . .	28
Figure 2.6	Measured demagnetization characteristics of a prototyped VFM . . . .	28
Figure 2.7	Dynamic equivalent circuits of PMSM neglecting core losses. . . . .	31
Figure 2.8	Block diagram of the variable flux machine using the basic model . .	31
Figure 2.9	Circuit diagram of a vector controlled variable flux machine drive . .	32
Figure 2.10	Experimental setup for the variable flux machine drive . . . . .	33
Figure 2.11	Vector control block diagram for a variable flux machine drive . . . .	34
Figure 2.12	Experimental result in a VFM drive . . . . .	35
Figure 2.13	Circuit connection to measure inductances using DC standstill test .	37

Figure 2.14	$dq$ voltage waveforms when pulsed $v_q$ is applied controlling $i_d$ . . . .	42
Figure 2.15	$dq$ current waveforms when pulsed $v_q$ is applied controlling $i_d$ . . . .	43
Figure 2.16	$dq$ voltage waveforms when pulsed $v_d$ is applied controlling $i_q$ . . . .	44
Figure 2.17	$dq$ current waveforms when pulsed $v_d$ is applied controlling $i_q$ . . . .	44
Figure 2.18	Experimental setup to measure inductances using vector controlled drive . . . . .	45
Figure 2.19	Schematic of vector control diagram . . . . .	45
Figure 2.20	Measured q-axis flux linkage at different currents for fully magnetized machine . . . . .	46
Figure 2.21	Measured d-axis flux linkage at different currents for fully magnetized machine . . . . .	46
Figure 2.22	Measured q-axis inductances at different currents for three different magnetization states . . . . .	47
Figure 2.23	measured d-axis inductances at different currents for three different magnetization states . . . . .	48
Figure 2.24	Comparison of q-axis inductances from different methods . . . . .	49
Figure 2.25	Comparison of d-axis inductances from different methods . . . . .	49
Figure 3.1	Theoretical flux linkage vs current characteristics of a saturated machine.	56
Figure 3.2	Schematic of vector control diagram . . . . .	57
Figure 3.3	Measured d-axis flux linkage due to stator excitation at 100% magne- tization level . . . . .	59
Figure 3.4	Measured q-axis flux linkage due to stator excitation at 100% magne- tization level . . . . .	59
Figure 3.5	Cross-magnetizing flux linkages at 100% magnetization level . . . . .	60
Figure 3.6	Incremental self inductances at 100% magnetization level . . . . .	60

Figure 3.7	Incremental cross-coupling mutual inductances at 100% magnetization level . . . . .	61
Figure 3.8	Apparent cross-coupling mutual inductances at 100% magnetization level . . . . .	61
Figure 3.9	Measured d-axis flux linkage due to stator excitation at 75% magnetization level . . . . .	62
Figure 3.10	Measured q-axis flux linkage due to stator excitation at 75% magnetization level . . . . .	62
Figure 3.11	Incremental cross-coupling mutual inductances at 75% magnetization level . . . . .	62
Figure 3.12	Apparent cross-coupling mutual inductances at 75% magnetization level . . . . .	63
Figure 3.13	Measured d-axis flux linkage due to stator excitation at 50% magnetization level . . . . .	63
Figure 3.14	Measured q-axis flux linkage due to stator excitation at 50% magnetization level . . . . .	63
Figure 3.15	Incremental cross-coupling mutual inductances at 50% magnetization level . . . . .	64
Figure 3.16	Apparent cross-coupling mutual inductances at 50% magnetization level . . . . .	64
Figure 4.1	Flux decomposition in unsaturated machine . . . . .	68
Figure 4.2	Flux decomposition in VFM considering cross-magnetization . . . . .	69
Figure 4.3	Calculated torque angle curves considering cross-coupling effects for a fully magnetized machine . . . . .	70
Figure 4.4	Calculated torque angle curves considering cross-coupling effects for a 75% magnetized machine . . . . .	70

Figure 4.5	Calculated torque angle curves considering cross-coupling effects for 50% magnetized machine . . . . .	71
Figure 4.6	Experimental setup for the torque-angle measurement . . . . .	73
Figure 4.7	Circuit diagram for the torque angle measurement . . . . .	74
Figure 4.8	Measured torque angle curve by varying rotor position for a fully magnetized VFM . . . . .	76
Figure 4.9	Measured torque angle curve by varying rotor position for a 75% magnetized VFM . . . . .	77
Figure 4.10	Measured torque-angle curves at fixed rotor position (a) 100% mag- netization (b) 75% magnetization. . . . .	78
Figure 4.11	Comparison of calculated and simulated torques with the measured torque using method I for 100% magnetization level . . . . .	79
Figure 4.12	Comparison of calculated and simulated torques with the measured torque using method I for 75% magnetization level . . . . .	80
Figure 4.13	Comparison of calculated and simulated torques with measured torque using method II for 100% magnetization level . . . . .	81
Figure 4.14	Measured torque ripple at 100% magnetization level at rated current and 90° torque angle . . . . .	83
Figure 4.15	Comparison of measured torque waveform with FEM simulation . . . . .	84

# List of Tables

Table 1.1 Electric Motor Drives Adoption in Automotive Industries . . . . . 6

Table 4.1 Maximum torque per ampere torque-angle variation at different magnetization levels . . . . . 71

Table A.1 Specification of the prototyped VFM . . . . . 98

# Chapter 1

## Introduction

Emissions from Vehicles driven by internal combustion engines (ICEs) is one of the major source of air pollution and green house gas emission. For instance, transportation in a typical city accounts for about 41% of the  $CO_2$  emissions [1]. Owing to the environmental impacts caused by the petroleum based transportation infrastructures and world-wide interest in clean energy, a renewed interest in alternative transportation technologies for industrial and commercial off-road vehicles is growing [2]. Studies suggested that replacement of conventional vehicles by alternative vehicles using clean and renewable source of energy can provide environmental as well as economic benefits [2]. Electric vehicles (EVs) and hybrid electric vehicles (HEVs) have lower emissions and higher energy efficiency compared to conventional ICE vehicles. Canada is projected to have at least 500,000 highway capable plug-in EVs, and numerous HEVs [3].

Electric vehicles use highly efficient electric motor for vehicle propulsion. The high efficiency is attributed by advancement in high quality materials, machine design and manufacturing technologies. This is in addition to the development of high power density battery technologies, advancements in power electronics and digital controllers. It is now possible to design more advanced electric and hybrid electric vehicles with improved performance and enhanced efficiency.

## 1.1 Electric Machines for EV Applications

Various types of electric machines have been used in EVs and hybrid electric vehicles (HEVs). Figure 1.1 shows the general overview of motor drives. The major requirements of an electric motor for traction applications are [4–6]:

- High torque and power density.
- High starting torque.
- High Efficiency over the whole operating range.
- Low torque ripple.
- Wide speed range, with a constant power range of around 3-4 times the base speed.
- Intermittent overload capability, typically twice the rated torque for short duration.
- Fast dynamic response.
- High reliability and robustness appropriate to the vehicle environment.
- Reasonable cost.
- Low acoustic noise.

Generally, the choice of the electric motor drive for EV applications is determined by the three dominant factors: cost, weight and size [7]. Thus, an electric machine for traction applications should be efficient and power dense within reasonable cost. Among these requirements, a wide speed range and energy efficiency are the two fundamental characteristics that are influenced by vehicle dynamics. Thus, among the number of competing and complementary electric motor drive technologies for HEV and EV applications, the selection of an electric machine require special attention to the speed range capability its energy efficiency.

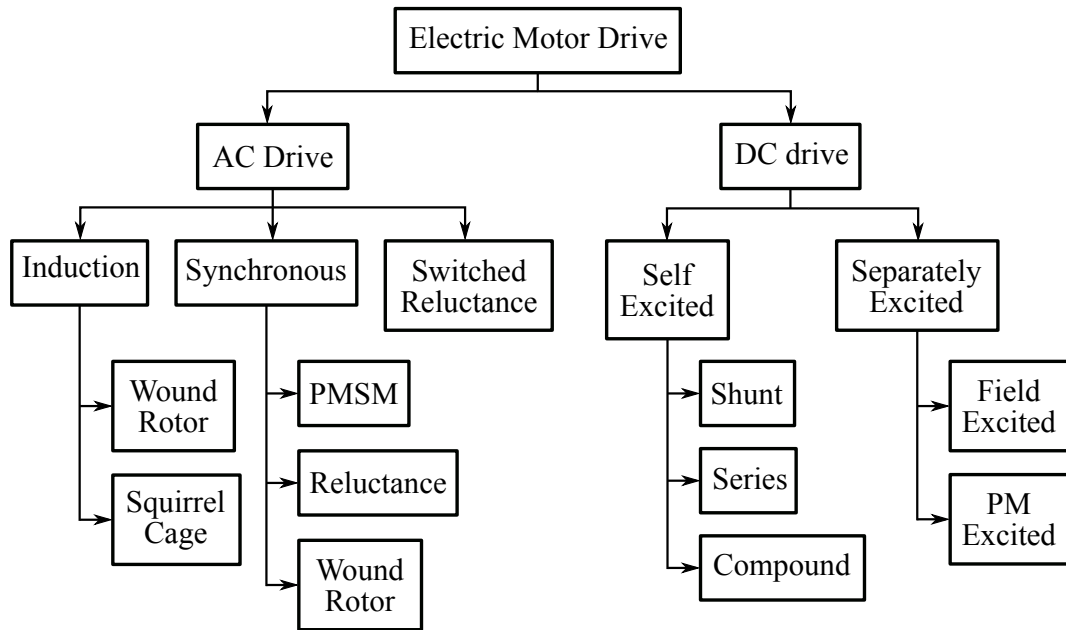


Figure 1.1: General overview of motor drives.

DC machines were used in EVs before the 1970s. They were easier to control than AC machines [8, 9]. They are still in use owing to their control simplicity and proper torque speed characteristics [4]. However, the major drawbacks of DC machines are the high rotor inertia, low power density, higher initial and maintenance cost. Because of these drawbacks, highly reliable and commutator less AC motors are a good alternative to DC machines. Development of special power electronic converters and advancement in digital controllers that can implement complex control strategy have also led to the growth of AC drives.

Induction machines(IMs) and permanent magnet synchronous machines (PMSMs) are widely used AC machines for traction applications [10]: This is because of the higher efficiency of PMSMs and lower cost of IMs [11]. The induction machine technology is the most mature among all AC machines. It is robust in structure, cost lower and it has well-established manufacturing techniques. A desirable characteristics of IMs, particular to automotive applications is that its speed range can be extended to four to five times the base speed [12]. An inverter fed IM permits the starting torque to as high as the maximum

torque, while high efficiency can be achieved by minimum slip control [13, 14]. However, IMs require magnetizing stator current which lowers the input power factor of the machine. Moreover, due to current in the rotor, there is increased copper losses in IMs compared to the PMSMs.

Permanent magnet synchronous machines have permanent magnets in the rotor that provide the necessary magnetic field in the air-gap. Magnets utilizing rare earth materials like Neodymium and Dysprosium can provide the highest magnetic field density per unit weight. Since there is no current flow in the rotor and no stator magnetizing current is required, the efficiency of PMSMs is higher. Compared to IMs, PMSMs have following advantages [15] which make them the most popular traction machines:

- Higher torque to inertia ratio.
- Higher efficiency due to lack of rotor copper losses.
- Smaller rectifier and inverter size due to absence of magnetizing current.
- High power and torque density.
- No problem in cooling the rotor.

Because of the above mentioned reasons, PMSMs have superior performance over all other machines. However, PMSMs have following drawbacks compared to IM drives [15].

- Undesirable cogging torque.
- Require expensive feedback position transducer.
- Higher cost due to expensive magnets.
- Lower field weakening range.
- Rotor operating temperature is limited by magnet properties.

- Safety issue (stator voltage is present if the wheel is spinning freely and braking torque in case of shorting).

Besides PMSMs and IMs, switched reluctance machines (SRM) and synchronous reluctance machines (SynRM) are alternative traction machines. The SRM rotor is the simplest rotor with no magnets and coils. The moment of inertia of the SRM is low that facilitate in faster dynamic response. The merits of a SRM which shows the strong potential for traction applications are as follows:

- Low cost.
- High efficiency.
- Simple and rugged structure.
- Fault tolerant operation and reliable converter topology.
- Easy to cool and high temperature operation.
- Simple stator coils.
- Very wide speed range.

Despite the excellent properties, the drawbacks of a SRM are higher torque ripple, higher acoustic noise generation, EMI noise generation, complexity in design and requirement of special converter topology.

The synchronous reluctance machine is similar to the conventional salient pole synchronous machine, but it neither has excitation windings nor magnets for field excitation. The rotor is constructed by barriers and segments to obtain magnetic saliency. The main advantages of the SynRM is elimination of rotor copper losses and lower cost. Due to its lower cost and higher torque capability, the SynRM is one possible alternative for traction drives in EV applications. The major drawbacks of a SynRM are low power factor and

Table 1.1: Electric Motor Drives Adoption in Automotive Industries

EV & HEV Model	Motor Drive System	EV & HEV Model	Motor Drive System
Peugeot-Citroen (France)	DC	Holden/ ECO (Australia)	SRM
BMW/X5 (Germany)	IM	Chevrolet/Silverado (USA)	IM
Daimler-Chrysler/Durango (Germany, USA)	IM	Tesla/S (USA)	IM
BMW/ I3 (Germany)	PMSM/IM	Toyota/ RAV4 (Japan)	PMSM/IM
Kia/ Soul (S. Korea)	PMSM	Toyota/ Prius (Japan)	PMSM
Honda/ Insite (Japan)	PMSM	Chevrolet/ Spark (USA)	PMSM
Nissan/ Leaf (Japan)	PMSM	Ford/ Focus (USA)	PMSM

higher torque ripple. Table 1.1 reviews a summary of different electric motor drives adopted in the automotive industries. It is apparent that both PMSMs and IMs are preferred by the automotive industry.

## 1.2 Permanent Magnet Synchronous Machine

Permanent magnet synchronous machines (PMSMs) are popular in low and medium power electric drives. The rotor has permanent magnets to provide a magnetic field for torque production. The high energy density of rare earth permanent magnets makes the PMSMs small and compact in size. The use of permanent magnets reduce the continuous copper loss that has to be supplied for machines without magnets. On the basis of the direction of the field flux, PMSMs are broadly classified into two categories: Radial field PMSMs and Axial field PMSMs. Radial field PMSMs are more common than axial field ones. Based on the magnet placement, the radial field PMSMs can have different topologies [16], some of which are shown in figure 1.2.

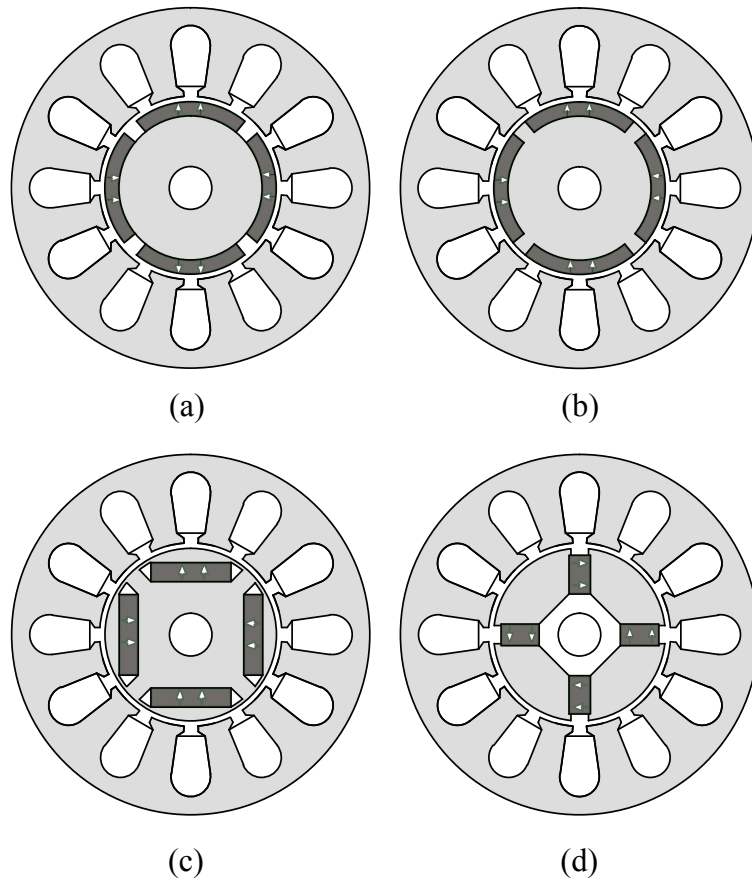


Figure 1.2: Different topologies for radial field PMSMs. (a) Surface PMSM. (b) Surface inset PMSM. (c) Interior PMSM. (d) Spoke type interior PMSM with circumferential orientation.

The surface PM arrangement provides the highest air gap flux density. As a result, surface mounted PMSMs have very high power density. These PM machines are not preferred for high speed applications. The surface inset PM arrangement provides the rotor some mechanical strength. The rotor surface is smooth and some magnetic saliency is introduced in this type of magnet placement. The magnets are held inside the rotor to provide mechanical robustness in interior PMSMs. Thus, they are suited for high speed operation. The circumferential orientation of the magnets in the spoke type PMSMs requires high volume of magnets. However, the air gap flux density can be made higher than the magnet flux density.

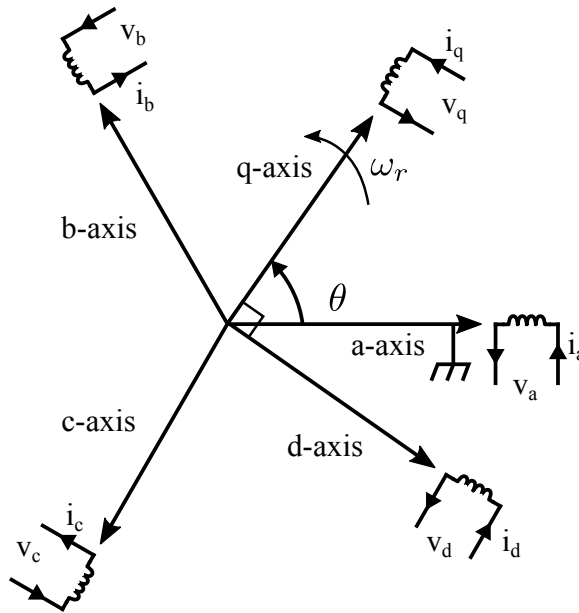


Figure 1.3: Three phase stationary coils and equivalent rotating d- and q- axes coils in rotor reference frame.

### 1.2.1 PMSM Modeling

Variable speed electric drives using PMSMs are converter-fed. Therefore, there is need to evaluate the dynamics of converter-fed variable speed drives for a given machine, and their interaction to determine the flow of currents in the converter and the machine [16]. The well established dq model of wound rotor synchronous machine is used to analyze the dynamics of the PMSMs [17].

In dq model, the three phase stator coils are modeled as two fictitious orthogonal coils. One of the fictitious coils is along the direct axis, and the other is along the quadrature axis which is  $90^\circ$  ahead of the direct axis. In the rotor reference frame, the direct axis is aligned with the magnet flux and both coils rotate synchronously with the rotor. Figure 1.3 shows the three phase stationary coils and the equivalent rotating d- and q- axes coils in the rotor reference frame. Expressions for d-axis voltage,  $v_d$  and q-axis voltage  $v_q$  are given by the equations (1.1) and (1.2).

$$v_d = \frac{2}{3}[v_a \sin \theta + v_b \sin(\theta - \frac{2\pi}{3}) + v_c \sin(\theta + \frac{2\pi}{3})] \quad (1.1)$$

$$v_q = \frac{2}{3}[v_a \cos \theta + v_b \cos(\theta - \frac{2\pi}{3}) + v_c \cos(\theta + \frac{2\pi}{3})] \quad (1.2)$$

where,  $v_a, v_b, v_c$  are the phase voltages and  $\theta$  is the position of q-axis from phase a-axis.

Dynamic equations for PMSMs can be written as the equations (1.3)-(1.6).

$$v_d = R_s i_d + \frac{d\lambda_d}{dt} - \omega_r \lambda_q \quad (1.3)$$

$$v_q = R_s i_q + \frac{d\lambda_q}{dt} + \omega_r \lambda_d \quad (1.4)$$

$$\lambda_d = L_d i_d + \lambda_f \quad (1.5)$$

$$\lambda_q = L_q i_q \quad (1.6)$$

where  $R_s$  is the stator resistance,  $i_d$  and  $i_q$  are d- and q-axes currents,  $\lambda_d$  and  $\lambda_q$  are d- and q-axes flux linkages,  $\lambda_f$  is the magnet flux linkage,  $\omega_r$  is the rotor speed,  $L_d$  and  $L_q$  are d- and q- axes inductances. The input power and the developed torque are given by the equations (1.7) and (1.8).

$$P_i = \frac{3}{2}[v_q i_q + v_d i_d] \quad (1.7)$$

$$T_e = \frac{3P}{2}[\lambda_f + (L_d - L_q)i_d]i_q \quad (1.8)$$

where  $P$  is the number of poles in the machine.

Often, the mathematical model of the PMSM is represented by equivalent circuits. Based on the equations (1.3)-(1.6), the dynamic equivalent circuits of PMSM neglecting core losses are shown in figure 1.4.

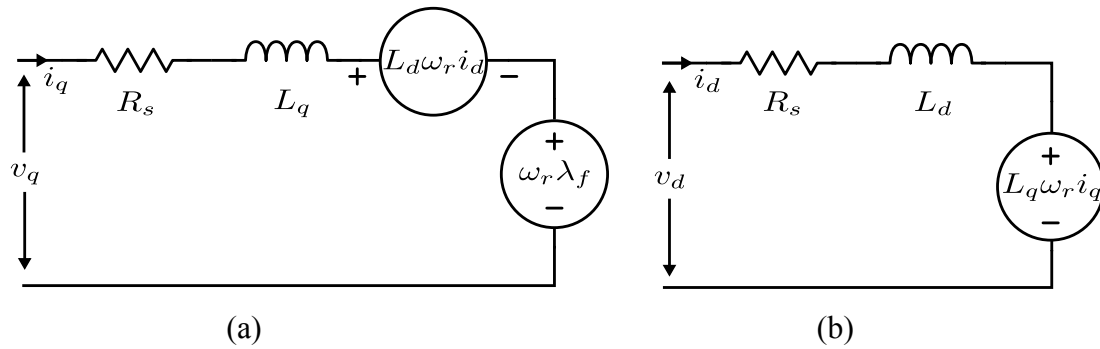


Figure 1.4: Dynamic equivalent circuits of PMSM neglecting core losses. (a) Stator q-axis dynamic circuit. (b) Stator d-axis dynamic circuit.

### 1.2.2 PMSM Parameters Measurements

The field oriented control of PMSM drives require the setting of motor electrical parameters for its proper functionality. The required parameters are number of poles, stator resistance, inductances and back-EMF constant. In the literature, there are various methods of determining these parameters [18–20].

#### Resistance measurement

The simplest method to measure the stator resistance  $R_s$  of the PMSM is to use a digital multimeter in the resistance mode. For a star connected stator windings, the resistance between two phases is measured in pair. The average of the measurement between each pair is divided by two to get the stator resistance. This technique works well for machines with higher values of resistance ( $>10\Omega$ ) [18].

Lower values of stator resistance can be measured using an RLC meter. Alternatively, two multi-meters can also be used to measure the voltage across the machine terminals and the current flowing through the windings, to reduce the effects of the test leads. The resistance is calculated using the voltmeter reading and ammeter reading. The calculated resistance should be corrected considering skin effect for the AC current. The accurate measurement of resistance also requires temperature compensation.

### Measurement of back-EMF constant

The back-EMF constant (or flux linkage of the PM denoted by  $\lambda_m$ ) is obtained by measuring the no-load peak voltage of the motor while it is driven by a prime mover at a constant speed [18]. The measurement can be performed at a few different speeds and average of the ratios of the peak value of the generated voltage to the speed of the shaft in rad/s gives the back-EMF constant.

### Measurement of inductances

Direct and quadrature axis inductances are the most important parameters of PM machines. They can be measured using both AC and DC tests. A method that use the time constant from current response to a DC voltage source to find the direct and quadrature axis inductances is described in [18]. The inductance is calculated by multiplying the measured time constant with the measured resistance. Figure 1.5 shows the connection diagrams to measure the direct and quadrature axes inductances using this method. The same circuit connection can be used in AC tests by replacing the DC source and freewheeling diode with a variable AC source. The RMS values of the applied voltage, input power and circuit current are recorded for an applied sinusoidal voltage. The impedance, resistance and inductances are calculated using equations (1.9) - (1.11) [21].

$$Z = \frac{V}{I} \quad (1.9)$$

$$R = \frac{P}{I^2} \quad (1.10)$$

$$L = \frac{1}{2\pi f} \sqrt{Z^2 - R^2} \quad (1.11)$$

Apart from the most basic methods described above, there are various other methods to determine the inductances [19–22]. Few of them use inverter fed AC source to determine both direct and quadrature axes inductances at the same time on the fly. The method can

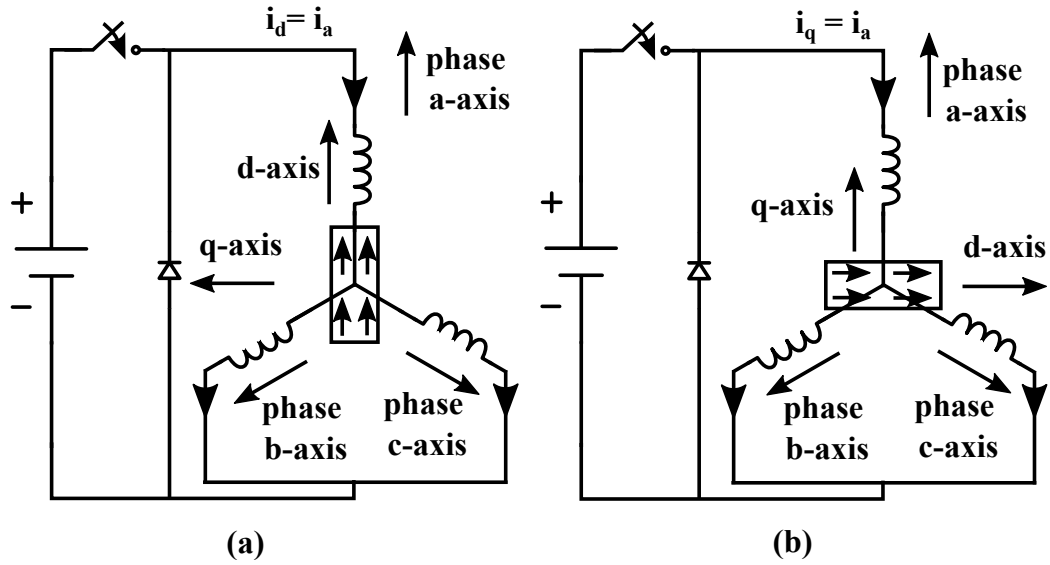


Figure 1.5: Circuit diagram to measure direct and quadrature axes inductances using a DC source (a) Circuit connection for direct axis inductance measurement. (b) Circuit connection for quadrature axis inductance measurement.

be used with some modification to determine the variation in inductances as well. Various methods to determine the inductances at standstill using step voltage and AC voltage from the measurement of current response to calculate flux linkage by using numerical integration technique are explained in detail in [19].

### 1.3 Variable Flux Machines

Variable flux machines (VFMs) are a new class of permanent magnet machines, for their ability to change the intensity of magnetization and memorize the flux density level in the magnets. The concept of VFM as memory motors is proposed in [23]. In VFMs, the magnetization of the magnets can be varied by a short duration current pulse. According to [23], memory motors have the combined advantages of a wound rotor machine (rotor flux can be varied) with those of wide speed PM machines that form a unique machine having the potential to find numerous applications in electric drives.

PMSMs utilize rare earth magnets having high remnant flux density and high coercivity. The high remnant flux density allows the PMSMs to be operated at high flux density giving high output torque and power density. The high coercivity makes the PMSMs tolerant to demagnetization from the stator current. A well designed PM machine should guarantee that the magnets remain fully magnetized under all operating conditions, including under short circuit faults.

As PMs cannot be re-magnetized in a conventional PMSM, the magnet thickness in the traditional PM machine is made large enough to keep the demagnetizing MMF of the armature reaction below the magnet coercive force under all operating conditions at the worst case operating temperature [24]. This is a serious disadvantage, as the costs of rare earth magnets that are used extensively in conventional PMSMs are high. Ferrite magnets are relatively lower in cost. However, they exhibit one third of the rare earth permanent magnet remnant flux density. Hence, their torque performance is not comparable to that of rare earth PMSMs [25].

Apart from the higher magnet cost, another issue with rare earth magnets is that their price is not stable. Due to increased interest in EVs and HEVs, the demand of these magnets is increasing but their supply is limited. This generates uncertainty of their availability and prohibits long term design planning in the automotive market [25, 26].

Since the magnet flux in PMSMs is fixed, the back-EMF of the machine is proportional to the speed only. As the operating speed increases, the back-EMF increases, reducing the voltage available to drive the current. For extended speed operation beyond the base speed, due to the limited inverter voltage, the PMSM requires continuous field weakening current which increases the machine losses. Thus, the efficiency of the PMSMs drops for operating speeds above the base speed. Additionally, the flux weakening stator current limits the torque producing component of the stator current which in turn limits the torque speed range of the machine. Therefore, oversized PMSMs are required to achieve a wide torque-speed range

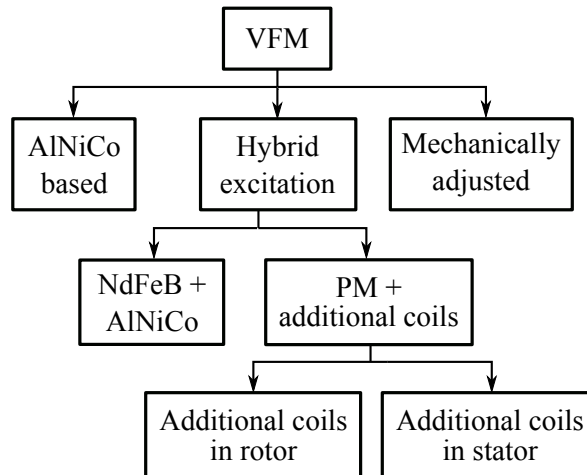


Figure 1.6: Categorization of VFMs according to the method of flux control.

for traction applications [5].

The drawbacks can be diminished in the variable flux memory motors. The use of less expensive and readily available permanent magnets make the variable flux PM machine a good alternative to rare earth based PM machines. The feature to vary the PM flux not only reduces the power loss at higher speeds, but also increases the torque-speed range.

### 1.3.1 VFM Classifications

With regards to the method of controlling flux, VFMs can be categorized into three types [27] as shown in figure 1.6. The first category uses AlNiCo magnets only as a source of field excitation. The second category uses a combination of different magnets or combination of magnets with additional coils to form hybrid-excitation. The last category uses mechanical methods to change the rotor's structure to achieve variable flux.

#### AlNiCo based VFMs

AlNiCo magnets have high remnant flux density that is comparable to rare earth magnets. However, their coercivity is very low which make them prone to demagnetization by stator

excitations during operation. Hence, AlNiCo magnets are rarely used in PM machines. The first proposed variable flux memory motor uses a sandwich of tangentially magnetized AlNiCo magnets [23, 28]. The magnets are magnetized using a short duration current pulse from the stator. The stator is the same as that of a three-phase PMSM. However, the manufacturing of sandwich rotor design is complex and the rotor has less mechanical strength compared to that of an interior PMSM. Moreover, the magnetization current requirement from the inverter is large, as a wider part of the magnets are near the rotor surface [24]. A variation in AlNiCo magnet based VFMs is proposed in [29–31] to get high torque density and reduce the inverter rating.

### **Hybrid excitations VFMs**

Hybrid excitation based VFMs utilizes two sources of magnetic fields. A class of these motors utilizes both rare earth magnets as a constant source of flux and low coercivity magnets to vary the air-gap flux density [32–35]. The NdFeB and AlNiCo magnets can be in the form of a sandwich or Y structure. The air gap flux is varied by controlling  $i_d$  to change the magnetization of AlNiCo magnets both in the positive and negative directions. The disadvantage with these designs is the requirement of a large current to vary the air gap flux due to the design of the rotor.

Another class of hybrid excitations VFMs utilizes either stator field coils or rotor field coils to vary the air gap flux. The field controllable axial flux PM motor proposed in [36] uses circumferentially wound DC field windings placed in between the inner and outer stator rings. The concept of using auxiliary stator windings for radial flux controlling purposes has been investigated in [37]. The PM machines described in [38, 39] has two rotor parts, one PM and one wound field, mounted on the same shaft separately. The design variation with either different magnetic circuits for PM and the wound field or the same magnetic paths has been explored.

### **Mechanically flux adjusted VFMs**

In mechanically flux adjusted VFMs, there is no need of d-axis current pulse or additional DC excitation windings to change the air gap flux. Mechanical arrangements are provided either to adjust the rotor structure or its location automatically. A rotor structure using centrifugal forces at different speeds to automatically adjust the magnets position was proposed in [40]. When the rotor speed exceeds the base speed, the magnetic conductor material will move outwards by the centrifugal force. The use of movable iron pieces to change the flux axially was proposed in [41]. At low speed, the iron pieces are kept out of the flux barrier so that the flux linkage due to PMs is not decreased. When the speed of the motor increases, the movable flux-shortening iron pieces can be inserted into the flux barriers of the rotor to get flux weakening effect.

### **1.3.2 Advantages of the VFM**

Variable flux machines exhibits significant feasibility for a wide speed range operations in electric vehicles and high speed machine tools. These machines possess several advantages over conventional PMSMs.

- The air-gap flux density can be changed so that a high efficiency characteristics of PM machine can be obtained with air-gap flux controllability of a wound rotor synchronous machine.
- The motor characteristics can be changed from high torque/low speed machine into a low torque/high speed machine through on-line control.
- For extended speed operation, the air-gap flux can be reduced by a short current pulse so that no sustained field weakening stator current is required. The stator copper loss is reduced improving the efficiency.

- As the field weakening current is not required, there is no limitation in torque producing current imposed by field weakening current. Thus, the torque speed curve is extended.
- As the machine is designed to change the magnetization, the magnet thickness need not be thick enough to prevent demagnetization due to stator current. Thus, the torque and power density is improved.
- Less expensive and readily available magnets are used.
- In conventional PMSMs there are safety issues due to large EMF caused by high speed rotation of the motor, but for VFMs this problem is controllable.
- The efficiency is increased in low speed operation as well as extended speed operation.
- The same hardware for PMSMs can be used for VFMs.

## 1.4 Cross Magnetization

In the dq model of a PMSMs described by the equations (1.3)- (1.6), the flux linkages  $\lambda_d$  and  $\lambda_q$  are dependent only on the currents  $i_d$  and  $i_q$  respectively. This is because the two coils (dq coils) are orthogonal to each other. The current in one coil cannot create a magnetic field in the other coil and vice-versa. However, in reality, because of the saturation of the core, the flux in d-axis tends to be affected by the current in q-axis and vice-versa. This phenomenon is called cross-magnetization or cross-saturation effects.

The cross-magnetization phenomenon is similar to the phenomenon of the demagnetizing effect of cross-magnetizing armature reaction in a DC machine and the phenomenon can also exist if the magneto-motive force (MMF) distributions are assumed to be sinusoidal [42]. The cross-magnetization effects arises from the non-linear magnetization characteristics of the electrical steel. Figure 1.7 shows a plot of the measured permeability of M19G29 electrical steel at 20 Hz sinusoidal excitation. From the plot it is seen that the permeability

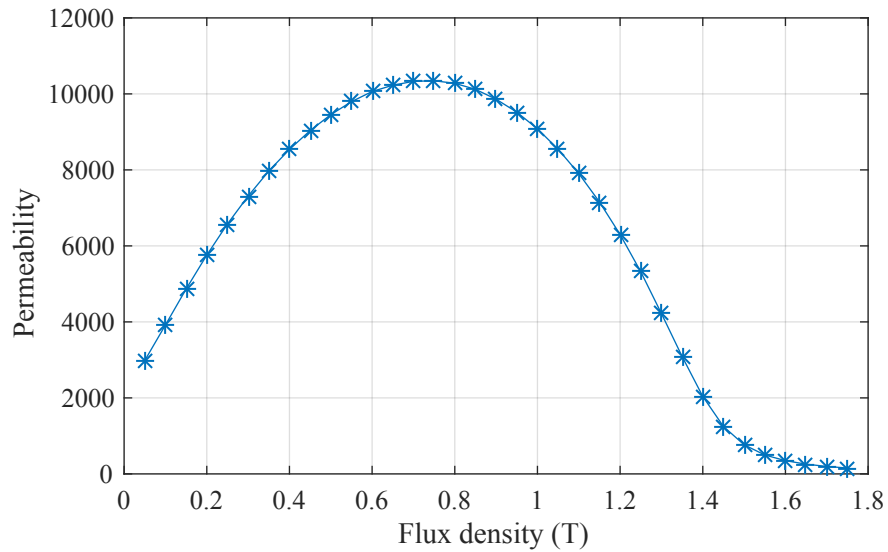


Figure 1.7: Measured permeability variation of M19G29 electrical steel at 20 Hz sinusoidal excitation.

of steel does not remain constant, but varies with excitation. For a magnetic circuit with two or more sources of excitations, the saturation effect causes the flux produced by one source to change when the excitations in another source is changed.

Cross-magnetization or cross-saturation effects are more prominent in interior magnet PMSMs and VFMs. It is because the air-gap is kept low to increase the air-gap flux density with less magnet thickness. In such a case, the reluctance of the steel is not negligible. As certain portion of the yoke and the rotor carries the magnetic flux from all the stator coils, the change of permeability of magnetic field path due to current in one coil affects the flux produced by another coil. In the  $dq$  model, though the two coils are orthogonal, the saturation of the common flux path by one coil will cause a change in the flux produced by another coil. Thus, there exists cross coupling flux linkages because of the cross-magnetization effects.

## 1.5 Research Objective

Variable flux machines are a new class of permanent magnet machines with added feature of control over the magnet flux. As control of the magnet flux requires an accurate control over the magnetizing current, precise measurement of the inductances is crucial. Moreover, the VFMs are designed with low air-gap to reduce the magnet thickness and the magnetizing current. Due to low air-gap, cross-magnetization effects become dominant in these machines. The consequence is that the inductances change not only with the magnetization level, but also with the load current. This will affect the performance of the flux controller and the pulse duration required to change the magnetization level in the VFM drive. For better flux control and lower torque ripple due to the pulsed current, accurate evaluation of inductance is necessary.

The estimation of the torque produced by the VFM requires the accurate estimate of the flux linkages. But, due to cross-magnetization, the flux produced along the d-axis is affected by the q-axis current and vice versa. Also, the inclusion of the cross-magnetization inductance is necessary to implement control strategies such as maximum torque per ampere and maximum efficiency per ampere. Thus, it is required to have a measurement technique to evaluate the cross-magnetizing effects in a VFM.

It is usual nowadays that an electric machine is designed using a finite element analysis design software. Apart from the accuracy of the algorithms employed, the material properties used in FEA software can cause deviation in the FEA design and the actual machine. To characterize and verify the designed machine, measurement techniques are important. This thesis focuses on the measurement techniques which can be used to measure inductance, to obtain torque-angle curves and, to measure the torque ripple of electric machines. The measurements obtained from the proposed method is compared with results from a FEA software. The techniques discussed and developed in this thesis are useful for drive designers and test engineers. The machine designers can use the proposed techniques to validate the

design. Moreover, the methods developed can also be useful in validation and improvement of machine design software.

Torque angle measurement and characterization is required in both machine design validation and drive design. It gives an idea of the current vector required to meet a certain load torque. Likewise, an electric machine is designed to have torque ripple within certain limit. A measurement technique is required to measure the torque ripple and validate the design requirements. The objectives of this thesis are therefore:

- To evaluate the existing PMSM parameter measurement techniques and to propose a rapid inductance evaluation method for the VFM
- To evaluate the cross-magnetization effects in the VFM.
- To measure the torque-angle curve and the torque ripple of an existing AlNiCo based VFM.

## **1.6 Organization of the Thesis**

This thesis is divided into five chapters.

**Chapter 2** starts with the fundamentals of AlNiCo based variable flux machines. This is followed by the experimental methods to find the characteristics of VFMs. Then, an existing model of a PMSM is modified to accommodate the variable flux property of the VFM. The VFM model is implemented in a vector controlled drive and experimental results are provided. The existing PMSM inductance measurement methods are discussed and an inductance measurement method using a vector controlled drive is proposed for VFMs. The experimental setup and results are discussed along with a comparison of the measured inductances from the proposed method with the flux linkage calculation method and the finite element analysis result.

**Chapter 3** discusses the cross-magnetization phenomenon in electric machines and its significance in variable flux machines. The  $dq$  model of the VFM presented in chapter 2 is modified to account for the cross-magnetization effects. Apparent and incremental inductances are defined and at the end, a method using a vector controlled drive for the measurement of the cross-coupling inductances of VFMs is discussed. Experimental results are provided for three different magnetization levels.

**Chapter 4** covers the measurement of torque-angle and torque-ripple of the VFM. The cross coupling inductances are used to calculate the steady state torque. An experimental method is given to measure the static torque-angle curves. The calculated and finite element analysis simulation torques are compared with the experimental torques.

**Chapter 5** summarizes the contributions of this thesis.

## 1.7 Publications

- R. Thike and P. Pillay. Vector Control Drive to Measure Inductances of Variable Flux Machine. Accepted in IEEE, Power Electronics, Drives and Energy Systems, 14-17 December 2016, Trivandrum, India

## Chapter 2

# Fundamentals of AlNiCo based VFMs

Despite having very high remnant flux density comparable to rare earth magnets, AlNiCo magnets are rarely used in electrical machines. This is because of their very low coercivity that makes them prone to demagnetization by armature reaction. A new class of permanent magnet machine using AlNiCo magnets to utilize its low coercive property to gain an extra benefit out of PMSMs technology and to opt out some limits in existing rare earth magnets based PMSMs was proposed in [23]. In [23], the proposed machine has the rotor built as a sandwich of AlNiCo magnet, electrical steel and a non-magnetic material. The trapezoidal magnet design in the proposed machine forces some of the magnet flux near the shaft to circulate through the rotor and the magnetization current is large which demands a larger size inverter and the manufacturing is quite complex [24].

Another variable flux machine using AlNiCo magnets is proposed in [29–31] to get a torque density comparable to that of rare earth PMSMs. This design also reduces the inverter rating by decreasing the full magnetization current of the machine. The designed machine uses tangentially magnetized rectangular magnets to balance the magnetization throughout the magnet length. To change the air-gap flux, a pulse of d- axis current is applied. The prototyped rotor cross section of the variable flux machine and its pictorial view showing the dq axes flux paths are shown in figure 2.1. The proposed machine has inverse saliency

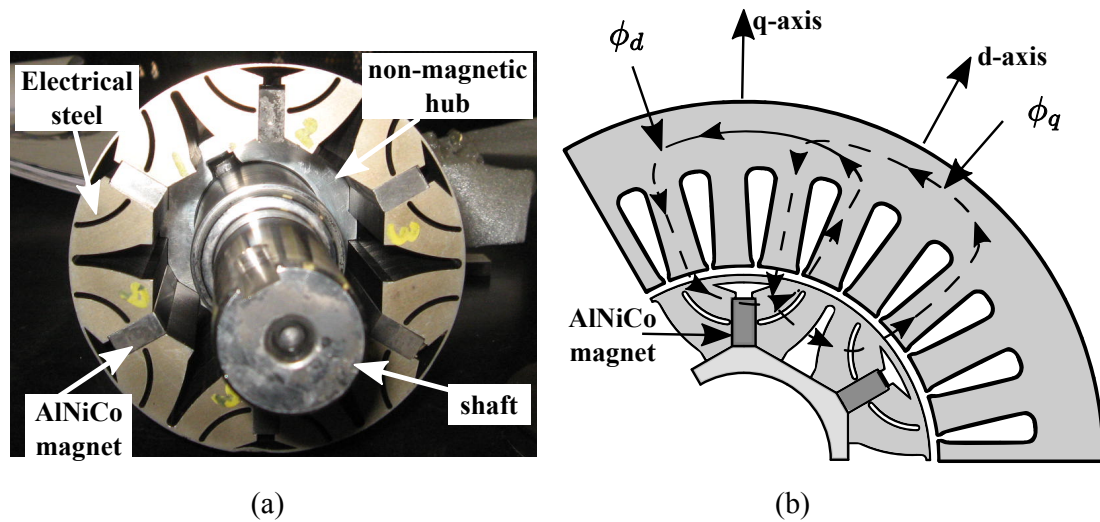


Figure 2.1: Variable flux machine using AlNiCo magnets (a) Prototyped VFM rotor construction (b) Pictorial view of the cross section of the prototyped VFM using AlNiCo magnets showing magnet locations and q- and d-axes flux paths.

( $L_d > L_q$ ) so that the machine can produce reluctance torque while applying a magnetizing current. The benefits of using AlNiCo magnets in VFMs can be listed as follows.

- Compared to rare earth magnets, AlNiCo magnets are less expensive and more readily available.
- The remnant flux density of AlNiCo magnets are comparable to rare earth magnets, i.e. high torque density comparable to rare earth PMSMs can be obtained.
- Lower coercivity of AlNiCo magnets require lower magnetizing and demagnetizing fields.
- The operating temperature of AlNiCo magnets is high compared to other permanent magnets.

The major challenges associated with variable flux machines are as follows.

- Overrating of the inverter to meet the magnetization current. The design challenge is to reduce the magnetization current close to the rated current.

- Torque ripple during magnetization and demagnetization process.
- Uncontrolled demagnetization of AlNiCo magnets by armature reactions due to low coercivity.

## 2.1 Characteristics of AlNiCo Magnets

A typical  $BH$  curve of a permanent magnet in second quadrant is shown in figure 2.2. The magnet operation is in the presence of external demagnetizing field  $H_a$ . In the figure,  $B_r$  is the full remnant flux density and  $H_c$  is the coercivity of the magnets. The operating point when no external field is applied is at point  $A$ ; the intersection of the air-gap line and the  $BH$  curve. When an external demagnetizing field ( $H_a$ ) is applied, the operating point moves towards the left of the operating point  $A$  along the  $BH$  curve. After the removal of the external field, the operating point returns to the original operating point  $A$ . If the external field is large enough to drive the operating point below the knee of the  $BH$  curve, there is some permanent loss in the remnant field and the magnet operating point recoils back along line  $BC$  parallel to the original demagnetization curve. The new operating point will be  $C$ , and the new remnant flux density will be  $B_r - \Delta B_i$  with a net loss of remnant flux density by  $\Delta B_i$ .

Once there is a permanent loss in magnet flux density, a magnetizing field large enough to drive the magnet to the saturation region in the first quadrant of the  $BH$  curve is required to re-magnetize the magnets. Figure 2.3 show the linearized  $BH$  loop in four quadrants.  $H_s$  is the required magnetizing field to fully magnetize the magnet. When the magnetizing field is removed, the magnet will recoil to the air-gap line along the demagnetization curve. If the demagnetizing field is  $H_d$ , the magnet will get completely demagnetized. As the coercivity of AlNiCo magnet is low, the  $BH$  curve for the AlNiCo magnets can be varied to control the air-gap flux density by applying an external field (magnetizing or demagnetizing).

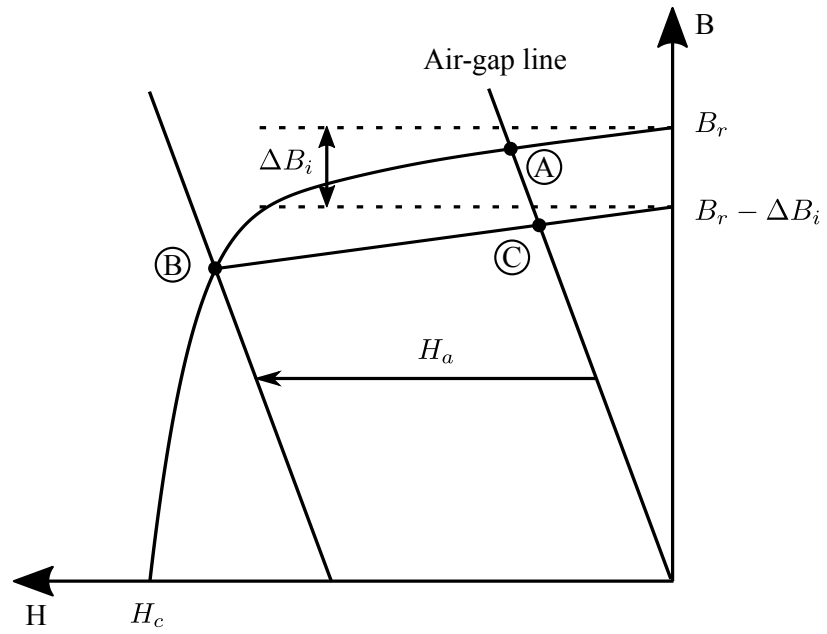


Figure 2.2: AlNiCo magnets operation under demagnetizing field

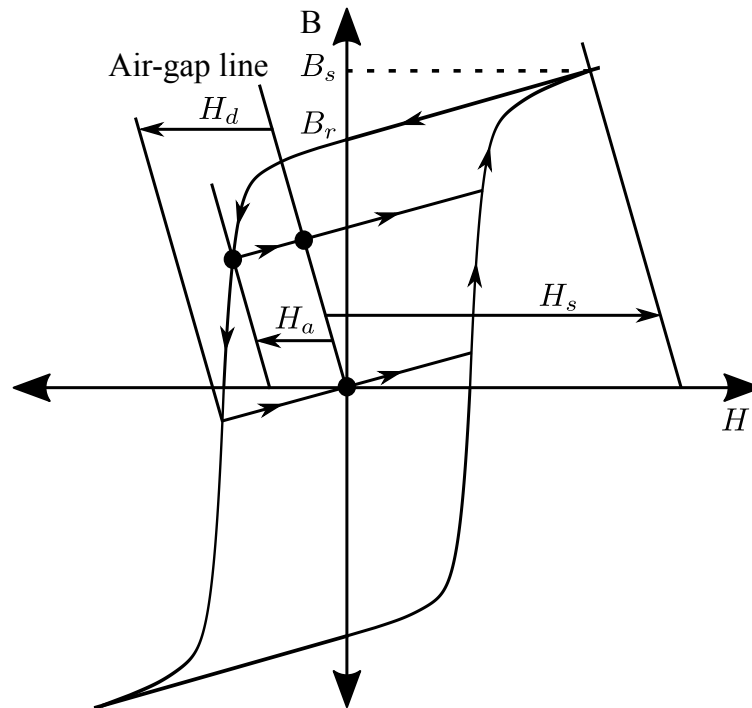


Figure 2.3: Linearized BH loop of AlNiCo magnets

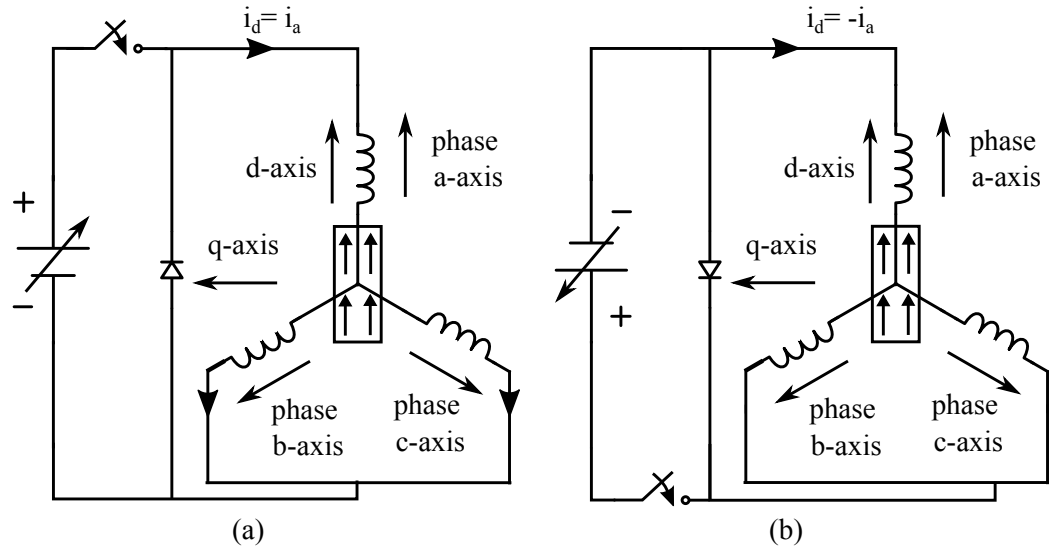


Figure 2.4: Circuit diagram showing machine terminal connections to measure (a) Magnetization characteristics (b) Demagnetization characteristics

Compared to rare earth magnets, the external field required to vary the operating point of AlNiCo magnet is very low.

## 2.2 Characteristics of a VFM

The difference between a regular PMSM and a VFM arises due to the controllability of the air-gap flux density in the latter. This is the most beneficial property of a VFM. To obtain advantages listed in section 1.3, accurate knowledge on the behavior of the machine under external excitation is important. When an external demagnetizing field drives the operating point below the knee in the  $BH$  curve of the magnet, there is a permanent loss in the magnet flux linkage. The measure of flux linkage of the VFM under demagnetizing current gives the demagnetization characteristics of the VFM. In a similar way, the measure of flux linkage of the VFM under magnetizing current gives the magnetization characteristics of the VFM.

### 2.2.1 Measurement of VFM Characteristics

The measurement of flux linkage of the VFM against the applied magnetizing and demagnetizing current gives the magnetization and demagnetization characteristics of the VFM respectively. The measurement of flux linkage of any permanent magnet machine can be done by running the machine as a generator using an external drive. The no-load back-EMF of the machine is measured at a certain speed. If the no-load line voltage at the terminals of the PM generator with  $P$  number of poles is  $V_{ll}$  when running at a speed of  $N$  rpm, the flux linkage is calculated using equation (2.1). The measurement is repeated for different speeds and an average is taken. This gives the measured flux linkage of the machine.

$$\lambda_f = \frac{\sqrt{2}V_{ll}}{2\pi\sqrt{3}\frac{P}{2}\frac{N}{60}} \quad (2.1)$$

The measurement technique of magnetization and demagnetization characteristics of a VFM is explained in [43]. To measure the magnetization characteristics of a VFM, the rotor direct axis is first aligned with phase-A axis. A variable voltage source is used to supply a positive d-axis current to a fully demagnetized machine. After each magnitude of d-axis current, the flux linkage of the machine is calculated using the measured speed and back-EMF data by driving the machine as a generator. The DC voltage is increased at each step to increase the d-axis current from the previous step. The connection diagram to supply the positive d-axis current is shown in figure 2.4 (a) and the measured magnetization curve of a prototyped VFM using AlNiCo magnets is shown in figure 2.5. From the magnetization curve it is seen that for the prototyped machine, the magnet flux is a non-linear function of the d-axis current. In similar way, to measure the demagnetization characteristics, a negative DC current is supplied to phase A winding of a fully magnetized machine while the machine is aligned with the phase A axis. The connection diagram is shown in figure 2.4

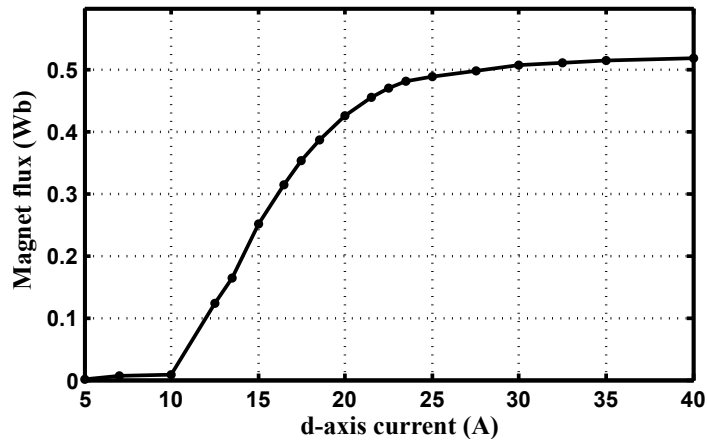


Figure 2.5: Measured magnetization characteristics of a prototyped VFM using AlNiCo magnets

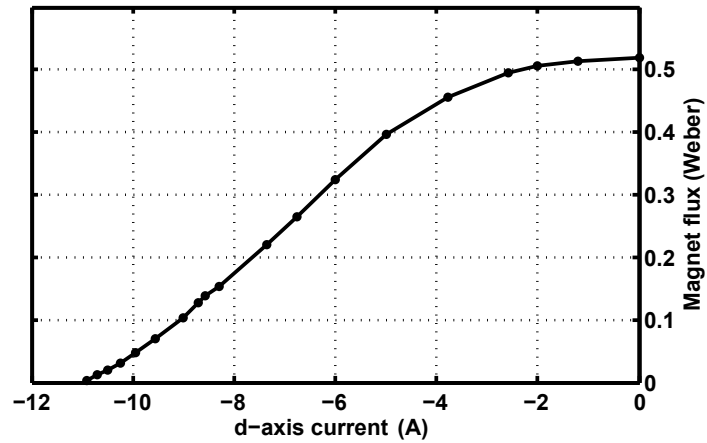


Figure 2.6: Measured demagnetization characteristics of a prototyped VFM using AlNiCo magnets

(b). The magnitude of the negative DC current is increased in each step and the magnet flux linkage is found via back-EMF and speed. Figure 2.6 shows the measured demagnetization characteristics of the same VFM which is a non-linear function of the d-axis current.

## 2.3 Modeling of a VFM

Variable flux machines can be mathematically modeled as a regular PMSM with some modifications. In PMSMs, the magnet flux is considered constant, while in VFMs, it is a non-linear function of d-axis current. Apart from the magnet flux being dependent on the present d-axis current, it also depends on the previous state of the magnet flux. As an example, if the magnet flux is already 100%, the magnet flux is not affected when any value of positive d-axis current is applied. Similarly, if the magnet flux is close to 0%, any negative d-axis current below the full demagnetization current will not affect the magnet flux. However, if the negative d-axis current is further increased, it will reverse the magnetization of the magnets. In other words, if the present magnetization state is known, the magnetization characteristics will be used if the d-axis current is positive. But, if the magnetization state corresponds to the supplied positive  $I_d$  is less than the present magnetization state, the current has no effect on the magnet flux linkage. Similarly, if the d-axis current is negative and the corresponding flux linkage in the demagnetization characteristics is higher than the present magnetization state, the current has no effect on the magnet flux.

### 2.3.1 Basic model of the VFM

Let  $v_a, v_b, v_c$  be the three phase stator voltages,  $i_a, i_b, i_c$  be the three phase stator currents. For field oriented control, the three phase quantities are transformed into synchronously rotating two phase quantities by using equations (1.1) and (1.2). The basic model of a VFM with constant magnet flux linkage, constant inductances and resistances are given by

equations (2.2) - (2.8).

$$v_d = R_s i_d + \frac{d\lambda_d}{dt} - \omega_r \lambda_q \quad (2.2)$$

$$v_q = R_s i_q + \frac{d\lambda_q}{dt} + \omega_r \lambda_d \quad (2.3)$$

$$\lambda_d = L_d i_d + \lambda_f \quad (2.4)$$

$$\lambda_q = L_q i_q \quad (2.5)$$

$$P_i = \frac{3}{2} [v_q i_q + v_d i_d] \quad (2.6)$$

$$T_e = \frac{3}{2} \frac{P}{2} [\lambda_f + (L_d - L_q) i_d] i_q \quad (2.7)$$

$$P_{em} = \frac{3}{2} \omega_r [\lambda_d i_q - \lambda_q i_d] \quad (2.8)$$

where,  $v_d$  and  $v_q$  are the d- and q- axes voltages,  $R_s$  is the stator resistance,  $i_d$  and  $i_q$  are d- and q-axes currents,  $\lambda_d$  and  $\lambda_q$  are d- and q- axes flux linkages,  $\lambda_f$  is the magnet flux linkage,  $\omega_r$  is the rotor electrical speed,  $L_d$  and  $L_q$  are d- and q- axes inductances,  $P_i$  is the input power,  $T_e$  is the developed electromagnetic torque and  $P_{em}$  is the developed electromagnetic power. The mathematical equations are represented in the form of an equivalent circuit to visualize in the circuit domain. The equivalent circuits for the basic  $dq$  model of a VFM are shown in figure 2.7. To account for the controllability of the magnet flux, the term  $\lambda_f$  in the equation 2.4 can be made a function of  $i_d$  and the previous value of  $\lambda_f$ .

For simulation and experimental work, the block diagram of a VFM considering the controllability of the magnet flux is shown in figure 2.8. In the block diagram, a memory block is used to memorize the magnet flux so that the new magnet flux is a function of the previous state of the magnet and the present d-axis current. Here,  $\tau_d$  and  $\tau_q$  are the d- and q-axes stator time constants respectively.

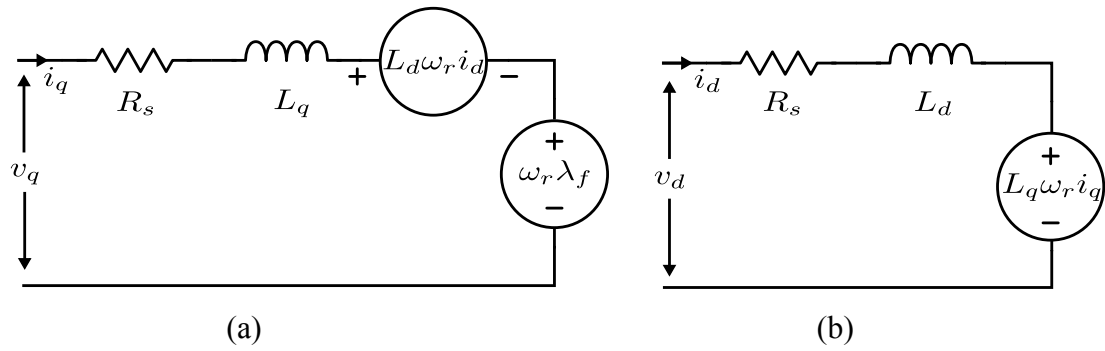


Figure 2.7: Dynamic equivalent circuits of PMSM neglecting core losses. (a) Stator q-axis dynamic circuit. (b) Stator d-axis dynamic circuit.

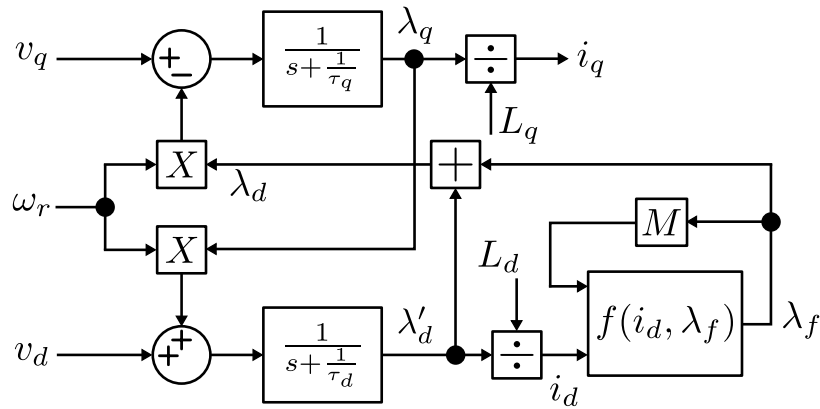


Figure 2.8: Block diagram of the variable flux machine using the basic model

### 2.3.2 VFM Drive

The purpose of an electric drive is to control the electric machine to meet both static and dynamic loads. A power electronic converter with an advanced modulation scheme is used to control the machine. The circuit diagram of a variable flux machine drive using a two level voltage source inverter used in this thesis is shown in figure 2.9. The drive consists of a three phase voltage source, a three phase rectifier, filter capacitor, three phase inverter, current and voltage sensors, a controller and a VFM with an encoder assembly. In this thesis, a space vector pulse width modulation (SVPWM) technique is employed for vector control of the VFM. Two out of the three phase currents are measured using sensors. The absolute

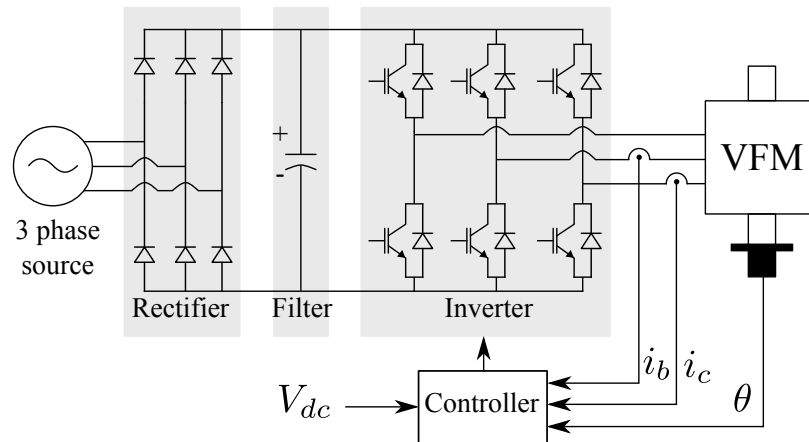


Figure 2.9: Circuit diagram of a vector controlled variable flux machine drive

encoder provides rotor position information. The controller converts the 3 phase quantities to dq quantities using dq transformation equations. Based on the commanded speed and the actual speed, the controller regulates the stator currents in the dq domain by supplying gating signals to the inverter using the SVPWM technique.

### 2.3.3 Experimental Tests

The variable flux machine drive experimental setup is shown in figure 2.10. The setup consists of a two level voltage source inverter, voltage and current sensors, a data acquisition system, controller (Opal-RT Wanda 4U real time simulator), dynamometer as load and prototyped variable flux machine with an encoder assembly. The schematic diagram of vector control technique for the VFM is shown in figure 2.11.

The vector control operation is constrained by the current limit and the voltage limit from the inverter. The speed controlled drive operates based on the feedback of the actual speed to find the error from the reference speed. The speed error is fed to a *PI* controller which generates the required torque producing current reference. To limit the instantaneous as well as the continuous stator current to the rated current, Block I is used to limit the torque producing reference current to the current controller. For normal operation below base

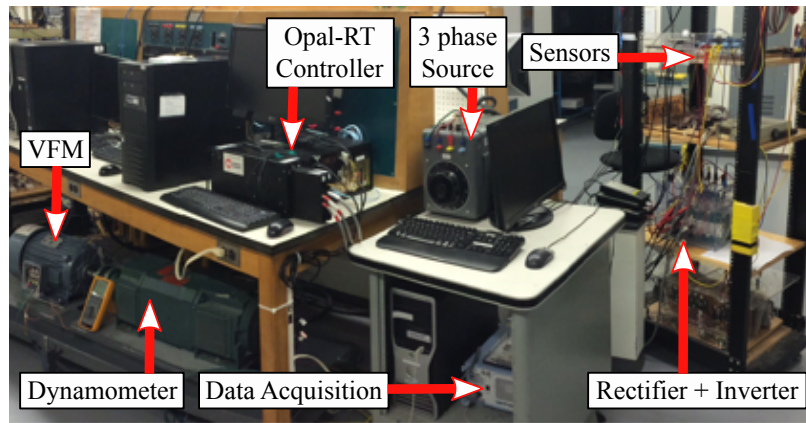


Figure 2.10: Experimental setup for the variable flux machine drive

speed, the reference d-axis current is controlled to maintain a zero value. In case of a speed reference higher than the base speed, Block II generates the reference field weakening current which is controlled by the d-axis current controller. The output of the current regulators are the reference dq voltages which are converted to the reference three phase voltages using  $dq$  to  $abc$  transformation. The SVPWM block generates the gating signal for the inverter to generate the reference phase voltages using space vector pulse width modulation technique. The phase currents are measured and fed back to the current regulators. Block III generates the reference demagnetizing current based on the measured speed and the off-line table containing speed and demagnetizing current requirements.

Block IV is the heart of the controller as it is unique to the variable flux PM machines. Based on the d-axis current, first it keeps track of the magnet flux, and secondly, it limits the field weakening current. The reason for the limit is that a fully magnetized machine will get demagnetized if field weakening current is applied. For other magnetization levels, there is a limit in the d-axis current which can be used to weaken the field without demagnetizing the magnets.

The experimental result of on-line magnetization and demagnetization of the VFM under test, is shown in figure 2.12. Figure 2.12(a) shows the field weakening operation



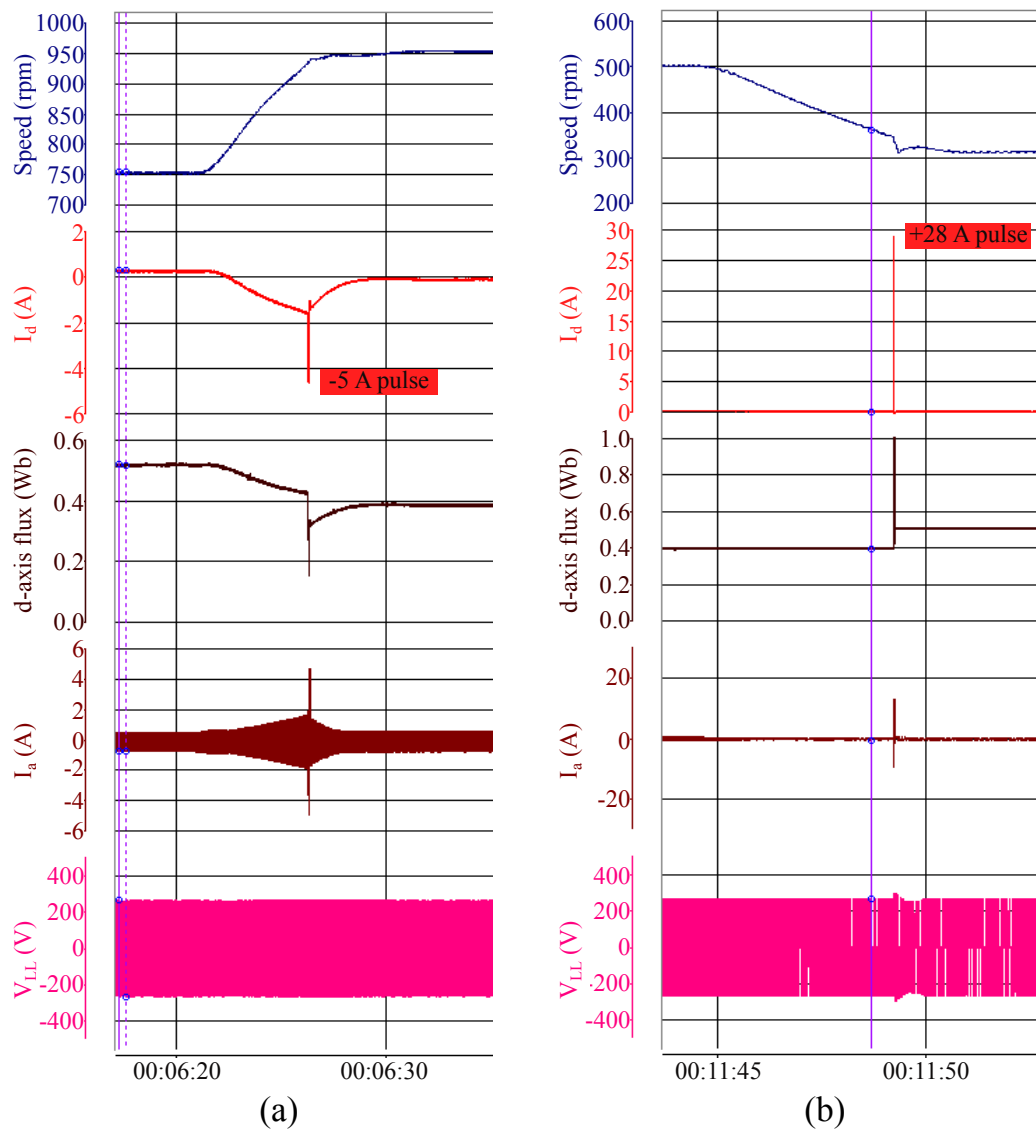


Figure 2.12: Experimental result in a VFM drive (a) Effect of demagnetizing current on the stator current and d-axis flux for operating speed over the base speed (b) Effects of magnetization current on stator current and d-axis flux for speed under the base speed.

## 2.4 Review on VFM Parameter Measurement

Machine parameters are of extreme importance for the design and operation of high performance drives. The basic electrical parameters of a VFM are the resistance, the inductances and the magnet flux. The mechanical parameters are the friction coefficient and the moment of inertia. The electrical parameters are used in the inner current control loop

and the mechanical parameters are used in the outer speed control loop in vector control. The methods to measure the electrical resistance and the magnet flux are covered in section 1.2.2. The inductance measurement method are considered in the next section.

### **2.4.1 Inductance Measurement**

The current dynamics of any machine depends on its inductance and resistance parameters. Accurate estimates of the inductances allows the design of high performance drives. For the VFM, the accuracy requirement is higher as the control strategy is to adjust the magnet flux that depends on the d-axis current. The magnet flux is adjusted by applying a short duration direct axis current pulse. whose duration affects the torque ripple [44]. During the demagnetizing/magnetizing current pulse period, if there is any overshoot/undershoot in the d-axis current, the magnet flux attained will be different from the desired one. So the controller must achieve the reference current level without any overshoot within the short period of time.

To reduce the magnetization and demagnetization current, the VFMs are designed to have a small air-gap. In such a case, the inductances also depends on the magnitude of current as well as the magnetization level of the magnets. The method to determine the inductances should be able to measure the inductances at different magnetization levels under various current magnitudes.

#### **DC Standstill Test**

In the DC standstill test, a VFM is exposed to a step DC voltage and the transient response of the machine is measured. Considering the first order response, the inductance is found from the time constant, which is the time required to rise the current from zero to 63.2% of the final steady state response. For the d-axis inductance measurement, the rotor is locked at the stator d-axis and a step voltage is applied to get the desired steady state DC current.

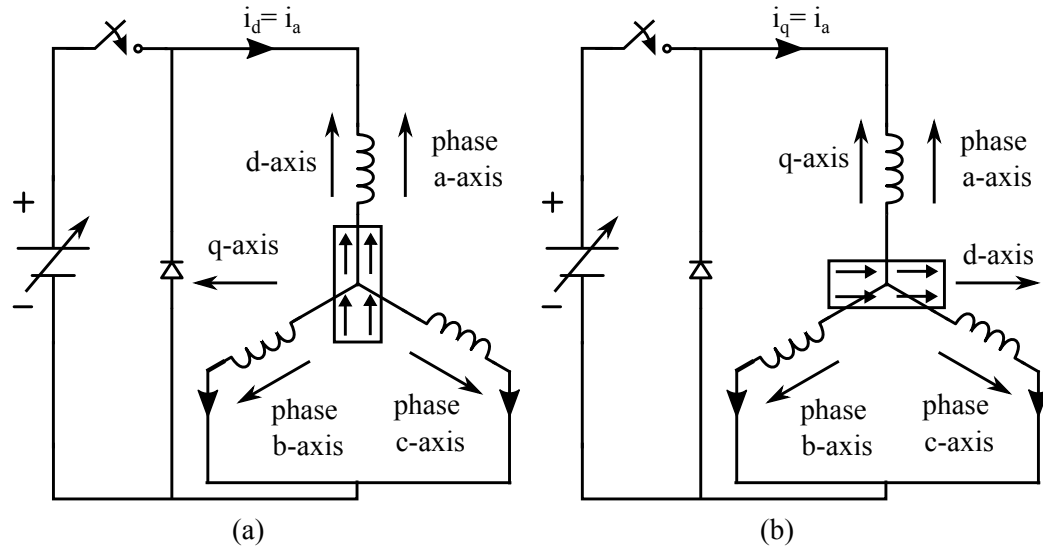


Figure 2.13: Circuit diagram showing machine terminal connections to measure (a) d-axis inductances (b) q-axis inductances, using DC standstill test method

The magnitude of the step voltage is changed to measure the inductance at different current levels. For the q-axis inductance measurement, the rotor is locked at the stator q-axis and a similar procedure for d-axis inductance measurement method is employed. Figure 2.13 shows the connection diagram to measure the inductances using the DC standstill test.

### AC Standstill Test

In the AC standstill test, an AC voltage source replaces the DC source and the freewheeling diode in figure 2.13. An AC voltage at a certain frequency (usually line frequency) is applied to get the desired peak current. The rms value of the applied voltage, the rms current and the consumed reactive powers are recorded. The reactance and then the respective inductance is calculated based on these measured quantities using equations 2.9 and 2.10.

$$X_L = \frac{Q}{I^2} \quad (2.9)$$

$$L = \frac{2}{3} \frac{X_L}{2\pi f} \quad (2.10)$$

where,  $Q$  is the measured reactive power,  $V$  is the rms voltage,  $I$  is the rms current,  $f$  is the applied AC frequency,  $X_L$  is the reactance and  $L$  is the inductance. When the rotor is locked to the direct axis, the measured inductance is d-axis inductance and the measured inductance is q-axis inductance when the rotor is locked to the quadrature axis. To find the inductances at different current, the magnitude of the AC voltage is changed.

A variant in the AC standstill test excites one phase with AC voltage and measure the induced voltage in other phases to find the self and mutual inductances as a function of rotor position. The  $dq$  inductances are then calculated based on equations 2.11 and 2.12.

$$L_d = (L_0 - M_0) - (L_1/2 + M_1) + L_{lk} \quad (2.11)$$

$$L_q = (L_0 - M_0) + (L_1/2 + M_1) + L_{lk} \quad (2.12)$$

where,  $L_0$  and  $M_0$  are the constant parts of the self and mutual inductances respectively,  $L_1$  and  $M_1$  are the peak values of the sinusoidal part of the self and mutual inductances and  $L_{lk}$  is the leakage inductance.

### **Inverter based Method**

This method uses a voltage source inverter to run the machine at certain speed. The currents and the PWM voltages are then measured using a low pass filter, or the fundamental is extracted from the FFT of the PWM voltage waveform. The steady state equations (2.13) and (2.14) of the VFM are used to find the  $dq$  inductances. In most cases the voltage drop in the switches are neglected and the measurement of the switching voltage is avoided by considering the reference  $dq$  voltage to the inverter as the actual  $dq$  voltages. When accuracy is needed without the measurement of the actual switching voltages, the switch drops are

considered and canceled from the reference by analyzing the power operation stage.

$$v_d = R_s i_d - \omega_r \lambda_q \quad (2.13)$$

$$v_q = R_s i_q + \omega_r \lambda_d \quad (2.14)$$

### Flux linkage Calculation Method

In this method, a current dependent flux linkage is calculated based on the applied pulsed voltage. The circuit connection diagram is the same as in figure 2.13. When the rotor is locked, the dynamic equations (2.2)-(2.5) for a VFM can be modified to find the flux linkages as defined by equations (2.15) and (2.16). The dq inductance can then be found using equations (2.17)-(2.18). To measure the d-axis inductance, the rotor is locked at the d-axis and a pulsed voltage is applied. The transient response to the pulsed voltage is measured and recorded. By using numerical integration, the d-axis inductance is calculated. Similarly, for the measurement of the q-axis inductance, the rotor is locked at the q-axis and the transient response to a pulsed q-axis voltage is recorded. For the measurement of the inductances at different current magnitude, the magnitude of the pulsed voltage is changed. In this way, the current dependent inductances for a full range of operating current is evaluated.

$$\lambda'_d = \int_0^t (v_d(\tau) - i_d(\tau)R_s) d\tau \quad (2.15)$$

$$\lambda'_q = \int_0^t (v_q(\tau) - i_q(\tau)R_s) d\tau \quad (2.16)$$

$$L_d = \frac{\lambda'_d}{i_d} \quad (2.17)$$

$$L_q = \frac{\lambda'_q}{i_q} \quad (2.18)$$

## 2.5 Inductance Measurement Method for the VFM

The flux in a variable flux machine is controlled by applying the d-axis current. The reduction of the inverter ratings requires that the magnetization current be as low as possible. The magnetization current is lowered during the design process by lowering the air-gap thickness. When the air-gap is reduced, the saturation of the steel shows its effects in the machine inductances. Thus, the assumption of constant inductances in a variable flux machine will be wrong. Therefore, current dependent inductances are required for high performance drive applications. Moreover, as the magnet flux is varied by the stator current, the inductances also changes. Hence, the inductances become a function of current and the magnetization level of the magnets. An appropriate inductance measurement technique should be able to measure the current and flux dependent inductances quickly and accurately.

### 2.5.1 Discussion on General Methods of Inductance Measurement

The DC standstill test uses the time constant to evaluate the inductance. Its accuracy is low and, requires frequent changes in the setup to measure the current dependent  $dq$  inductances at different magnetization levels.

The AC standstill test performed using a single phase coil requires considerable amount of measurements for a set of  $dq$  inductances, at one current value. While the measurement technique using three phase connection, and calculation of inductance from power measurement is simple and quick, the method can only measure the  $q$  axis inductance. It is not suitable in the measurement of the  $d$  – axis inductance, as the negative cycle of the AC current demagnetizes the magnets in variable flux machines.

The inverter based method is convenient as it uses the existing drive and no further equipments are required. However, this method requires the loading of the machine to find the current dependent inductances.

The flux linkage calculation method using a DC source gives an accurate measure of

the inductances. However, the measurement of current dependent inductances at different magnetization states requires changes to the setup.

## **2.5.2 The Proposed Method**

The proposed method to measure inductances of VFMs uses a vector controlled drive to supply a pulsed voltage in the locked rotor condition. The inductances are evaluated based on the calculated flux linkages by numerical integration on the measured voltages and currents. The main advantage of a vector controlled drive is that the measurement of both direct and quadrature axis inductances can be performed at any rotor position. This is in addition to the measurement of inductances at a given rotor position for any current and the magnetization level. The vector controlled drive allows arbitrary orientation of the excitation pulse with respect to the d- or q- axis. The measurement process is fast, since there is no need to change the rotor position.

The method uses the magnetization and demagnetization characteristics discussed in section 2.2.1. The rotor is locked at an arbitrary position. The magnet flux linkage is fixed by applying a pulse of d-axis current. The current dependent q-axis inductances are measured by applying a pulsed voltage in q-axis. After that, the current dependent d-axis inductances are measured. After a set of measurement, the magnetization level is changed by applying the d-axis current pulse. The measurement of inductances is repeated for that magnetization level. In this way, a vector controlled drive can be used to measure the current dependent inductances at various magnetization levels.

## **2.5.3 q-axis Inductance Measurement**

To measure the q-axis inductance, the rotor is locked at any arbitrary position and the q-axis voltage pulse is given as a reference while the d-axis current is controlled to zero. The pulse width of the voltage is chosen such that the transient currents in the q-axis settles

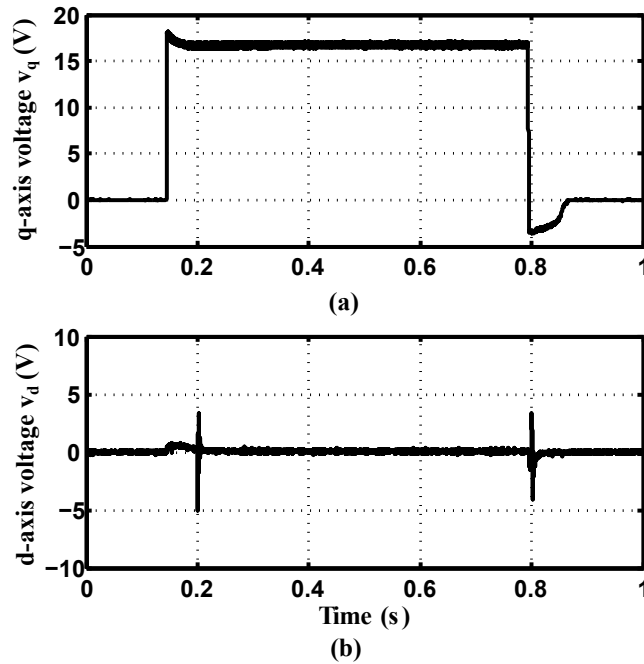


Figure 2.14: Measured voltages in d- and q-axis when  $i_d$  is maintained zero and a pulsed voltage  $v_q$  is applied (a)  $v_q$  (b)  $v_d$

down. A data acquisition system is used to record the q-axis voltage and the corresponding current response. Figure 2.14 shows the measured  $dq$  voltages and Figure 2.15 shows the measured  $dq$  currents for an arbitrary value of q-axis voltage reference. From the recorded data, equation (2.16) is used to calculate the q-axis flux linkage and equation (2.18) is used to find the q-axis inductance at a particular steady state q-axis current. Here, the stator resistance is calculated as the quotient of the average steady state voltage and the average steady state current. To find  $L_q$  at different current levels, the amplitude of  $v_q$  is changed in the reference. In this way, inductance,  $L_q$  at any current level can be calculated.

## 2.5.4 d-axis Inductance Measurement

For the measurement of the d-axis flux linkages and inductances at different current levels, the position of the rotor is kept intact while the control algorithm is modified to maintain the q-axis current to zero and supply pulsed voltage to the d-axis. A data acquisition system records

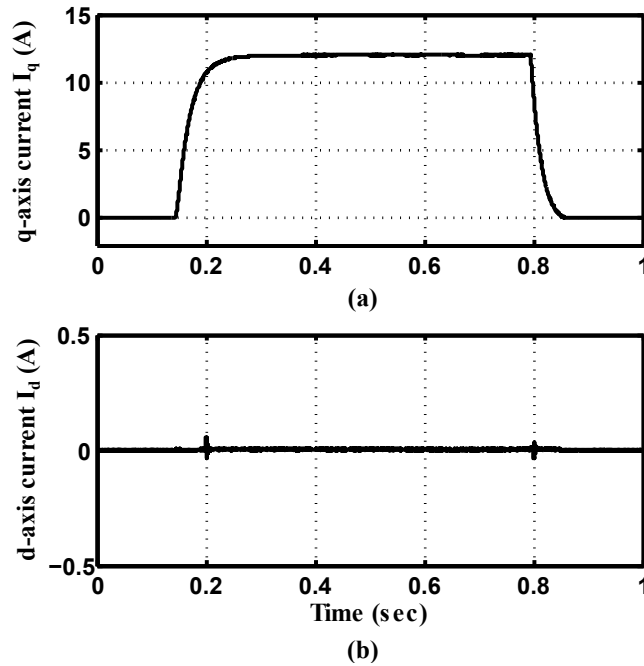


Figure 2.15: Measured currents in d- and q-axis when  $i_d$  is maintained zero and a pulsed voltage  $v_q$  is applied (a)  $i_q$  (b)  $i_d$

the d-axis voltage and the corresponding current response. Figure 2.16 shows the measured  $v_d$  and  $v_q$  and figure 2.17 shows the measured  $i_d$  and  $i_q$  for an arbitrary values of d-axis voltage reference. From the recorded data, equations (2.15) and (2.17) are used to calculate the d-axis flux linkage and inductance. Similar to the q-axis inductance measurement method, the stator resistance is calculated as the quotient of steady state  $v_d$  and  $i_d$ . For inductance at different  $i_d$ , the amplitude of  $v_d$  is changed in the reference.

### 2.5.5 Experimental Setup and Control Structure

The experimental setup for the measurement of  $dq$  inductances using a vector controlled drive is shown in figure 2.18. It consists of a voltage source inverter using IGBT switches (SKM50GB123D), hall effect current (LA 100-P) and voltage sensors (LV 20-P), controller (Opal-RT Wanda-4u system), data acquisition system (SL1000), dynamo-meter and VFM with an encoder assembly.

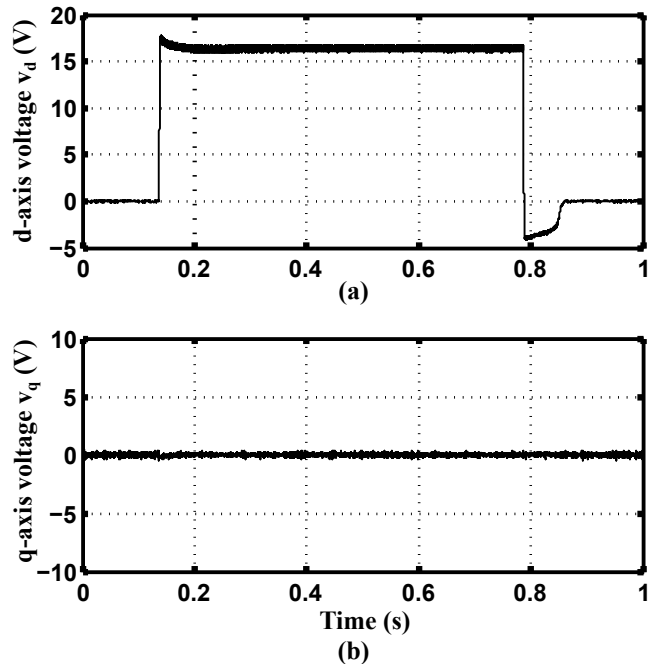


Figure 2.16: Measured voltage in d- and q-axis when  $i_q$  is maintained zero and a pulsed voltage  $v_d$  is applied (a)  $v_d$  (b)  $v_q$

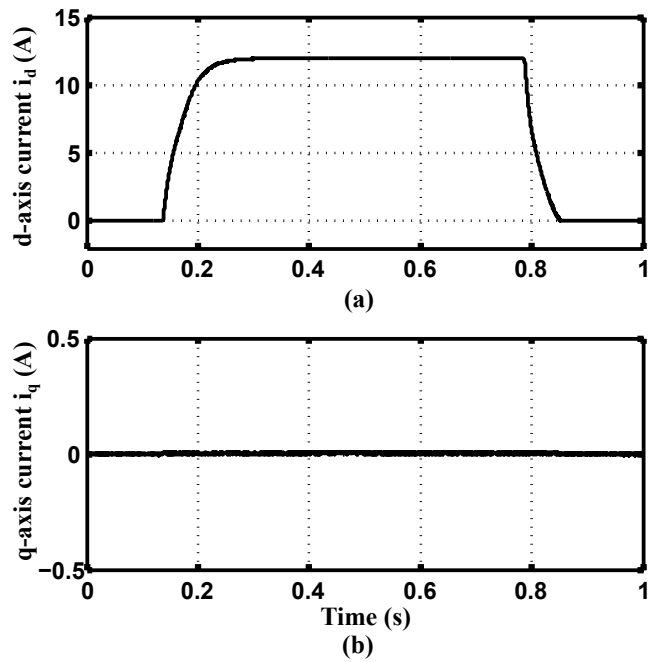


Figure 2.17: Measured currents in d- and q-axis when  $i_q$  is maintained zero and a pulsed voltage  $v_d$  is applied (a)  $i_d$  (b)  $i_q$

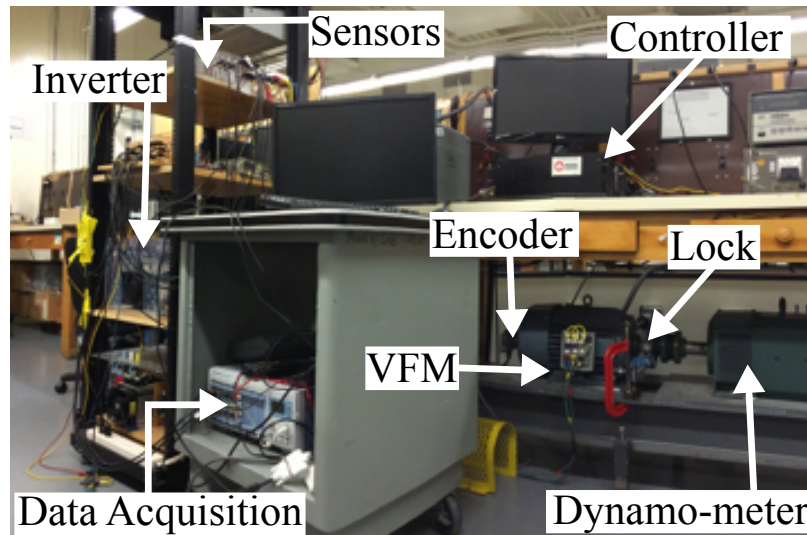


Figure 2.18: Experimental setup to measure inductances using vector controlled drive

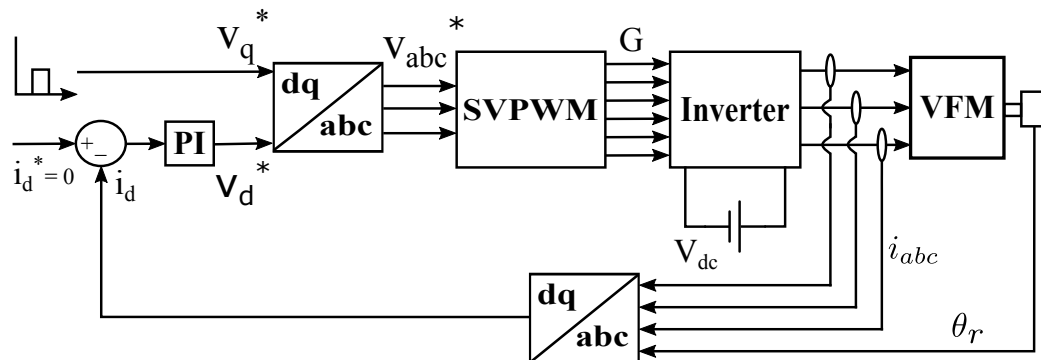


Figure 2.19: Schematic of vector control diagram

Figure 2.19 shows the vector control strategy to measure the q-axis inductance. The three phase currents are measured using current sensors and are transformed to  $dq$  currents using position information. The calculated  $i_d$  is compared with the reference (which is set to zero) and using a PI controller, reference  $v_d$  is generated. A pulsed voltage command is given as a reference for  $v_q$ . The gate signals are generated from the required phase voltages using a space vector pulse width modulation technique switching at 6 kHz. The data acquisition unit stores the response of the machine. To measure inductances at different magnetization levels, the reference voltage,  $v_q$  is set to zero and a required pulsed reference  $i_d$  from the magnetization and demagnetization characteristics is commanded to change the magnetization level. The

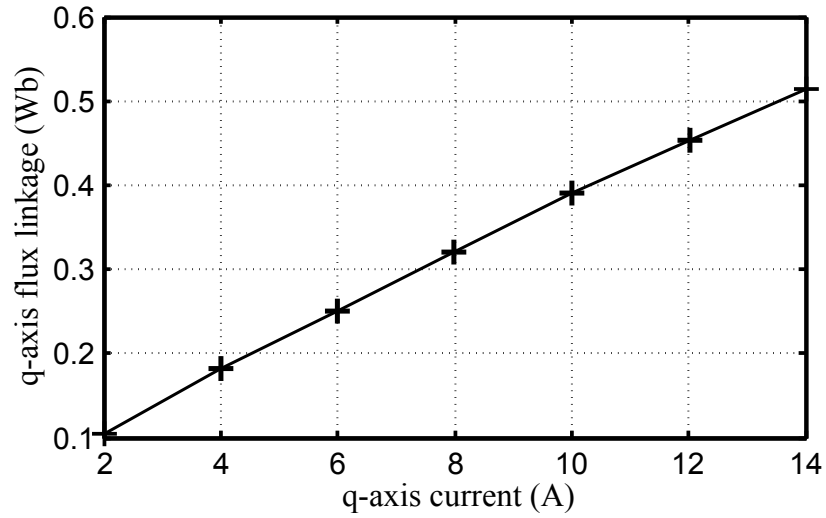


Figure 2.20: Measured q-axis flux linkage at different currents for fully magnetized machine

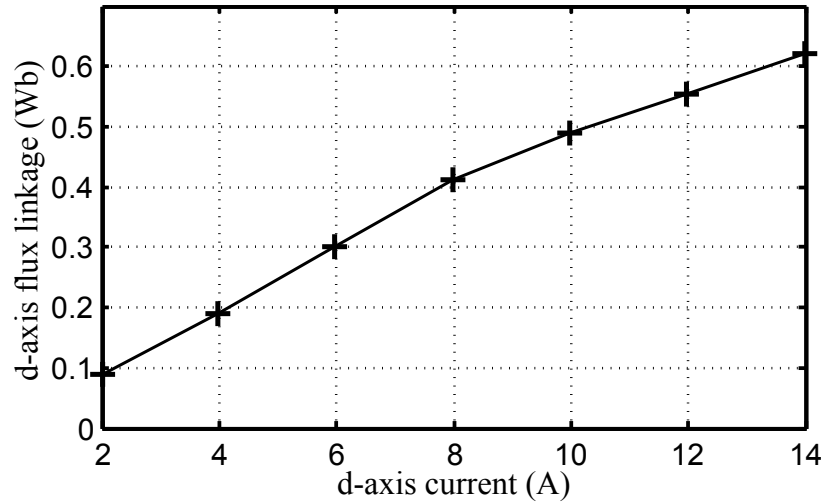


Figure 2.21: Measured d-axis flux linkage at different currents for fully magnetized machine

process is repeated to measure both the d- and q- axes inductances at the new magnetization level. This technique is versatile, as the excitation vector is controlled with respect to both the d- and q-axis, instead of manually changing the rotor position.

## 2.5.6 Results

Figures 2.20 and 2.21 show the measured flux linkages of a fully magnetized machine at different currents. The inductances calculated as the quotient of the flux linkages and the

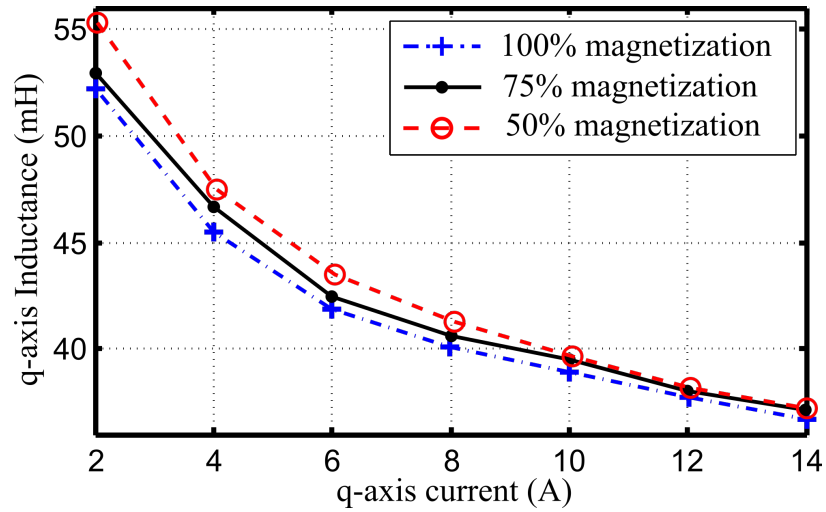


Figure 2.22: Measured q-axis inductances at different currents for three different magnetization states

currents are shown in figures 2.22 and 2.23. The plots show that both the inductances are non-linear functions of current. The figures also compares the inductances at three different magnetization states (100%, 75% and 50%). It is seen that  $L_q$  and  $L_d$  decreases with increase in the magnet flux at all current levels. While  $L_q$  seems to fall exponentially with increase in the current,  $i_q$  for all magnetization levels,  $L_d$  at first rises with increase in  $i_d$  up to some current and then drops with further increase. The plot of  $L_d$  verses  $i_d$  skew towards higher current with an increase in the magnet flux. The nature of the d-axis inductance variation with current can be explained by analyzing the magnetization property of the electrical steel. As shown in figure 1.7, the permeability of the electrical steel increases up to a certain flux density. With a further increase in the flux density, the permeability decreases. Since, the air-gap in the VFM is small, the effect of steel reluctance become significant. Thus, the inductance increases with current as the steel permeability increases and it decreases with a further increase in the current due to reduction in the steel permeability.

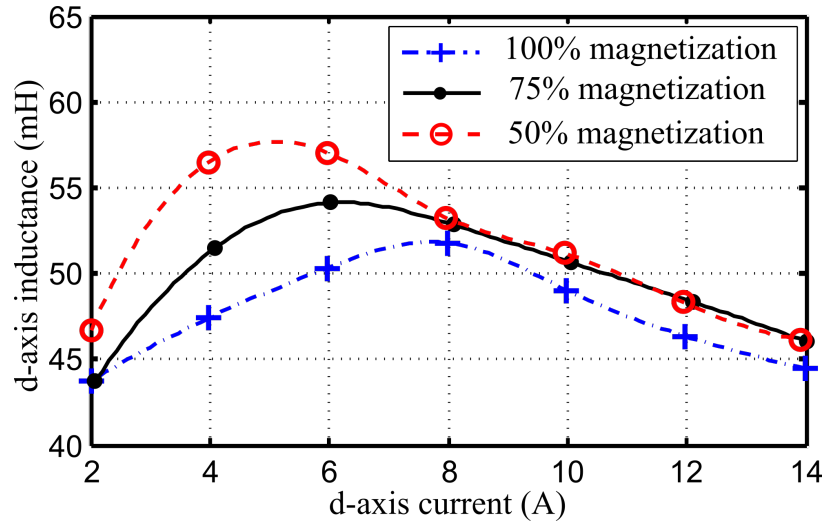


Figure 2.23: measured d-axis inductances at different currents for three different magnetization states

## 2.6 Comparison of Techniques

Figure 2.24 shows the comparison of the q-axis inductances measured using the vector controlled technique with the inductances measured using flux linkage method and the inductances from the MotorSolve finite element method (FEM) simulation. Similarly, figure 2.25 shows the comparison of the d-axis inductances for the fully magnetized machine from the vector controlled technique, flux linkage method and MotorSolve simulation. The results shows a good agreement between the two measurement methods. Further, the FEA simulation result is in good agreement with the measured inductances except some deviations at low current levels.

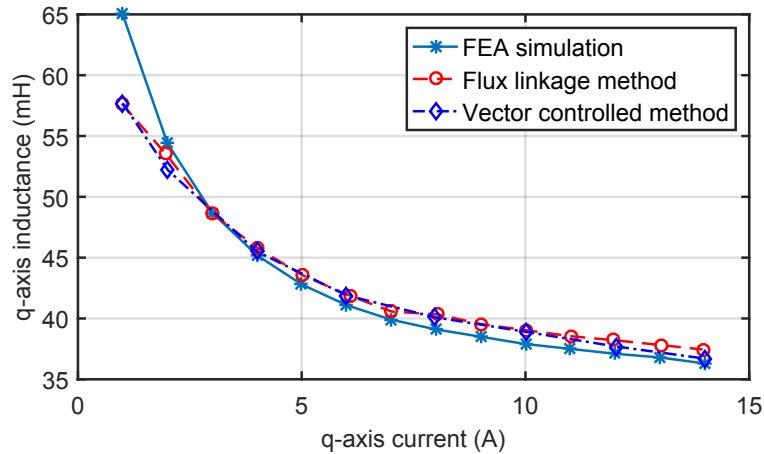


Figure 2.24: Comparison of q-axis inductances measured using vector control drive with flux linkage method and FEA simulation.

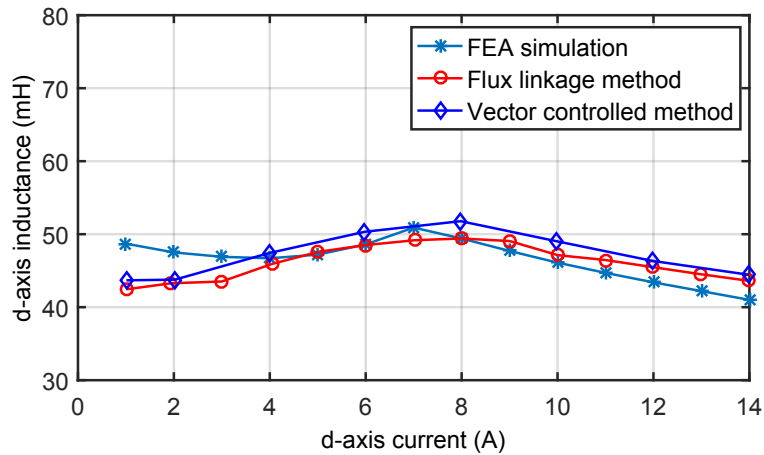


Figure 2.25: Comparison of d-axis inductances measured using vector control drive with flux linkage method and FEA simulation.

## 2.7 Summary

In this chapter, the fundamentals of AlNiCo based VFMs were discussed. The benefits of AlNiCo magnets over other magnets were reviewed and challenges listed. The characteristics of AlNiCo based VFMs were discussed and evaluated experimentally. The basic model of PMSM was modified to adapt for the flux controllability of VFM. The model was used in experiment to demonstrate the flux control. Different existing parameter measurement methods were reviewed and a vector controlled drive based inductance measurement method

was proposed for fast and convenient inductance measurement. The proposed method was utilized to measure the inductances at various magnetization levels. A good agreement in results between the inductances from the proposed method and the flux linkage calculation method was found. There was a slight deviation in inductance values measured using the vector control technique and the finite element method at low currents.

## Chapter 3

# Cross Magnetization Effects in VFMs

The cross-magnetization or cross-saturation in electrical machines is a phenomenon in which the magnetic flux produced by one coil is affected by the currents in perpendicular coils sharing the common magnetic path. It is similar to armature reaction in a DC machine [45] and it can also exist if the magnetomotive force (MMF) distributions are assumed to be sinusoidal [42]. The cross-magnetization effects arise due to the non-linear magnetization characteristics of the electrical steel. For a magnetic circuit with two or more sources of excitations, the saturation effect causes the flux produced by one source to change when the excitations in another source is changed.

The concept of cross-magnetization studies for the AC electrical machines goes back to the early 80's. A detailed analysis of the phenomenon for smooth air-gap electrical machines is done in [42] which identifies two static and two dynamic inductances. The cross-coupling effect disappears not only when a single coil is excited, but also under linear magnetic circuit conditions [42]. Therefore, the sole cause of cross-magnetization effect is due to the magnetic non-linearity or the saturation effect.

### 3.1 Cross-Magnetization in PM Machines

Three phase PM machines are the most common in high performance applications. The analysis and control of PM machines are done using field oriented control ( $dq$  model). In the  $dq$  model, the flux linkages in the  $dq$  domain are considered to be dependent only on the current in their respective axis. This assumption is true for surface mounted PM machines with large air-gaps. However, the high torque and power density interior PMSMs have very small air-gaps. Due to this reason, the non-linear characteristics of the steel causes the cross-magnetization effects. The cross-magnetization effects causes a variation in the direct and the quadrature inductances by introducing cross-coupling inductances. Therefore, the uncoupled  $dq$  model with constant parameters is not suitable to represent accurately the performance of an electrical machine predisposed to cross-saturation.

The inductances play a significant role in the controller and estimator design. For PMSMs, the inclusion of cross-magnetization is necessary for performance prediction improvement. In addition, the direct and quadrature axes inductances determine a part of the torque; the reluctance torque and hence the required terminal voltage. Thus consideration of cross-magnetization offers more accurate torque calculations [46, 47]. Apart from that, PMSM drives using magnetic saturation based sensorless control to eliminate the use of the position sensor is significantly influenced by the cross-saturation effect in the rotor position estimation [48, 49]. Thus cross-magnetization is an important phenomenon to be considered in permanent magnet machines.

Generally, the cross-magnetization effects are integrated in the mathematical model based on an off-line calculation using finite element methods [50, 51]. In this method, the direct and quadrature flux linkages are determined as a function of the direct and quadrature axis currents by an offline FEM. For steady state torque analysis, the torque is decomposed into four components, viz. the main magnet torque, main reluctance torque, cross-magnet torque and the cross-reluctance torque [52, 53]. Each torque component is determined using

the inductances from FEM calculations. Analytic calculations methods can also be combined with FEM results or measurement results [54].

## 3.2 Cross-Magnetization in VFMs

Variable flux machines are designed such that the magnet flux can be controlled using the stator current. To reduce the magnetizing current and considering the manufacturing feasibility, the air gap length of the VFM has to be minimized [31, 55]. Due to the small air-gap, the saturation of the steel contributes significantly to the reluctance of the magnetic circuit during loading. Firstly, as in interior PMSMs, due to the common magnetic path between the d-axis current and the q-axis current, the dq axes inductances vary depending on the dq axes currents. Additionally, the saturation level of the machine is also changed as the magnetization level is varied and it also affects the dq inductances. Thus, unlike conventional PMSMs, the VFMs have one more parameter to be considered, as their dq inductances are functions of the dq currents and the magnetization level.

## 3.3 VFM Model including Cross-Magnetization

When cross-magnetization effects are negligible, the magnetic flux linkages in the q-axis is dependent only on the q-axis current and the magnetic flux linkage in the d-axis is dependent only on the d-axis current and the magnet flux. When cross-magnetization is significant, both the d-axis and q-axis flux linkages depend on both the  $dq$  currents and the magnet flux linkage.

The dynamic equations including cross-magnetization with the flux linkages as the variable are given by equations (3.1) and (3.2), where  $v_d$  and  $v_q$  are the  $dq$  voltages,  $R_s$  is

the stator resistance and  $\omega_r$  is the rotor electrical speed.

$$v_d = R_s i_d + \frac{d\lambda_d}{dt} - \omega_r \lambda_q \quad (3.1)$$

$$v_q = R_s i_q + \frac{d\lambda_q}{dt} + \omega_r \lambda_d \quad (3.2)$$

For linear assumptions the d-axis flux linkage,  $\lambda_d$  is only dependent on the d-axis current  $i_d$  and the magnet flux  $\lambda_f$ . Similarly, the q-axis flux linkage  $\lambda_q$  is dependent on the q-axis current  $i_q$  only. Due to the cross-magnetization effects, the  $dq$  flux linkages depend on both the  $dq$  currents and the magnet flux linkage. For such case the  $dq$  flux linkages can be decomposed as given by equations (3.3) and (3.4).

$$\lambda_d(i_d, i_q, \lambda_f) = \lambda_{dd}(i_d, \lambda_f) + \lambda_{dq}(i_d, i_q, \lambda_f) + \lambda_f(i_d, i_q) \quad (3.3)$$

$$\lambda_q(i_d, i_q, \lambda_f) = \lambda_{qd}(i_d, i_q, \lambda_f) + \lambda_{qq}(i_q, \lambda_f) \quad (3.4)$$

where  $\lambda_{dd}$  and  $\lambda_{qq}$  are the  $dq$  self flux linkages,  $\lambda_{dq}$  is the d-axis cross-coupling flux linkage,  $\lambda_{qd}$  is the q-axis cross-coupling flux linkage and  $\lambda_f$  is the magnet flux linkage. As inductance values are more meaningful in terms of circuit analysis and controller design, it is common to express the flux linkages in inductances terms. The  $dq$  axes flux linkages can be expressed as a function of several inductances as given in equations (3.5) and (3.6).

$$\lambda_d(i_d, i_q, \lambda_f) = L_{dd}(i_d, \lambda_f)i_d + L_{dq}(i_d, i_q, \lambda_f)i_q + \lambda_f(i_d, i_q) \quad (3.5)$$

$$\lambda_q(i_d, i_q, \lambda_f) = L_{qd}(i_d, i_q, \lambda_f)i_d + L_{qq}(i_q, \lambda_f)i_q \quad (3.6)$$

where  $L_{dd}$  and  $L_{qq}$  are the direct and the quadrature axis self inductances,  $L_{dq}$  and  $L_{qd}$  are the direct and quadrature axis cross-coupling inductances. For the VFMs, self and cross-coupling inductances depend on the magnet flux  $\lambda_f$  and currents  $i_d$  and  $i_q$ .

### 3.3.1 Apparent and Incremental Inductances

Based on the analysis requirement, as suggested in [42, 56], two types of inductance exists. The first one is the incremental inductances which affects the dynamic behavior and the other is the apparent inductances which gives the steady state characteristics. Both the inductances are the same for the unsaturated machine. For a saturated machine, the two are not same. Figure 3.1 illustrates the theoretical flux linkage vs current characteristics of a saturated machine. At a specific operating point,  $(i_0, \lambda_0)$ , the apparent inductance is defined as the ratio of the flux linkage  $\lambda_0$  and the corresponding current  $i_0$  while the incremental inductance is defined as the ratio of the differential variation in the flux linkage,  $\partial\lambda$  to the differential variation in current,  $\partial i$  around the operating point [56]. Based on the definition, the apparent and incremental inductances of the VFM can be defined by the following equations.

$$L_{dd(app)} = \frac{\lambda_{dd}}{i_d} \qquad L_{dq(app)} = \frac{\lambda_{dq}}{i_q} \qquad (3.7)$$

$$L_{qq(app)} = \frac{\lambda_{qq}}{i_q} \qquad L_{qd(app)} = \frac{\lambda_{qd}}{i_d} \qquad (3.8)$$

$$L_{dd(inc)} = \frac{\partial\lambda_{dd}}{\partial i_d} \qquad L_{dq(inc)} = \frac{\partial\lambda_{dq}}{\partial i_q} \qquad (3.9)$$

$$L_{qq(inc)} = \frac{\partial\lambda_{qq}}{\partial i_q} \qquad L_{qd(inc)} = \frac{\partial\lambda_{qd}}{\partial i_d} \qquad (3.10)$$

### 3.3.2 Cross-Coupling Inductance Evaluation

The measurement of cross-coupling inductances is not as simple as the measurement of self inductances. The AC standstill test can be modified to find the cross-coupling inductances. But it requires the change in the rotor position and the application of the AC voltage at standstill, which should be converted to dq voltages and currents. Since, the

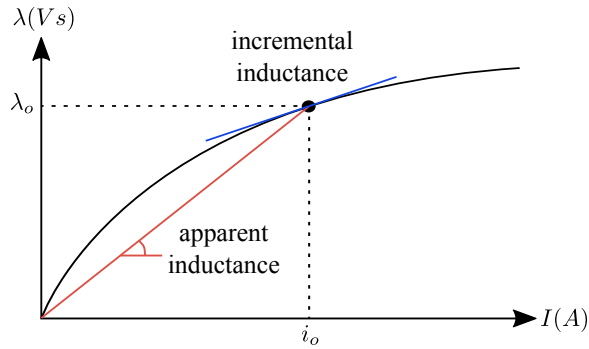


Figure 3.1: Theoretical flux linkage vs current characteristics of a saturated machine.

measured quantities are abc quantities, the choice of the required dq values requires several calculations and the accuracy requirements in rotor-position measurement is high. Moreover, the method requires instantaneous data measurement compared to the conventional AC standstill tests, which only requires rms values. Apart from that, the AC current in the d-axis is prone to change the magnetization state making the method not applicable to variable flux machines.

The flux linkage calculation methods for PMSMs explained in [56–58] can be used for VFMs with some modifications. In [57], a square wave voltage with both positive and negative cycles is used to measure the transient response of the machine at the locked rotor condition. However, for VFMs, any negative voltage (and thus current) in the d-axis at locked rotor condition should be avoided to prevent demagnetization of the magnets.

For the self and cross-coupling inductances defined by equations (3.7) - (3.10), the respective flux linkages should be known. The current dependent flux-linkages can be evaluated by applying a pulsed voltage in any axis keeping the current in the other axis constant. For example, to evaluate the q-axis current dependent flux-linkage from the test, the VFM is supplied by a VSI at locked-rotor position and the d-axis current is kept constant while a pulsed voltage is applied in the q-axis. The dynamic equations for a VFM given by

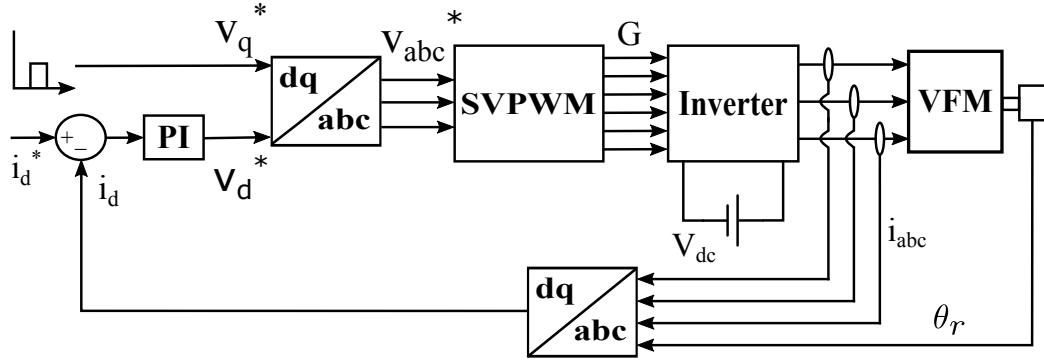


Figure 3.2: Schematic of vector control diagram

equations (3.1) and (3.2) for the locked rotor condition can be written as follows.

$$\lambda'_d = \int_0^t [v_d(\tau) - i_d(\tau)R_s] d\tau \quad (3.11)$$

$$\lambda'_q = \int_0^t [v_q(\tau) - i_q(\tau)R_s] d\tau \quad (3.12)$$

### 3.3.3 Experimental Tests

The experimental setup for the measurement of current dependent  $dq$  flux linkages due to the stator excitations is shown in chapter 2 (figure 2.10). It consists of a test VFM with encoder assembly, voltage source inverter using IGBT switches (SKM50GB123D), controller (wanda-4U), hall effect current (LA 100-P) and voltage sensors (LV 20-P), data acquisition system (SL1000) and dynamo-meter. An existing vector control drive is used to measure the current dependent flux linkages requiring no extra equipments.

Fig. 3.2 shows the vector control strategy to supply a pulsed  $v_q$  while controlling  $i_d$  to a constant value. The gate signals are generated from the required phase voltages using space vector pulse width modulation technique, switching at 6 kHz. The data acquisition unit stores the response of the machine. The procedure is repeated for different levels of  $i_d$  to obtain current dependent q-axis flux linkage at different d-axis current level. After the test is completed for the q-axis flux linkage,  $\lambda'_q$ , the control algorithm is switched to control

the q-axis current and  $v_d$  pulse is supplied to find the current dependent d-axis flux linkage. The procedure is repeated for different levels of q-axis current. Once the measurement is complete for a full magnetization level, the whole procedure is repeated to measure the current dependent flux linkages at 75% and 50% magnetization levels.

From the measured d- and q-axes flux linkages at various magnetization level, the self and cross-coupling flux linkages can be calculated using equations (3.13) – (3.16) [51]. And the self and cross-coupling inductances considering the steady state or transient effects can be calculated using equations (3.7) - (3.10).

$$\lambda_{dd}(i_d, \lambda_f) = \lambda_{d'}(i_d, i_q, \lambda_f) - \lambda_d(0, i_q, \lambda_f) \quad (3.13)$$

$$\lambda_{dq}(i_d, i_q, \lambda_f) = \lambda_{d'}(i_d, i_q, \lambda_f) - \lambda_d(i_d, 0, \lambda_f) \quad (3.14)$$

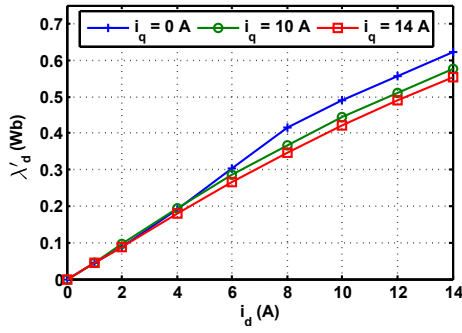
$$\lambda_{qq}(i_q, \lambda_f) = \lambda_{q'}(i_d, i_q, \lambda_f) - \lambda_q(i_d, 0, \lambda_f) \quad (3.15)$$

$$\lambda_{qd}(i_d, i_q, \lambda_f) = \lambda_{q'}(i_d, i_q, \lambda_f) - \lambda_q(0, i_q, \lambda_f) \quad (3.16)$$

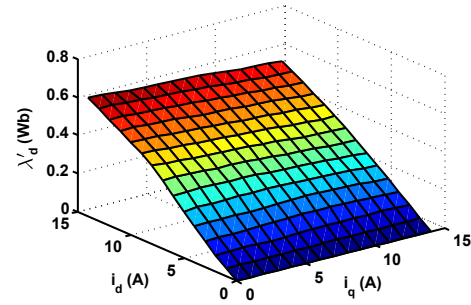
### 3.3.4 Results and Discussions

For a fully magnetized VFM, the variation of the d- and q-axes flux linkages due to the stator excitations are shown in figures 3.3 and 3.4 respectively. It is seen that the d-axis flux drops with an increase in the q-axis current for the same value of the d-axis current. From figure 3.3, it is seen that the d-axis flux produced by the d-axis current drops from 0.63 Wb to 0.55 Wb at 14A of  $i_d$  when the q-axis current is increased from zero to 14 A. This means that increasing the q-axis current reduces the d-axis flux. Similarly, the q-axis flux also drops with increasing d-axis current. That is, there is a drop in the q-axis flux from 0.52 Wb to 0.47 Wb at the rated  $i_q$  of 14 A when the d-axis current is increased from zero to 14 A.

The cross-magnetizing flux linkages  $\lambda_{dq}$  and  $\lambda_{qd}$  are shown in figure 3.5. The plots show that the cross-coupling flux linkages are negative for most of the currents in  $i_d i_q$  plane and increases as the current in another axis is increased. However, the q-axis flux linkage due

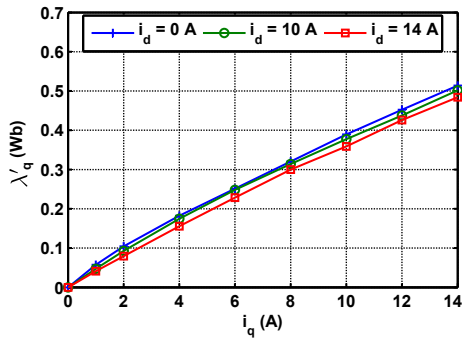


(a)

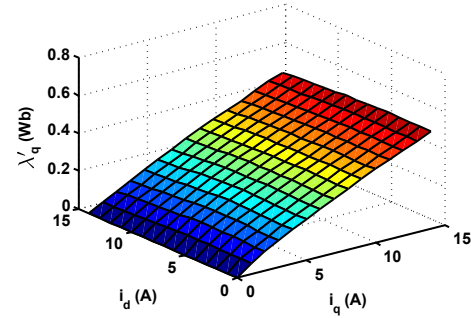


(b)

Figure 3.3: Measured d-axis flux linkage due to stator excitation at 100% magnetization level



(a)

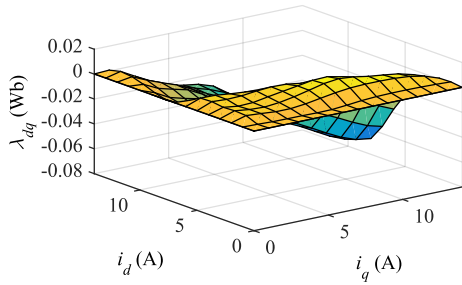


(b)

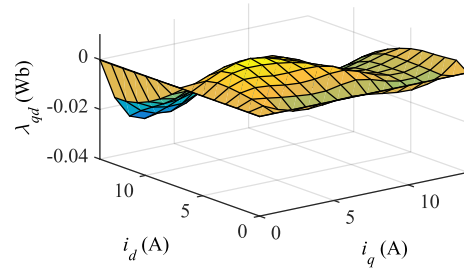
Figure 3.4: Measured q-axis flux linkage due to stator excitation at 100% magnetization level

to the d-axis current increases in some regions. This can be explained from the d-axis self inductance measurement result. The result in chapter 2, section 2.5.6 shows that the d-axis inductance increases up to a certain range of d-axis current. What actually happens is that the d-axis current up to a certain value drives the core to a higher permeability region that causes an increase in the flux produced by the stator currents.

The incremental self inductances are shown in figures 3.6. A similar trend to the self inductances measurement in chapter 2, section 2.5.6 can be seen in the self inductances. As the q-axis current is increased, the d-axis current at which the inductance  $L_{dd(inc)}$  has a peak is shifted towards the zero, and the peak itself is reduced in magnitude. Similarly, the q-axis self inductance decreases as the d-axis current increases.

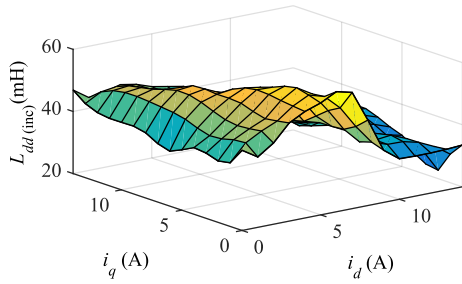


(a)

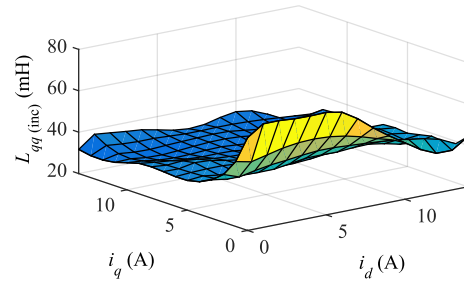


(b)

Figure 3.5: Cross-magnetizing flux linkages at 100% magnetization level (a) d-axis flux linkage due to q-axis current (b) q-axis flux linkage due to d-axis current



(a)



(b)

Figure 3.6: Incremental self inductances at 100% magnetization level (a) d-axis incremental self inductances (b) q-axis incremental self inductances

The incremental cross-coupled inductances are shown in figure 3.7. While, the apparent cross-coupled inductances are shown in figure 3.8. It is seen that the cross-coupling inductances are higher for higher values of the currents and the effects in the cross-coupling inductances show that they saturate at higher values of  $d - q$  currents.

For a 75% magnetized machine, the variation of the d-axis flux linkage due to stator excitations are shown in figure 3.9 and the variation of the q-axis flux linkage due to the stator excitations are shown in figure 3.10. Similar to the effect of q-axis inductance in d-axis flux in 100% magnetized machine, the d-axis flux decreases with increase in the q-axis current. Also comparing figures 3.3 and 3.9, the d-axis flux for the same  $i_d$  and  $i_q$  is higher in the 75% magnetized machine. The incremental cross-coupled inductances are shown in figure 3.11. Finally, the apparent cross-coupled inductances are shown in figures 3.12. The

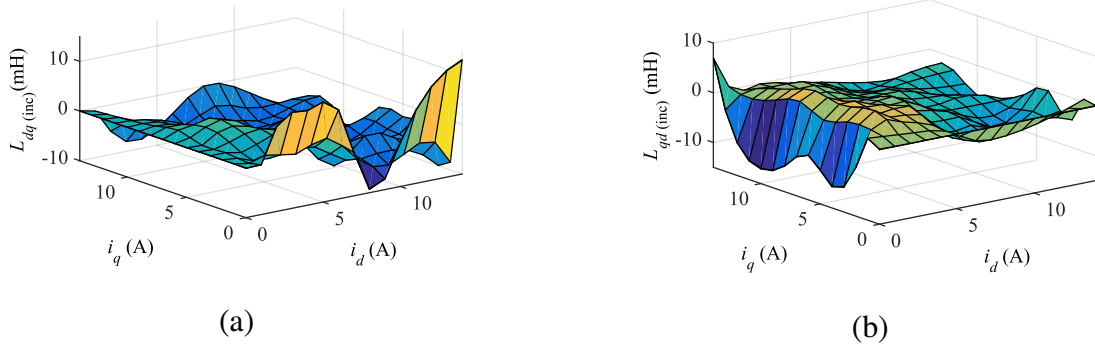


Figure 3.7: Incremental cross-coupling mutual inductances at 100% magnetization level (a) d-axis incremental cross-coupling inductances (b) q-axis incremental cross-coupling inductances

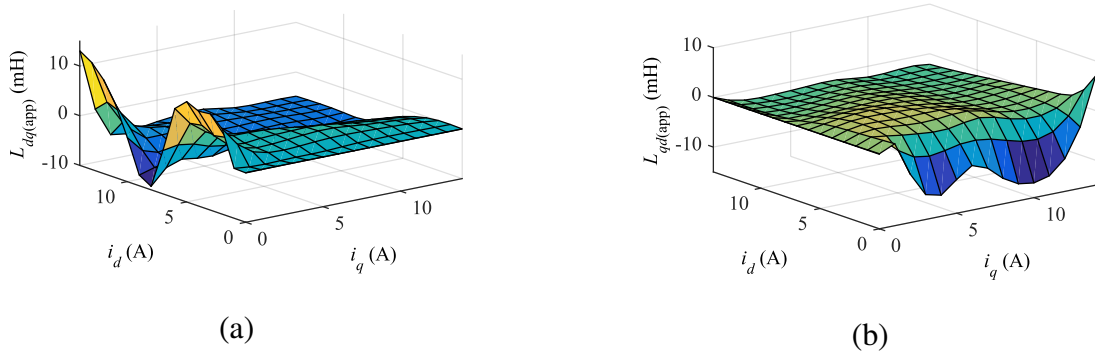
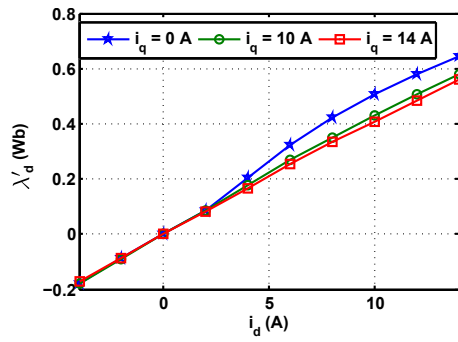


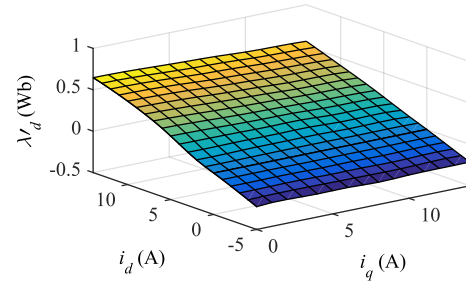
Figure 3.8: Apparent cross-coupling mutual inductances at 100% magnetization level (a) d-axis apparent cross-coupling inductances (b) q-axis apparent cross-coupling inductances

cross-coupling inductances at 75% magnetization level follows similar trends to those at 100% magnetization level.

For a 50% magnetized machine, the variation of the d- and q-axes flux linkage due to the stator excitations are shown in figures 3.13 and 3.14, respectively. The trend is similar to the 100% and the 75% magnetization level, but the values are slightly higher. For example, the d-axis flux linkage at the highest values of  $dq$  currents is 0.58 Wb for 50% magnetization level while it is 0.55 Wb for the full magnetization level. The incremental cross-coupled inductances are shown in figure 3.15. Finally, the apparent cross-coupled inductances are shown in figure 3.16.

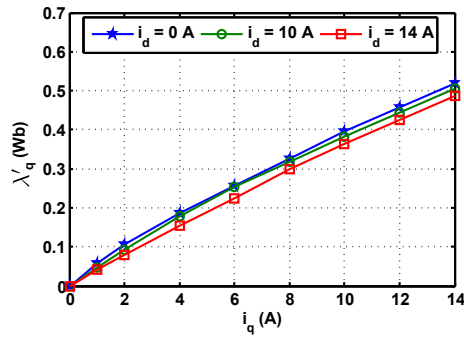


(a)

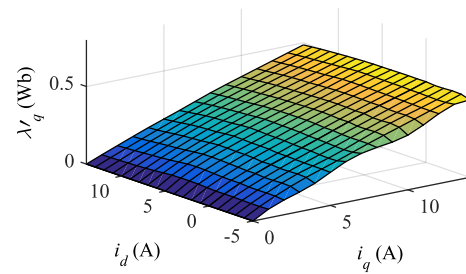


(b)

Figure 3.9: Measured d-axis flux linkage due to stator excitation at 75% magnetization level

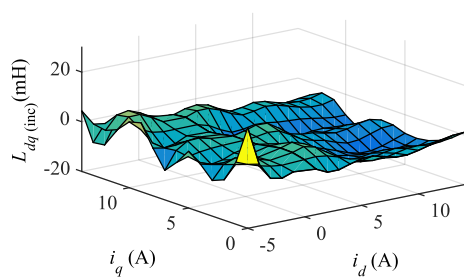


(a)

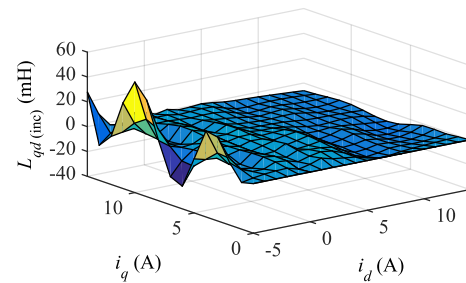


(b)

Figure 3.10: Measured q-axis flux linkage due to stator excitation at 75% magnetization level

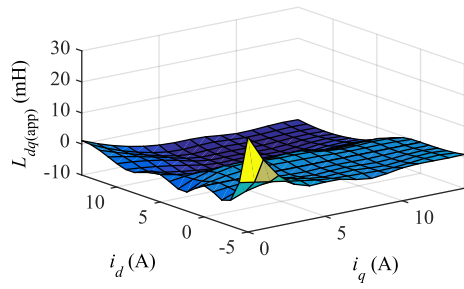


(a)

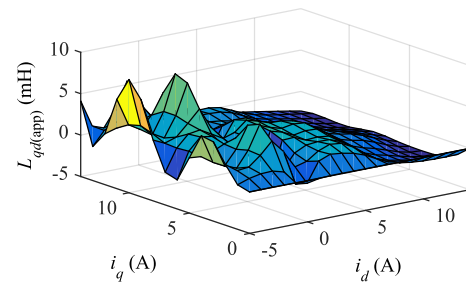


(b)

Figure 3.11: Incremental cross-coupling mutual inductances at 75% magnetization level (a) d-axis cross-coupling inductance due to q-axis current (b) q-axis cross coupling inductance due to d-axis current

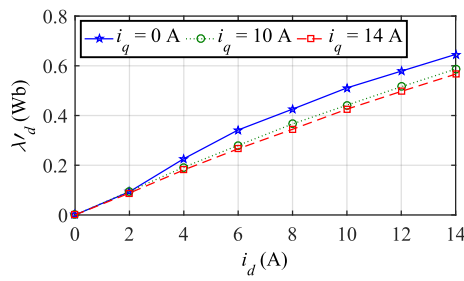


(a)

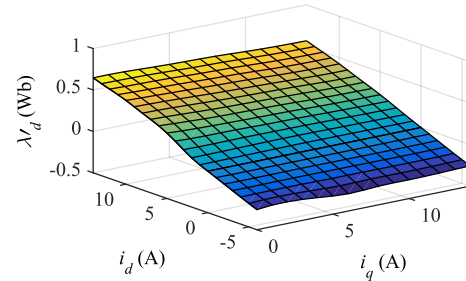


(b)

Figure 3.12: Apparent cross-coupling mutual inductances at 75% magnetization level (a) d-axis cross-coupling inductance due to q-axis current (b) q-axis cross coupling inductance due to d-axis current

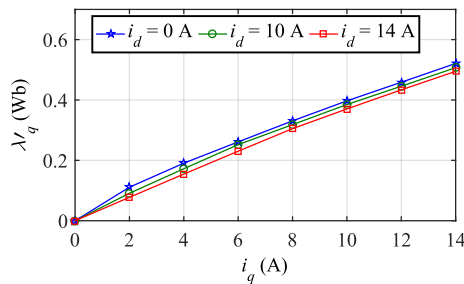


(a)

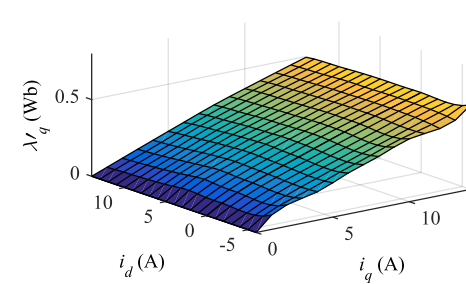


(b)

Figure 3.13: Measured d-axis flux linkage due to stator excitation at 50% magnetization level

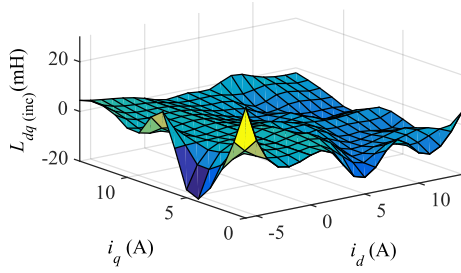


(a)

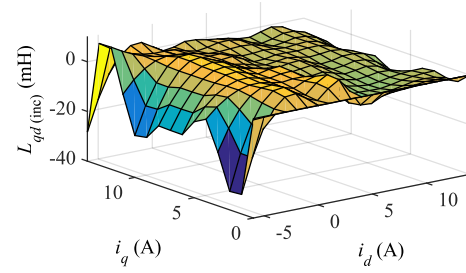


(b)

Figure 3.14: Measured q-axis flux linkage due to stator excitation at 50% magnetization level

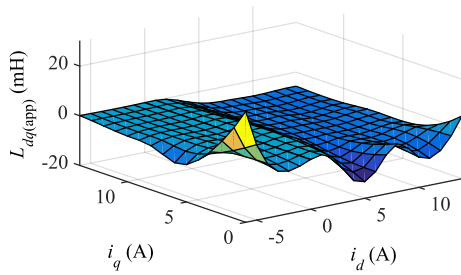


(a)

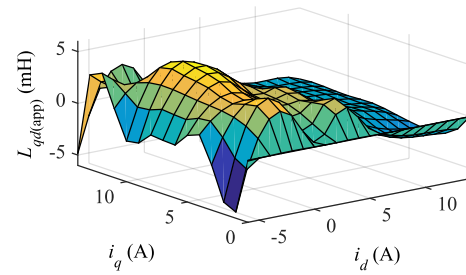


(b)

Figure 3.15: Incremental cross-coupling mutual inductances at 50% magnetization level (a) d-axis cross-coupling inductance due to q-axis current (b) q-axis cross coupling inductance due to d-axis current



(a)



(b)

Figure 3.16: Apparent cross-coupling mutual inductances at 50% magnetization level (a) d-axis cross-coupling inductance due to q-axis current (b) q-axis cross coupling inductance due to d-axis current

## 3.4 Summary

In this chapter, the cross-magnetization phenomenon in electric machines and its significance in variable flux machines is discussed. The dq model of the VFM is modified to account for the cross-magnetization effects. The apparent and incremental inductances are defined along with their significance. The method proposed in chapter 2 that uses a vector control drive is used to determine the cross-coupling and self inductances. Three different magnetization levels are discussed based on the experimental results.

## Chapter 4

# Torque Performance of VFMs

For all electric motors, electromagnetic torque is the most important output variable that determines the mechanical dynamics of the machine. An electric machine is designed for a certain value of rated torque. The electromagnetic torque in variable flux machine arises from first, the interaction of the magnetic field from the magnets and the stator field, and second, the variation in the reluctance of the magnetic field path. For electric machines with magnetic saliency, the reluctance torque can be used to reduce the stator current in the machine. As the power losses in the machine and the converter driving the machine increases with the rise in the current, it has been in practice to utilize the reluctance torque to get the highest possible torque for a given current. For such cases, the inductance parameters are used to find the minimum current to drive a given load torque.

The variable flux machine is peculiar to normal PM machines in the respect that the same torque can be generated by varying the magnet flux as well. So, estimation of the current that produces a required torque is not simple. Moreover, due to cross-saturation effects, there exist two more torque components apart from the magnet torque and the reluctance torque. These torque components may be aid or oppose the main torque. For a drive designer, it is necessary to have a torque vs current angle curve for a proper selection of the operating point. The torque performance of an electrical machine is studied as torque vs current angle

that gives the maximum torque per current, and the torque ripple performance that gives the spatial variation of the torque around the rotor circumference.

## 4.1 Steady State Torque Calculation

The steady state electromagnetic torque in any PM machine in the  $dq$  domain is given by equation (4.1). For non-saturated electric machine, the torque equation in terms of inductances can be written as equation (4.2).

$$T_e = \frac{3P}{2} \frac{1}{2} [\lambda_d i_q - \lambda_q i_d] \quad (4.1)$$

$$T_e = \frac{3P}{2} \frac{1}{2} [\lambda_f + (L_d - L_q) i_d] i_q = T_{PM} + T_R \quad (4.2)$$

where,  $\lambda_d$  is the d-axis flux, which is the sum of the magnet flux and the flux produced by the d-axis current component of the stator current,  $\lambda_q$  is the q-axis flux produced by the q-axis component of the stator current.  $T_{PM}$  is the magnet torque as a result of the interaction between the magnet flux and the stator current.  $T_R$  is the reluctance torque generated by the difference in the magnetic reluctance along the d- and q-axis. Figure 4.1 shows the flux decomposition in an unsaturated machine.

When there is magnetic saturation in the steel core, or the variation in the steel reluctance can not be neglected in comparison to the air gap reluctance, the inductances  $L_d$  and  $L_q$  do not remain constant. In fact, the inductance in one axis is affected by the current in another axis. This cross-magnetization effect causes deviation in the torque predicted by equation (4.2). The flux linkages considering the cross-coupling effects can be written as given in equations (4.3) and (4.4). Here, the d-axis flux is decomposed into three fluxes: the first one  $\lambda_{dd}$  being the flux produced by the current in the same axis, the second one  $\lambda_{dq}$  is the flux in the d-axis produced by the current in the q-axis and the last one  $\lambda_f$  is the flux produced by the magnets in the d-axis. Similarly, the q-axis flux is decomposed into two fluxes: the first

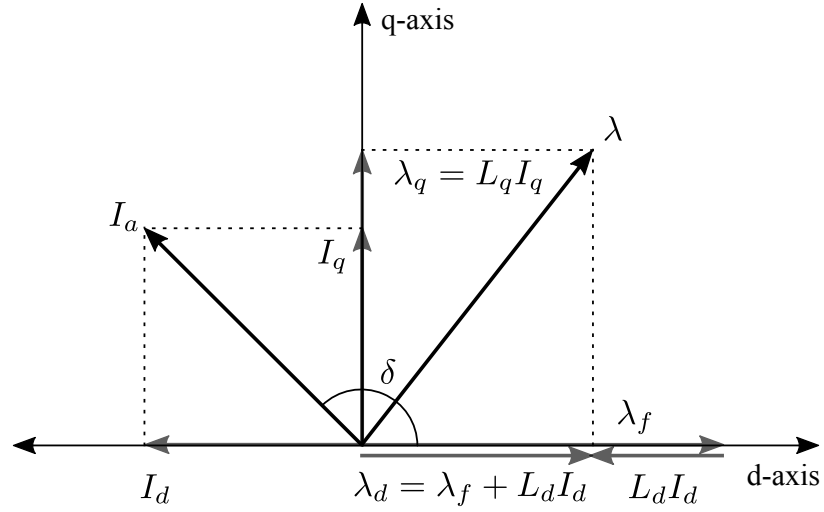


Figure 4.1: Flux decomposition in unsaturated machine

one  $\lambda_{qq}$  is the flux produced by the current in the same axis, the second one  $\lambda_{qd}$  is the flux produced by the d-axis current.

$$\lambda_d = \lambda_{dd} + \lambda_{dq} + \lambda_f \quad (4.3)$$

$$\lambda_q = \lambda_{qd} + \lambda_{qq} \quad (4.4)$$

Writing the flux in terms of inductance values, the equations (4.3) and (4.4) can be written as follows.

$$\lambda_d = L_{dd}i_d + L_{dq}i_q + \lambda_f \quad (4.5)$$

$$\lambda_q = L_{qd}i_d + L_{qq}i_q \quad (4.6)$$

where  $L_{dd}$ ,  $L_{dq}$ ,  $L_{qd}$  and  $L_{qq}$  are the current and magnet flux dependent self and cross-coupling cross-inductances. Figure 4.2 shows the flux decomposition in a VFM considering cross-coupling effects. Substitution of equations (4.5) and (4.6) in equation (4.1) gives the

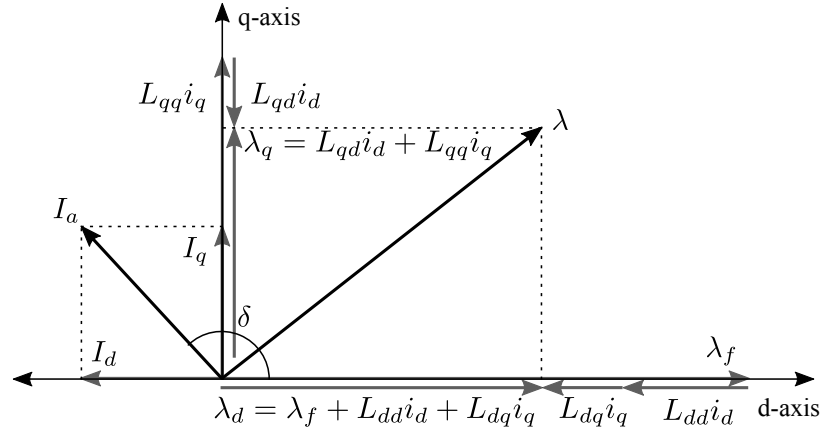


Figure 4.2: Flux decomposition in VFM considering cross-magnetization

following expression for the electromagnetic torque.

$$T_e = \frac{3P}{2} [\lambda_f i_q + (L_{dd} - L_{qq}) i_q i_d + (L_{dq} i_q^2 - L_{qd} i_d^2)] \quad (4.7)$$

The first term is the main magnet torque, the second term is the main reluctance torque and the last term is the cross reluctance torque caused by the mutual inductance between the d- and q-axes. In equations (4.3)-(4.6), the q-axis flux attributed by the magnet is considered negligible. This assumption is valid for a properly designed machine, and it leads to the torque attributed by the phase delay of the magnet flux being negligible.

The electromagnetic torque produced by the variable flux machine is calculated based on equation (4.7) and the cross-coupling inductances found in chapter 3. However, as the magnet flux can also be varied, the torque has to be calculated for different magnet flux. Figures 4.3, 4.4 and 4.5 show the calculated torque angle curves for 100%, 75% and 50% magnetization levels for a prototype VFM. The curves show that for a fixed current, the torque increases with an increase in the torque-angle, attains maximum value, and decreases with the further increase in the torque-angle. The maximum value of torque increases with an increase in the current magnitude and the magnetization level. Table 4.1 shows the variation in torque angle for maximum torque at three different magnetization levels.

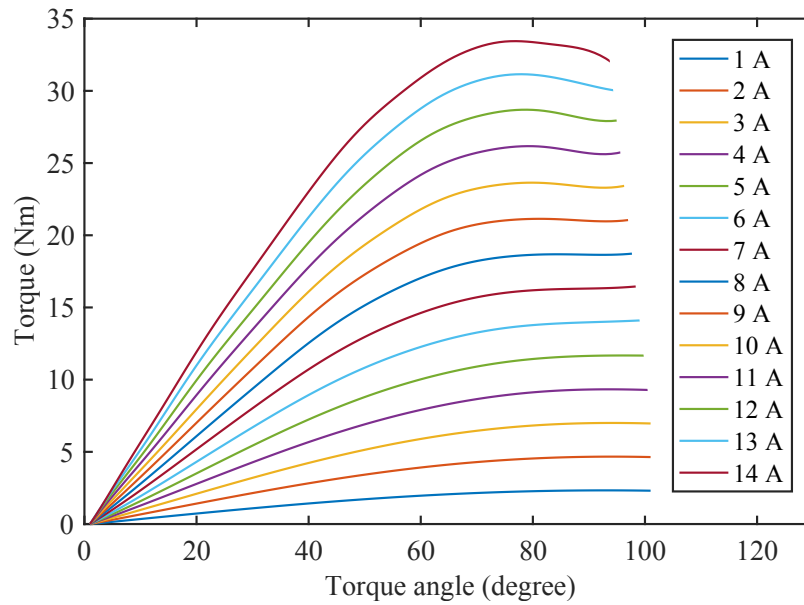


Figure 4.3: Calculated torque angle curves considering cross-coupling effects for a fully magnetized machine

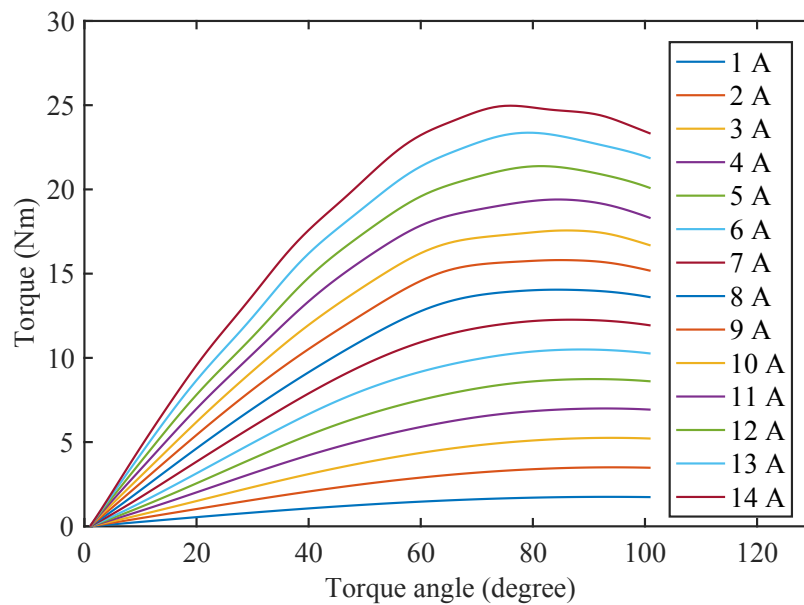


Figure 4.4: Calculated torque angle curves considering cross-coupling effects for a 75% magnetized machine

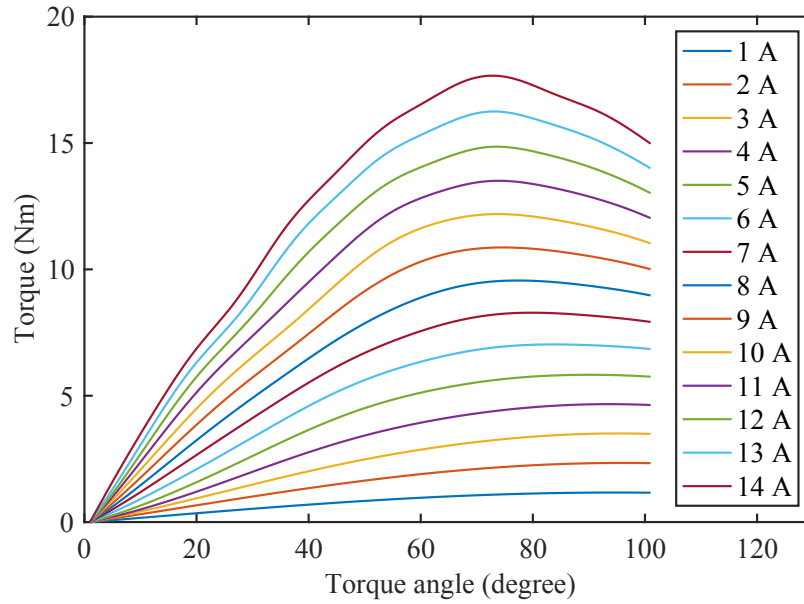


Figure 4.5: Calculated torque angle curves considering cross-coupling effects for 50% magnetized machine

Table 4.1: Maximum torque per ampere torque-angle variation at different magnetization levels

Peak current(A)	100%	75%	50%
1	93	93	95
2	94	94	96
3	94	94	95
4	93	93	94
5	95	91	90
6	95	89	84
7	95	87	80
8	84	84	77
9	81	85	75
10	80	86	74
11	79	85	74
12	79	81	74
13	78	79	73
14	77	76	73

## 4.2 Measurement of Static Torque-Angle Characteristics

The torque-angle refers to the difference in angle between the magnetic flux produced by the stator current and the magnetic flux produced by the permanent magnet. In practice, the current characteristics of a PM machine rarely matches the ideal characteristics. The simulation result from the finite element analysis are usually taken to be close to the actual result. However, the measurement result has to verify the simulation result.

Usually, a DC source is used to supply the required DC current to measure the torque-angle characteristics through a lock rotor test method [7, 59]. One phase (phase A) of the three phase machine is connected to the positive of the DC power supply while the others are shorted and connected to the negative of the DC power supply. The torque is measured using a torque sensor at a fixed 'phase A' current. The torque-angle characteristics is obtained by varying the rotor position. In this method, a current regulated DC power supply is needed for steady current and torque readings. While the fluctuations caused by heating is taken care by the use of a current regulated DC power supply, the effect of unequal coil resistance is not taken care.

In this thesis, two methods using a vector controlled drive are presented to obtain static torque-angle characteristics. In the first method, the torque is measured at different rotor positions keeping the current vector fixed. In the second method, the torque is measured at a fixed rotor position while the current vector direction is varied. Both of the methods use the same experimental setup shown in figure 4.6. The test set-up includes a torque transducer, a dc dynamo-meter, a voltage source inverter, current and voltage sensors and the VFM with an encoder assembly. The VFM is coupled to the dynamo-meter through the torque transducer.

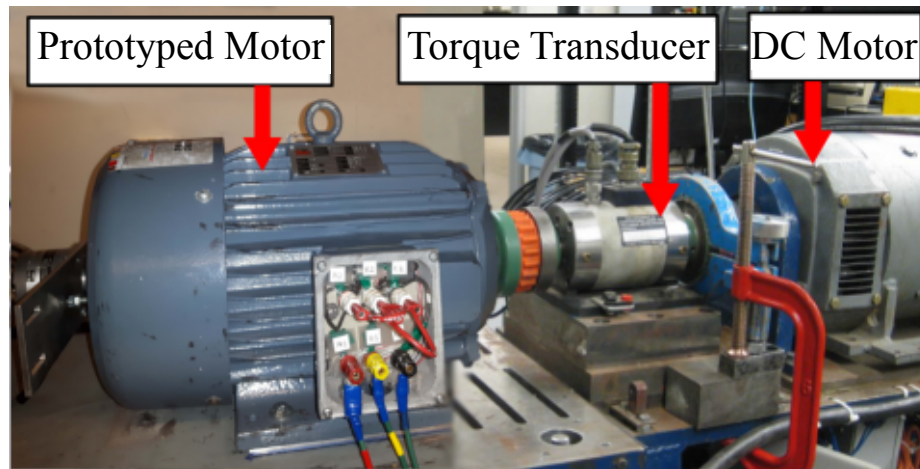


Figure 4.6: Experimental setup for the torque-angle measurement

#### 4.2.1 Method I: Varying Rotor Position

In this method, the rotor position is varied and the current vector is controlled constant to obtain the static torque-angle characteristics. Figure 4.7 shows the circuit diagram of the measurement set-up. A dc voltage from the rectifier is fed to the DC bus of the inverter. A DC current in 'phase A' is produced by controlling the 'phase A' current to a fixed value while the 'phase B' and 'phase C' currents are controlled to remain half of the 'phase A' current with opposite polarity. The benefit of using an existing drive is that no extra DC supply is required. Further, the effects of heating and unequal phase resistances are taken care by the controller. To obtain the torque-angle characteristics at different magnetization levels, the magnetization and demagnetization characteristics of the VFM are used to set the magnetization level of the machine.

At the beginning, the magnetization level is set to 100%. The VFM is locked at the d-axis of the rotor on the test bench. A DC current  $I_a$  of magnitude 1A is supplied to the stator windings. The controller will generate the gating signals so that  $I_a$  is maintained 1A and both  $I_b$  and  $I_c$  are maintained at  $-0.5A$ . The torque reading from the torque-meter along with the 'phase A' current and the present rotor position (or torque-angle) is recorded. The

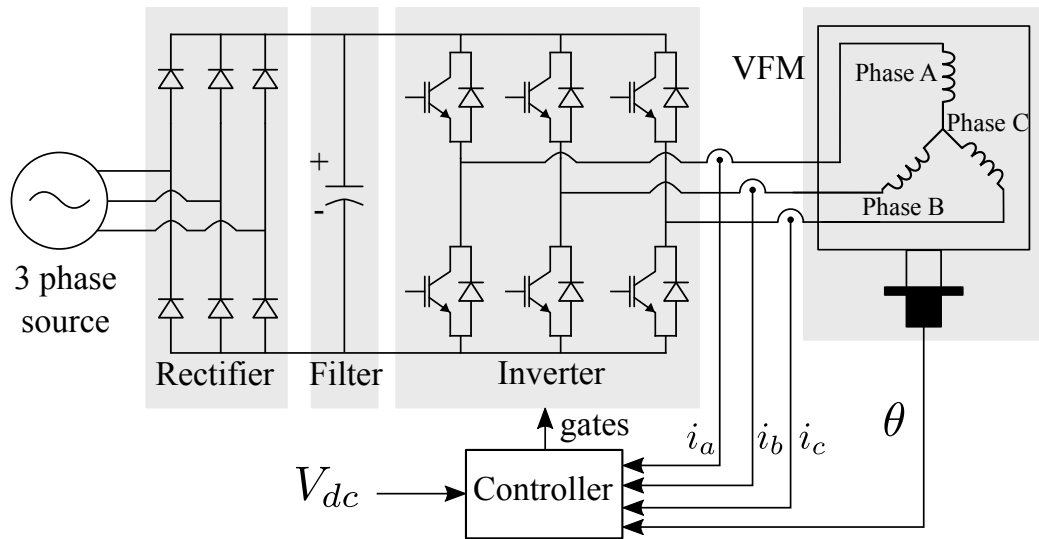


Figure 4.7: Circuit diagram for the torque angle measurement

next step is to increase the reference current. The controller is commanded to increase the current by 1A in each measurement until the readings are recorded for the rated current of 14A. Once the measurement is done for one rotor position, the rotor position is changed and then the above procedure is repeated. The measurement is done for various rotor positions for currents from 1A to 14A.

After the measurement for full magnetization state is complete, the controller is commanded to demagnetize the machine to 75% magnetization level according to the magnetization/demagnetization characteristics. The above measurement procedure is repeated until the torque values are recorded for the current range of 1A to 14A over the range of rotor positions. The procedure is repeated to obtain the torque values at various current levels and various rotor positions for 50% magnetization level.

Figures 4.8 and 4.9 shows the measured torque vs angle curves for full magnetization and 75% magnetization levels respectively for full range of currents. The figures shows that the torque varies with the torque angle and has a maximum value at certain torque angle. The same torque can be obtained with different current by operating at different torque angles.

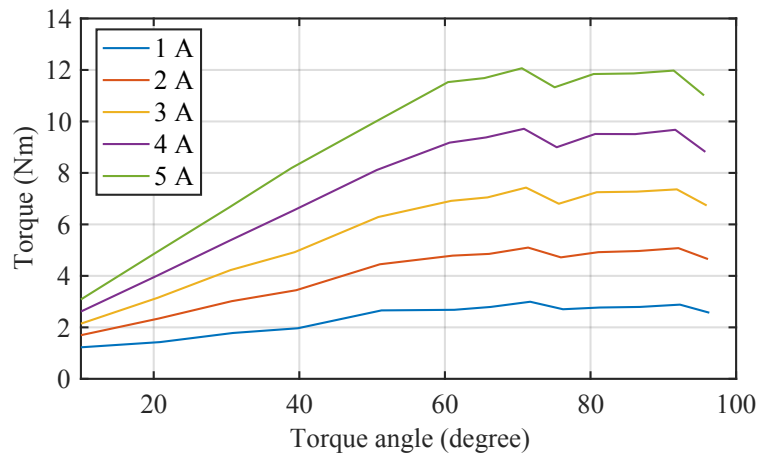
Moreover, the lower values of torques can be obtained by changing the magnetization level to lower values. The torque angles for maximum torque changes with the current supplied. Additionally, the torque angle for the maximum torque at the same current varies with the magnetization level.

#### **4.2.2 Method II: Varying Current Vector**

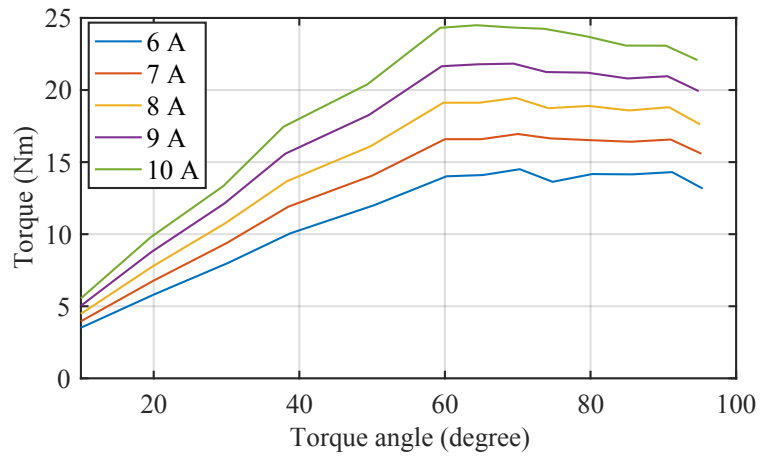
In this method, the rotor position is kept fixed while the current vector is rotated to obtain the static torque-angle characteristics. The circuit connection is the same as that shown in figure 4.7. The three phase currents are measured and fed-back to the controller. A reference current and torque angle are given to the controller. Based on the current and position feed-backs, the controller generates the gating signals to control the  $dq$  currents. The reference torque angle is varied to measure the torque angle characteristics at a current level. The process is repeated at various currents. To obtain the torque-angle characteristics at different magnetization levels, the magnetization and the demagnetization characteristics of the VFM are used to vary the magnetization level. However, the reference current and torque-angle should guarantee that the magnetization level of the machine does not change during the measurement process.

Figure 4.10(a) and 4.10(b) show the measured torque-angle characteristics at 100% and 75% magnetization levels respectively. Unlike the torque-angle curves obtained by varying the rotor position, the figures 4.10(a) and 4.10(b) show that the torque-angle curves obtained using method II are smooth.

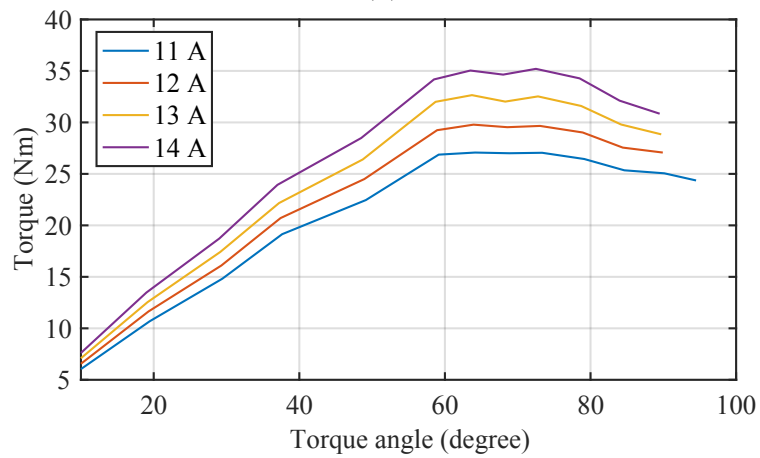
The benefit of this method to obtain the torque-angle characteristics is that the measurement process is faster and can be automated. The effects of heating and unequal phase resistances are automatically taken into account. Moreover, as the torque-angle characteristics calculated using inductances are smooth curves, this method gives a basis for comparison.



(a)

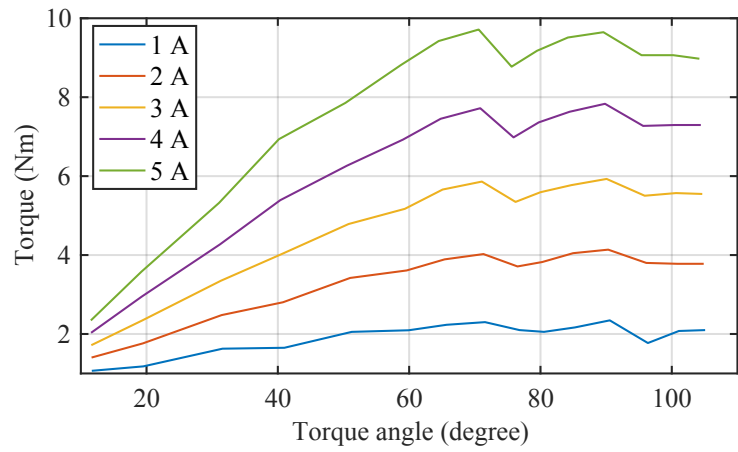


(b)

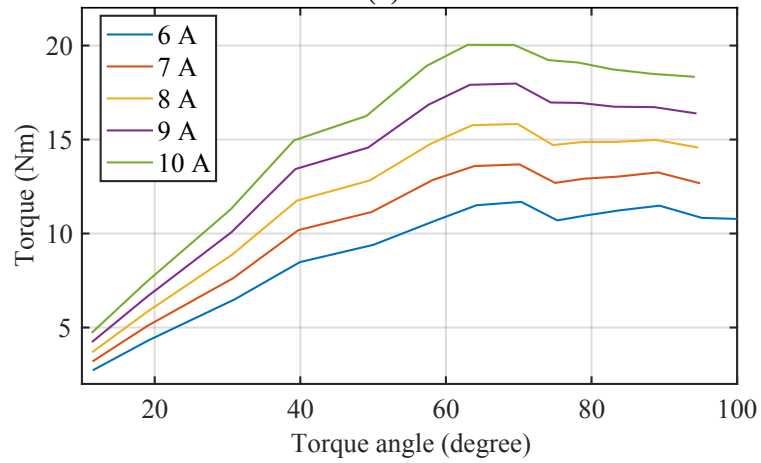


(c)

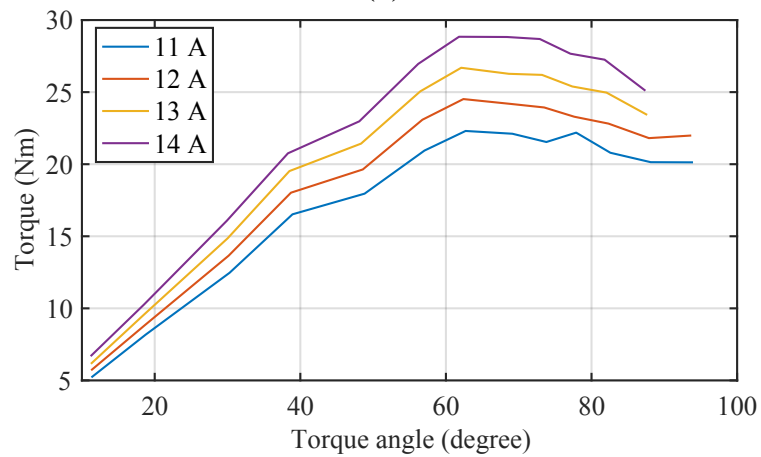
Figure 4.8: Measured torque angle curve by varying rotor position for a fully magnetized VFM



(a)

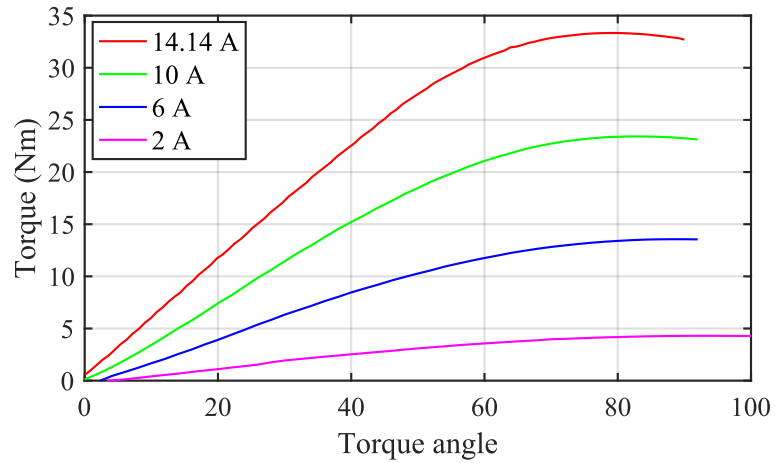


(b)

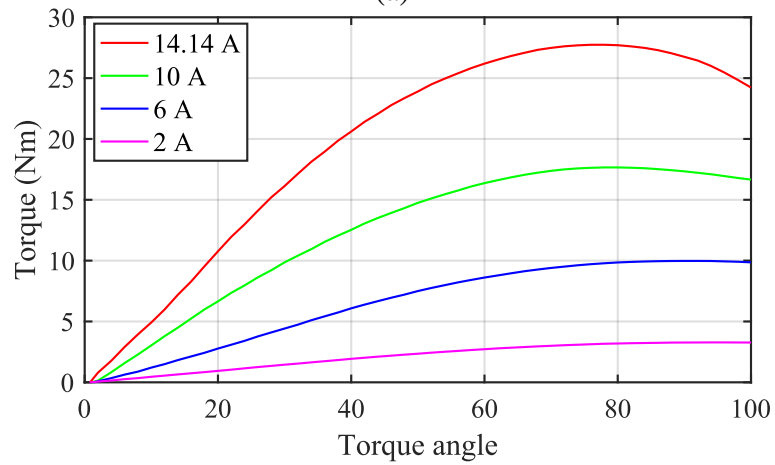


(c)

Figure 4.9: Measured torque angle curve by varying rotor position for a 75% magnetized VFM



(a)

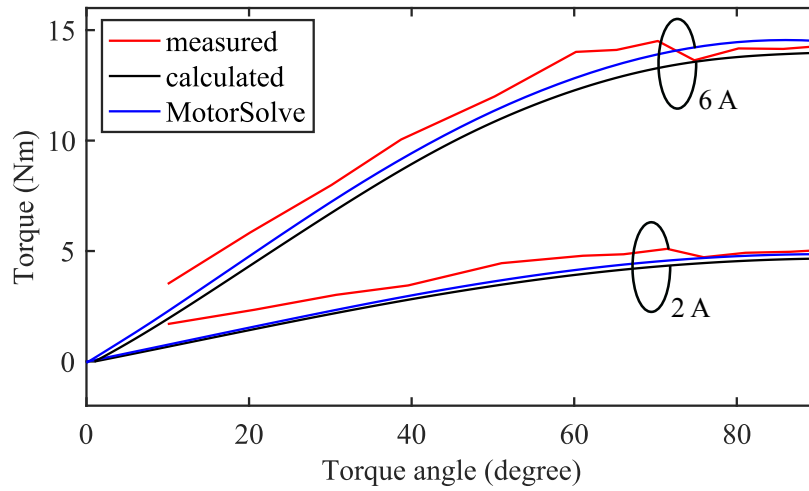


(b)

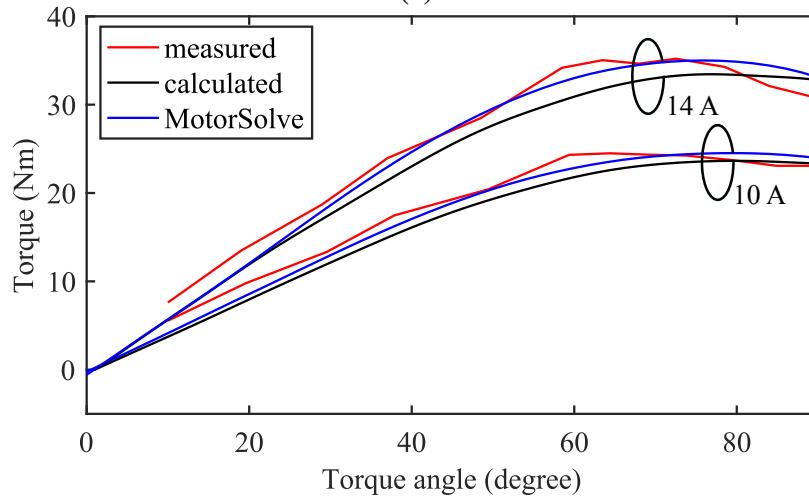
Figure 4.10: Measured torque-angle curves at fixed rotor position (a) 100% magnetization (b) 75% magnetization.

### 4.3 Torque Angle Comparison

In this section, the torque-angle characteristics measured using the two methods are compared with the torque calculated using cross-coupling inductances and FEM simulation. Figures 4.11 and 4.12 compare the torque measured using method I with the calculated and FEM simulation torque-angle characteristics for peak currents of 2A, 6A, 10A and 14A at 100% and 75% magnetization levels respectively. For full magnetization level, all the measured, calculated and simulated torques are in good agreements. For 75% magnetization



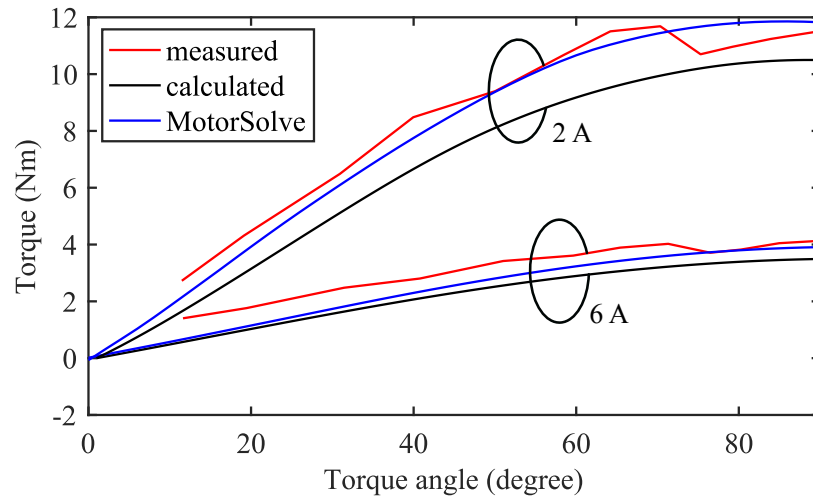
(a)



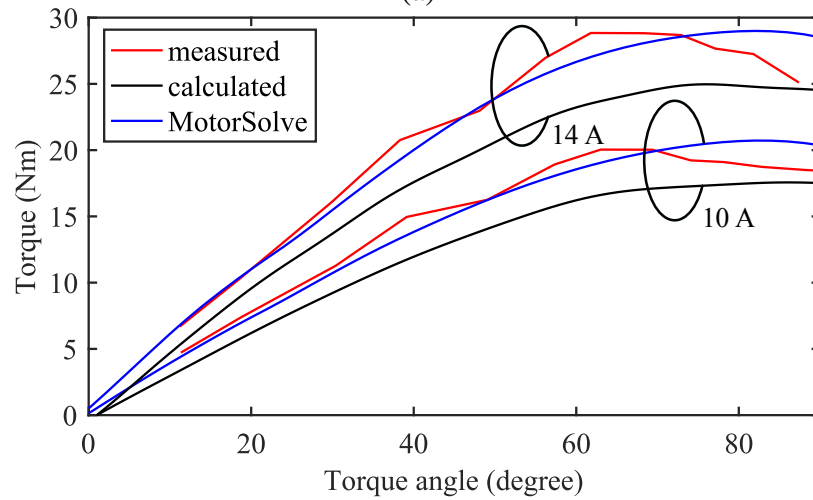
(b)

Figure 4.11: Comparison of calculated and simulated torques with the measured torque using method I for 100% magnetization level

level, the measured simulated torques are closer, while there are some deviations with the calculated torques. Figures 4.13 shows a comparison of torque angle characteristics measured using method II with the calculated and FEM simulation torque angle characteristics. The comparison shows that the measured and calculated torques are in very good agreement while the MotorSolve simulation torque is higher. The reason might be due to higher magnet flux linkage in FEM simulation (0.56 Wb) than the actual flux linkage in the physical machine(0.515 Wb).

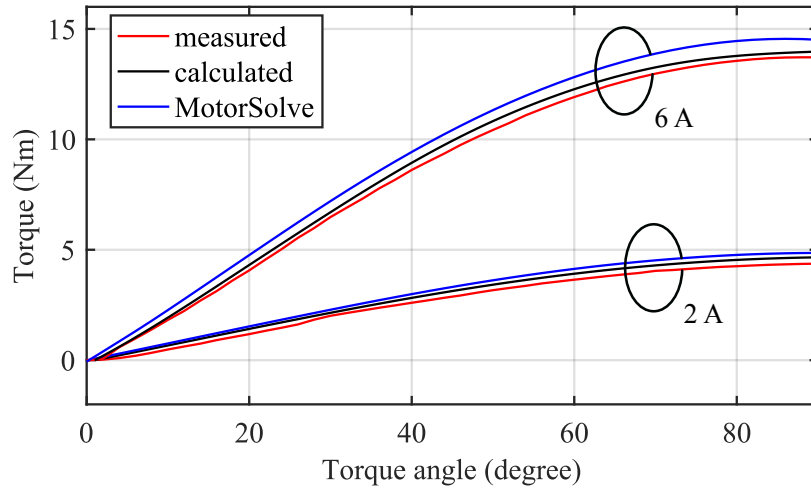


(a)

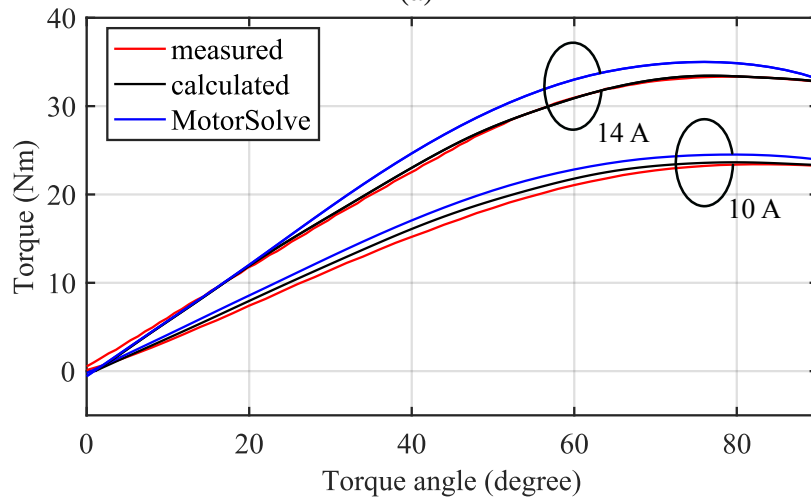


(b)

Figure 4.12: Comparison of calculated and simulated torques with the measured torque using method I for 75% magnetization level



(a)



(b)

Figure 4.13: Comparison of calculated and simulated torques with measured torque using method II for 100% magnetization level

## 4.4 Torque Ripple Performance

Low torque ripple is one of the requirements in high performance drives in traction applications. The torque ripple produce vibrations in an electric vehicle. The torque ripple causes additional losses, reducing the efficiency when the machine needs to operate at constant power region. The torque ripple additionally causes decrease in the average torque, produces audible noise, and imposes mechanical pulsation on the shaft [7]. It is desirable to have as low torque ripple as possible.

The torque ripple in permanent magnet machine is mainly due to the fluctuations of the field distribution and armature MMF. The reluctance variation along the air-gap due to stator slotting and the rotor saliency is another source of torque ripple [60]. The torque ripple due to stator slots harmonics effects can be reduced by skewing, but it is not preferable for variable flux machines with low coercive field magnets. The reason is the possibility of irreversible magnet demagnetization in part of the machine axial length [24].

Improvement in torque ripple performance is one of the machine design issues. The specifications for the torque ripple is set and finite element analysis simulates and evaluates the torque ripple performance during machine design. However, for the verification of finite element analysis design, it is desirable to have an actual torque ripple of the physical machine.

### 4.4.1 Torque Ripple Measurement

Two methods to measure the torque ripple are presented in [61]. Although the first method uses a torque sensor of lower range than the rated machine torque, the measured torque ripple depends on several factors. The second method is an indirect method that assumes all the magnetic quantities to be sinusoidal and the torque ripple is calculated based on the current ripple. Similar technique to measure the torque ripple that uses sinusoidal current is explained in [60]. The drawbacks of those methods are the complexity of their design and requirement of the extra components that reduce the accuracy.

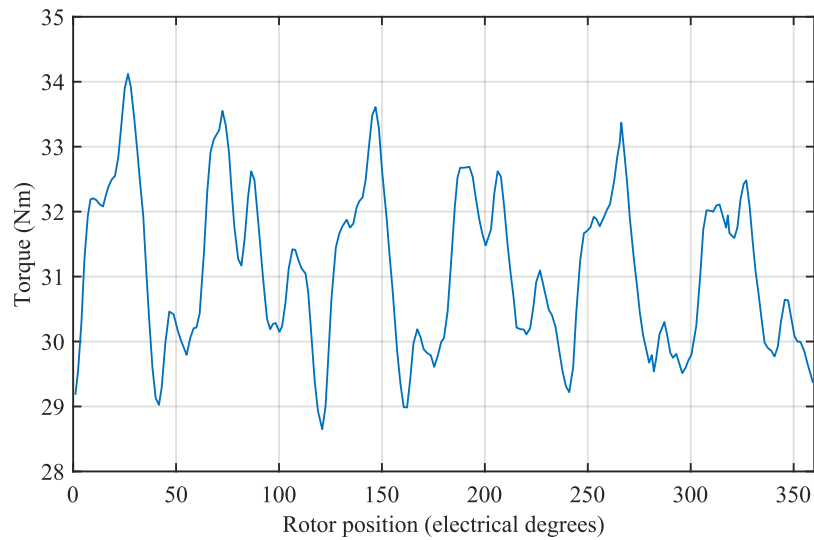


Figure 4.14: Measured torque ripple at 100% magnetization level at rated current and 90° torque angle

In this thesis, a vector controlled drive based static torque measurement technique is proposed to measure the torque ripple. The experimental setup for the measurement of the static torque-angle curve is the same as shown in figure 4.6. The test set-up include a torque sensor, a dc dynamo-meter, a voltage source inverter, current and voltage sensors and the VFM with an encoder assembly. The VFM is coupled with the dynamo-meter through the torque sensor. A mechanical lock is used to hold the shaft at the dynamo-meter side. The benefit of this method is that the same existing setup for the torque-angle measurement is used. Moreover, the same controller with minimal or zero modification can be used.

The circuit connection for the torque ripple measurement is show in figure 4.7. A three phase source feeds the rectifier/inverter. The three outputs of the three phase inverter is connected to the three terminals of the star connected VFM. The rotor shaft is locked at a fixed position by mechanical arrangements. The reference  $dq$  currents are given as input to the controller. Based on the position and stator currents feedbacks, the controller generates the gate signals to control the currents in  $dq$  domain. When the stator currents reached steady state, the toque and the rotor position are recorded. Next, the shaft position is advanced

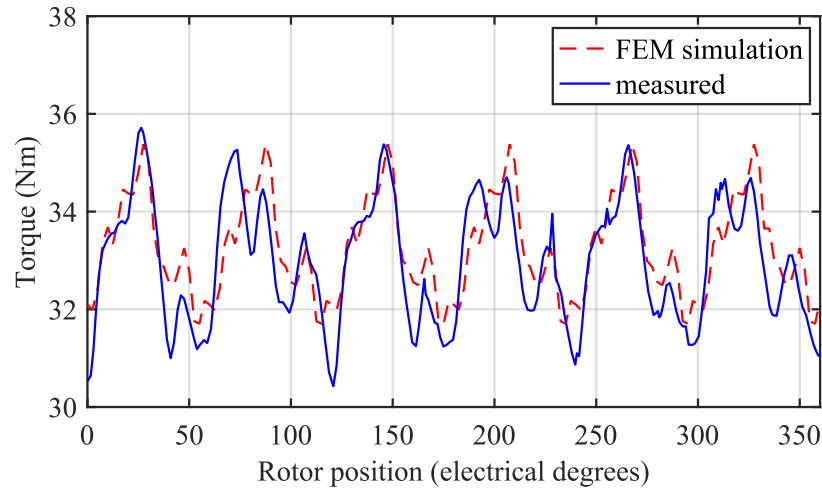


Figure 4.15: Comparison of measured torque waveform with FEM simulation for 100% magnetization level at rated current and  $78^\circ$  torque angle

and the torque reading is recorded for that position at the same  $dq$  currents. The process is repeated to record the torque and rotor positions for a complete electrical cycle.

Figure 4.14 shows the plot of the measured torque vs the rotor position at the rated current and  $90^\circ$  torque angle. The torque waveform shows the harmonics present in the air-gap torque. The torque harmonics are the result of non-sinusoidal air-gap flux due to stator slots, and their interaction with the rotor structure. The comparison between the measured and finite element simulation torque vs rotor position at full magnetization and  $78^\circ$  torque angle is presented in figure 4.15. The FEM simulation was done in Infolytica MotorSolve where, maximum accuracy option was selected. Since, the measurement was done for the magnet flux corresponding to 30 A magnetizing current, the magnet flux during the test was  $0.50 \text{ Wb}$ . However, the magnet flux from the FEM simulation in MotorSolve was  $0.54 \text{ Wb}$ . So, the demagnetization curve of the AlNiCo magnet was modified to reduce the magnetization level in the FEM simulation to match it with the experimental magnetization level. The plot shows similarity in the nature of the measured and the simulated torque waveforms. The average value of torque in both waveforms are  $33 \text{ Nm}$ . However, there are differences in the magnitude of trough at some rotor positions.

The same procedure can be repeated to measure the torque ripple at different value of  $dq$  currents and even at different magnetization levels. To do that, the reference stator current and/or reference torque angle is changed. To measure the torque ripple at another magnetization level, the magnet flux can be changed without any modification in the setup. The proposed method is good for design and performance evaluation of a newly designed PM machine. Moreover, the proposed technique can be used to characterize the torque waveform of the PM machine with the design software.

## 4.5 Summary

In this Chapter, the importance of the torque vs torque angle curve is discussed. Mathematical equation for torque produced by a VFM is modified to account for the saturation and cross-magnetization effects. A method to calculate the torques from the cross-magnetization inductances is described. Two methods are presented to measure the static torque-angle characteristics. Both of them utilizes the same existing vector controlled drive while taking care of the effects due to heating and unequal resistances. The first method is able to get the effect of slots in the torque. The second method gives a very good agreement of the measured torque with calculated and FEM simulation results. In addition to the torque-angle characteristics measurement, the same vector control technique is used to measure the torque ripple of the VFM at various torque angle and magnetization states. A comparison of the measured torque ripple with FEM simulation is presented. Although the measured torque has a lower average value, the comparison shows a good agreement in the torque waveform.

# Chapter 5

## Conclusions And Recommendations

This thesis explored in detail a new class of PM machine called the variable flux machine that has a feature to control the magnet flux by the stator current. The variable flux machines have a combined advantages of a wound rotor machine with highly efficient PM machine that form a unique machine with potential in numerous applications in electric drives. For high performance drives for electric vehicle applications, VFM is one of the suitable candidate as it has higher operating efficiency below the base speed, as well as above it. The magnet flux is varied by applying a short duration pulse of d-axis current. Consequently, the accurate control of the magnet flux requires a good estimate of the inductances. The main contributions of this thesis is the analysis and development of parameters measurement method for a VFM.

### 5.1 Conclusion

Based on the work done in this thesis, following conclusions are drawn.

**Chapter 2** discussed the basics of AlNiCo based variable flux machines and its modeling. The  $dq$  model of a permanent magnet machine is modified to account for the variable flux property. Various inductance measurement techniques are evaluated and a vector controlled

drive based inductance measurement technique is proposed for variable flux machine. The proposed technique uses an existing drive; requiring no extra power supply. It is fast as there is no need for mechanical rotation and locking of the rotor at different angles. The rotor is locked only in one position. However, the inductances can be measured at any magnetization level. The method was then validated using existing methods.

**Chapter 3** described the significance of the cross-magnetization phenomenon in variable flux machines. The  $dq$  model of the VFM is modified to account for the cross-magnetizing effects. The method proposed in chapter 2 was used to evaluate the cross-coupling flux linkages as well as the cross-coupling inductances. Experimental results for three different magnetization levels showed that VFMs are predisposed to cross-magnetization phenomenon which has a significant effect in the flux linkages and the inductances. The benefit of the proposed technique is that, the existing drive is used in the measurement and, no extra hardware is required.

**Chapter 4** presented the use of the cross-coupling inductances to evaluate the torque performance of the VFM. Two methods based on the vector controlled technique are presented to measure the static-torque angle curve. The first method measures the torque at various rotor positions at fixed current vector. The second method measures the torque at various current angle at a fixed rotor position. Both the methods eliminate the need of a DC power supply and takes into account the effects of heating and unequal phase resistances. Thus, the proposed methods ensure the right current vector is applied which is not guaranteed while using a DC source. The comparison of the measured torque angle curves with the calculated and FEM simulation ones are in a good agreement. The same vector control technique is used to evaluate the torque ripple of the VFM. Comparison of the measured and FEM simulation torque ripples show a good agreement in the torque waveforms. This method to measure the torque ripple performance is not only useful in evaluating the designed machine,

but it is also useful in the evaluation of a machine design software.

## 5.2 Future Works

This thesis evaluated the inductances including the cross-magnetization effects of an AlNiCo based VFM. The evaluation of steady state torque by considering cross-magnetization can be easily done. However, in the control of the magnet flux, taking account of cross-magnetization effects is challenging. During the magnetization and the demagnetization process, the pulsed current results in a torque ripple which becomes more severe as the pulse duration is increased. For performance improvement of the VFM drives, it is necessary to minimize such torque ripple while controlling the magnet flux accurately. Following are some recommendations.

- In this thesis, a slower d-axis current controller was used to avoid current overshoot which requires a longer pulse duration that may not be required. Evaluation of the minimum pulse duration considering the measured cross-coupling inductances will reduce the torque ripple during magnetization/demagnetization and its implementation in real time control is a good research topic for further improvement of VFM drives.
- This thesis proposes a mathematical model of VFM considering cross-saturation. The performance of the drive based on this model needs to be evaluated.
- This thesis evaluated the static torque performance of the VFM. These static torque characteristics are useful for operating the VFM at maximum torque per amp control strategy and maximum efficiency control strategy. The use of these torque characteristics in improving the overall efficiency of the drive or its use in reducing the ampere load drawn from the battery operated VFM drive is also an important area of research.

# Bibliography

- [1] W. Xu, J. Zhu, Y. Zhang, Y. Wang, and G. Sun. Characterization of advanced drive system for hybrid electric vehicles. In *Electrical Machines and Systems (ICEMS), 2010 International Conference on*, pages 487–492, Oct 2010.
- [2] Iqbal Husain. *Electric and Hybrid Vehicles , Design Fundamentals*. CRC, second edition, August 2010.
- [3] Natural Resource Canada. Electric vehicle technology roadmap for canada. Technical report, Government of Canada, 2009.
- [4] S.E. Gay A. Emadi M. Ehsani, Y.Gao. *Modern Electric, Hybrid Electric, and Fuel Cell Vehicles*, volume I. CRC Press, 2004 edition, December 2005.
- [5] Z. Q. Zhu and D. Howe. Electrical machines and drives for electric, hybrid, and fuel cell vehicles. *Proceedings of the IEEE*, 95(4):746–765, April 2007.
- [6] M. Zeraoulia, M. E. H. Benbouzid, and D. Diallo. Electric motor drive selection issues for HEV propulsion systems: A comparative study. *IEEE Transactions on Vehicular Technology*, 55(6):1756–1764, Nov 2006.
- [7] S. Taghavi. *Design of Synchronous Reluctance Machines for Automotive Applications*. PhD thesis, Concordia University, 2015.

- [8] Z. Wang and K. T. Chau. Design, analysis, and experimentation of chaotic permanent magnet DC motor drives for electric compaction. *IEEE Transactions on Circuits and Systems II: Express Briefs*, 56(3):245–249, March 2009.
- [9] J. M. Knežević. Low-cost low-resolution sensorless positioning of DC motor drives for vehicle auxiliary applications. *IEEE Transactions on Vehicular Technology*, 62(9):4328–4335, Nov 2013.
- [10] G. Pellegrino, A. Vagati, P. Guglielmi, and B. Boazzo. Performance comparison between surface-mounted and interior PM motor drives for electric vehicle application. *IEEE Transactions on Industrial Electronics*, 59(2):803–811, Feb 2012.
- [11] G. Pellegrino, A. Vagati, B. Boazzo, and P. Guglielmi. Comparison of induction and PM synchronous motor drives for EV application including design examples. *IEEE Transactions on Industry Applications*, 48(6):2322–2332, Nov 2012.
- [12] M. Ehsani, K. M. Rahman, and H. A. Toliyat. Propulsion system design of electric and hybrid vehicles. *IEEE Transactions on Industrial Electronics*, 44(1):19–27, Feb 1997.
- [13] Z. M. Zhao, S. Meng, C. C. Chan, and E. W. C. Lo. A novel induction machine design suitable for inverter-driven variable speed systems. *IEEE Transactions on Energy Conversion*, 15(4):413–420, Dec 2000.
- [14] Tiecheng Wang, Ping Zheng, Qianfan Zhang, and Shukang Cheng. Design characteristics of the induction motor used for hybrid electric vehicle. *IEEE Transactions on Magnetics*, 41(1):505–508, Jan 2005.
- [15] P. Pillay and R. Krishnan. Application characteristics of permanent magnet synchronous and brushless DC motors for servo drives. *IEEE Transactions on Industry Applications*, 27(5):986–996, Sep 1991.

- [16] R. Krishnan. *Permanent magnet Synchronous and Brushless DC Motor Drives*. CRC Press, 2010.
- [17] P. Pillay and R. Krishnan. Modeling, simulation, and analysis of permanent-magnet motor drives. I. the permanent-magnet synchronous motor drive. *IEEE Transactions on Industry Applications*, 25(2):265–273, Mar 1989.
- [18] V. Bobek. PMSM electrical parameters measurement. *Freescale Semiconductor*, 2013.
- [19] G. Stumberger, B. Polajzer, B. Stumberger, M. Toman, and D. Dolinar. Evaluation of experimental methods for determining the magnetically nonlinear characteristics of electromagnetic devices. *IEEE Transactions on Magnetics*, 41(10):4030–4032, Oct 2005.
- [20] F. Senicar, M. Džupker, A. Bartsch, B. Krájčiger, and S. Soter. Inverter based method for measurement of PMSM machine parameters based on the elimination of power stage characteristics. In *Industrial Electronics Society, IECON 2014 - 40th Annual Conference of the IEEE*, pages 702–708, Oct 2014.
- [21] Gorazd TUMBERGER, Eljko PLANTI. Determining parameters of a three phase permanent magnet synchronous machine using concontrol single phase voltage source. *PRZEGLAD ELEKTROTECHNICZNY (Electrical Review)*, 87:0033–2097, 2011.
- [22] R. Dutta and M. F. Rahman. A comparative analysis of two test methods of measuring d - and q -axes inductances of interior permanent-magnet machine. *IEEE Transactions on Magnetics*, 42(11):3712–3718, Nov 2006.
- [23] V. Ostovic. Memory motors. *IEEE Industry Applications Magazine*, 9(1):52–61, Jan 2003.

- [24] M. Ibrahim. *Application of magnetic Hysteresis Modeling to the Design and Analysis of Electric Machines*. PhD thesis, Concordia University, Montreal, Quebec, Canada, November 2014.
- [25] J. Goss, M. Popescu, and D. Staton. A comparison of an interior permanent magnet and copper rotor induction motor in a hybrid electric vehicle application. In *Electric Machines Drives Conference (IEMDC), 2013 IEEE International*, pages 220–225, May 2013.
- [26] T. Miura, S. Chino, M. Takemoto, S. Ogasawara, Akira Chiba, and Nobukazu Hoshi. A ferrite permanent magnet axial gap motor with segmented rotor structure for the next generation hybrid vehicle. In *Electrical Machines (ICEM), 2010 XIX International Conference on*, pages 1–6, Sept 2010.
- [27] Huang Jia, Wang Xinjian, and Sun Zechang. Variable flux memory motors: A review. In *Transportation Electrification Asia-Pacific (ITEC Asia-Pacific), 2014 IEEE Conference and Expo*, pages 1–6, Aug 2014.
- [28] V. Ostovic. Memory motors-a new class of controllable flux PM machines for a true wide speed operation. In *Industry Applications Conference, 2001. Thirty-Sixth IAS Annual Meeting. Conference Record of the 2001 IEEE*, volume 4, pages 2577–2584 vol.4, Sept 2001.
- [29] M. Ibrahim, L. Masisi, and P. Pillay. Design of variable-flux permanent-magnet machines using Alnico magnets. *IEEE Transactions on Industry Applications*, 51(6):4482–4491, Nov 2015.
- [30] M. Ibrahim, L. Masisi, and P. Pillay. Design of variable flux permanent-magnet machine for reduced inverter rating. *IEEE Transactions on Industry Applications*, 51(5):3666–3674, Sept 2015.

- [31] M. Ibrahim and P. Pillay. Design of high torque density variable flux permanent magnet machine using Alnico magnets. In *Energy Conversion Congress and Exposition (ECCE), 2014 IEEE*, pages 3535–3540, Sept 2014.
- [32] Chen Yiguang, Pan Wei, Wang Ying, Tang Renyuan, and Wang Jing. Interior composite-rotor controllable-flux PMSM - memory motor. In *2005 International Conference on Electrical Machines and Systems*, volume 1, pages 446–449 Vol. 1, Sept 2005.
- [33] K. Sakai, K. Yuki, Y. Hashiba, N. Takahashi, and K. Yasui. Principle of the variable-magnetic-force memory motor. In *Electrical Machines and Systems, 2009. ICEMS 2009. International Conference on*, pages 1–6, Nov 2009.
- [34] Z. Changqing, W. Xiuhe, and W. Bei. Study of a novel permanent magnet synchronous motor with composite-rotor. In *Electrical Machines and Systems (ICEMS), 2010 International Conference on*, pages 1044–1047, Oct 2010.
- [35] G. Zhou, T. Miyazaki, S. Kawamata, D. Kaneko, and N. Hino. Development of variable magnetic flux motor suitable for electric vehicle. In *Power Electronics Conference (IPEC), 2010 International*, pages 2171–2174, June 2010.
- [36] M. Aydin, Surong Huang, and T. A. Lipo. A new axial flux surface mounted permanent magnet machine capable of field control. In *Industry Applications Conference, 2002. 37th IAS Annual Meeting. Conference Record of the*, volume 2, pages 1250–1257 vol.2, Oct 2002.
- [37] J. A. Tapia, F. Leonardi, and T. A. Lipo. Consequent pole permanent magnet machine with field weakening capability. In *Electric Machines and Drives Conference, 2001. IEMDC 2001. IEEE International*, pages 126–131, 2001.

- [38] N. Naoe and T. Fukami. Trial production of a hybrid excitation type synchronous machine. In *Electric Machines and Drives Conference, 2001. IEMDC 2001. IEEE International*, pages 545–547, 2001.
- [39] D. Fodorean, A. Djerdir, I. A. Viorel, and A. Miraoui. A double excited synchronous machine for direct drive application 2014; design and prototype tests. *IEEE Transactions on Energy Conversion*, 22(3):656–665, Sept 2007.
- [40] Kou Baoquan, Li Chunyan, and Cheng Shukang. A new flux weakening method of permanent magnet synchronous machine. In *2005 International Conference on Electrical Machines and Systems*, volume 1, pages 500–503 Vol. 1, Sept 2005.
- [41] Lei Ma, M. Sanada, S. Morimoto, Y. Takeda, and N. Matsui. High efficiency adjustable speed control of ipmsm with variable permanent magnet flux linkage. In *Industry Applications Conference, 1999. Thirty-Fourth IAS Annual Meeting. Conference Record of the 1999 IEEE*, volume 2, pages 881–887 vol.2, 1999.
- [42] P. Vas, K. E. Hallenius, and J. E. Brown. Cross-saturation in smooth-air-gap electrical machines. *IEEE Transactions on Energy Conversion*, EC-1(1):103–112, March 1986.
- [43] L. Masisi, M. Ibrahim, and P. Pillay. Control strategy of a variable flux machine using AlNiCo permanent magnets. In *Energy Conversion Congress and Exposition (ECCE), 2015 IEEE*, pages 5249–5255, Sept 2015.
- [44] C. Y. Yu, T. Fukushige, N. Limsuwan, T. Kato, D. D. Reigosa, and R. D. Lorenz. Variable-flux machine torque estimation and pulsating torque mitigation during magnetization state manipulation. *IEEE Transactions on Industry Applications*, 50(5):3414–3422, Sept 2014.

- [45] A. M. El-Serafi and J. Wu. Determination of the parameters representing the cross-magnetizing effect in saturated synchronous machines. *IEEE Transactions on Energy Conversion*, 8(3):333–342, Sep 1993.
- [46] S. T. Lee, T. A. Burress, and L. M. Tolbert. Power-factor and torque calculation with consideration of cross saturation of the interior permanent magnet synchronous motor with brushless field excitation. In *Electric Machines and Drives Conference, 2009. IEMDC '09. IEEE International*, pages 317–322, May 2009.
- [47] Min-Seok Kim, Won Jeon, Yu-Seok Jeong, and Sang-Yong Jung. Numerical identification of synthetic flux linkages considering cross-magnetization for interior PM synchronous motor and its effective availability on design and control. In *Industrial Electronics, 2008. IECON 2008. 34th Annual Conference of IEEE*, pages 1299–1304, Nov 2008.
- [48] T. Frenzke. Impacts of cross-saturation on sensorless control of surface permanent magnet synchronous motors. In *Power Electronics and Applications, 2005 European Conference on*, pages 10 pp.–P.10, Sept 2005.
- [49] Y. Li, Z. Q. Zhu, D. Howe, C. M. Bingham, and D. Stone. Improved rotor position estimation by signal injection in brushless ac motors, accounting for cross-coupling magnetic saturation. In *Industry Applications Conference, 2007. 42nd IAS Annual Meeting. Conference Record of the 2007 IEEE*, pages 2357–2364, Sept 2007.
- [50] L. Chedot and G. Friedrich. A cross saturation model for interior permanent magnet synchronous machine. application to a starter-generator. In *Industry Applications Conference, 2004. 39th IAS Annual Meeting. Conference Record of the 2004 IEEE*, volume 1, page 70, Oct 2004.

- [51] G. Almandoz, J. Poza, M. A. Rodriguez, and A. Gonzalez. Modeling of cross-magnetization effect in interior permanent magnet machines. In *Electrical Machines, 2008. ICEM 2008. 18th International Conference on*, pages 1–6, Sept 2008.
- [52] K. Yamazaki and M. Kumagai. Torque analysis of interior permanent-magnet synchronous motors by considering cross-magnetization: Variation in torque components with permanent-magnet configurations. *IEEE Transactions on Industrial Electronics*, 61(7):3192–3201, July 2014.
- [53] K. Yamazaki and M. Kumagai. Rotor design of interior permanent magnet motors considering cross magnetization caused by magnetic saturation. In *Electrical Machines and Systems (ICEMS), 2011 International Conference on*, pages 1–6, Aug 2011.
- [54] K. J. Meessen, P. Thelin, J. Soulard, and E. A. Lomonova. Inductance calculations of permanent-magnet synchronous machines including flux change and self- and cross-saturations. *IEEE Transactions on Magnetics*, 44(10):2324–2331, Oct 2008.
- [55] N. Limsuwan, T. Kato, K. Akatsu, and R. D. Lorenz. Design and evaluation of a variable-flux flux-intensifying interior permanent-magnet machine. *IEEE Transactions on Industry Applications*, 50(2):1015–1024, March 2014.
- [56] A. Pouramin, R. Dutta, M. F. Rahman, and D. Xiao. Inductances of a fractional-slot concentrated-winding interior PM synchronous machine considering effects of saturation and cross magnetization. In *2015 IEEE Energy Conversion Congress and Exposition (ECCE)*, pages 6075–6081, Sept 2015.
- [57] B. Stumberger, G. Stumberger, D. Dolinar, A. Hamler, and M. Trlep. Evaluation of saturation and cross-magnetization effects in interior permanent-magnet synchronous motor. *IEEE Transactions on Industry Applications*, 39(5):1264–1271, Sept 2003.

- [58] A. Pouramin, R. Dutta, M. F. Rahman, J. E. Fletcher, and D. Xiao. A preliminary study of the effect of saturation and cross-magnetization on the inductances of a fractional-slot concentrated-wound interior PM synchronous machine. In *Power Electronics and Drive Systems (PEDS), 2015 IEEE 11th International Conference on*, pages 828–833, June 2015.
- [59] L. Masisi. *Design and Development of Novel Electric Drives for Synchronous Reluctance and PM Synchronous Machines*. PhD thesis, Concordia University, April 2015.
- [60] S. Hossain, D. Smith, S. Gebhart, and U. Deshpande. Torque ripple tester for a permanent magnet synchronous motor. In *IEEE International Conference on Electric Machines and Drives, 2005.*, pages 1020–1024, May 2005.
- [61] Li Sun, Hanying Gao, Qingliang Song, and Jianhong Nei. Measurement of torque ripple in PM brushless motors. In *Industry Applications Conference, 2002. 37th IAS Annual Meeting. Conference Record of the*, volume 4, pages 2567–2571 vol.4, Oct 2002.

# Appendix A

## Machine Specifications

The specifications of the machine used in this thesis are given below

Table A.1: Specification of the prototyped VFM

Number of poles	6
Number of slots	27
Stator outer diameter (mm)	200
Axial length (mm)	120
Air gap length (mm)	0.4-0.75
Magnet material	AlNiCo 9
Steel material	M19G29
DC bus voltage (V)	600
Rated current (A)	10
Rated torque (Nm)	36.8
Base speed (rpm)	1200